New Methodology for use in Rotating Field Nuclear Magnetic Resonance

By

Rebecca Corina Jachmann

B.S. (University of Utah) 2002

A Dissertation submitted in partial satisfaction of the

requirements for the degree of

Doctor of Philosophy

in

Chemistry

in the

Graduate Division

of the

University of California, Berkeley

Committee in charge:

Professor Alexander Pines, Chair

Professor David Wemmer

Professor Jeff Reimer

Spring 2007

Abstract

High-resolution NMR spectra of samples with anisotropic broadening are simplified to their isotropic spectra by fast rotation of the sample at the magic angle 54.7°. This dissertation concerns the development of novel Nuclear Magnetic Resonance(NMR) methodologies which would rotate the magnetic field instead of the sample, i.e. rotating field NMR. It also provides an overview of the NMR concepts, procedures, and experiments needed to understand the methodologies that will be used for rotating field NMR.

A simple two-dimensional shimming method based on harmonic corrector rings provides arbitrary multiple order shimming corrections that are necessary for rotating field systems, but can be used in shimming other systems as well. Those results demonstrate, for example, that quadrupolar order shimming improves the linewidth by up to a factor of ten. An additional order of magnitude reduction is in principle achievable by utilizing this shimming method for *z*-gradient correction and higher order *xy* gradients.

Additionally, initial investigations into a specialized pulse sequence for the rotating field NMR experiment, which allows for spinning at angles other than the magic angle and spinning slower than the anisotropic broadening is discussed. This will be useful for rotating field NMR because there are limits on how fast a field can be spun and difficulties of reaching the magic angle. This pulse sequence is a combination of the previously established projected magic angle spinning (p-MAS) and magic angle turning (MAT) pulse sequences. One of the goals of this project is for rotating field NMR to be used on biological systems. The p-MAS pulse sequence was successfully tested on bovine tissue samples, which suggests that it will be a viable methodology to use in rotating field NMR.

A side experiment on steering magnetic particles by MRI gradients was also carried out. Initial investigations indicate some movement, but for total steering control, further experiments are needed.

Acknowledgements

This work was supported by the Director, Office of Science, Basic Energy Sciences, U.S. Department of Energy under Contract No. DE-AC02-05CH11231. The Author would like to give a special thanks to Louis Bouchard, Dimitris Sakelleriou, Rachel Martin for the endless hours of help given to understand NMR material and in helping with the experiments. The author also thanks Pete Doniaz, Marcus H. Donaldson, Dimitris Sakelleriou, Alec Sorensen, Lana Chavez, Susan Jachmman, Tyler Meldrum, Arron Johnson and Eric Philbrick for carefully proof-reading the manuscript and William Gath for the assembly of the Halbach magnet array and for help during the design and assembly of the shimming device. She also thanks Alex Pines for all the great experiences, inspiration, and support he gave during this work.

She is especially grateful for the love and support that was given to her from her family and friends.

Contents

Chapter 1

Forward

1.1 The Thesis

Many PhD topics can be, well, boring and there's no way that I could do that! I wanted to be on the edge of the impossible and I think that's right where I am. We're at an exciting stage of research right now, and it's only going to get more exciting as things once thought impossible become possible. Once when discussing my project with a friend they told me that it sounded like I was inventing the tricorder from Star Trek. The fictional, small, handheld, device identifies chemical composition by simply pointing it towards an area of interest. In some senses this is the goal of my research. It seems imposible to make such a fictional device, but I'm helping fiction become a reality. It's amazing how the technology of tomorrow is arriving today.

Nuclear Magnetic Resonance(NMR) is different than the majority of popular techiniques in that is doesn't destroy the sample being examined. This makes it perfect to probe the world around us. Today we're working on *ex-situ* rotating field NMR, and in the future it will be completely portable which is a lot like the fictional tricorder. [1] The basic idea is to have

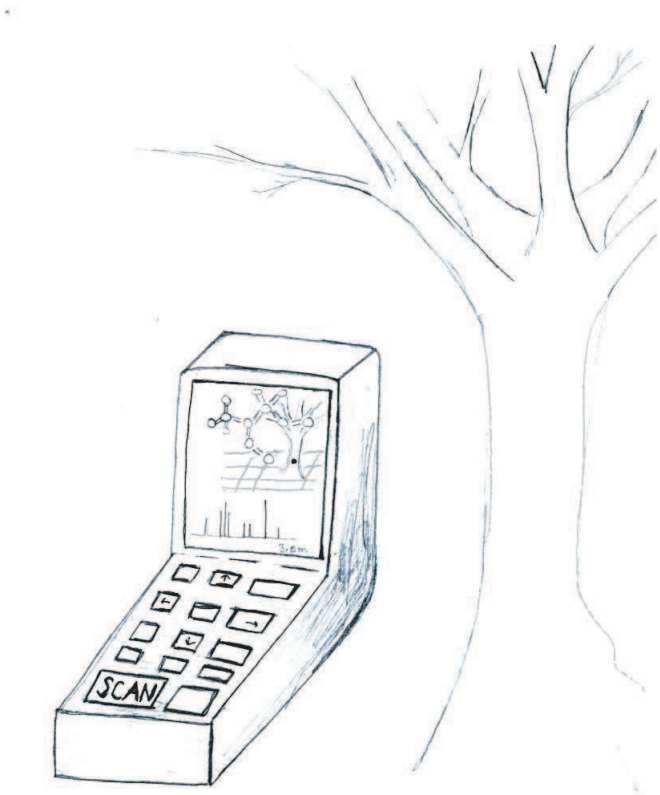

Figure 1.1: A pictorial of an imaginary NMR tricorder which could image, give spectra, and identify chemicals at the push of a button.

a portable machine that can do chemical analysis and imaging wherever you want without disturbing the sample you are analysizing. For instance, it could take an image of a tree, like in Figure 1.1, and also scan for the chemicals which make it up. This technique would have endless uses, in field studies, like imaging a tree to see how old it is, in a doctors office to see broken bones, in industry to check the quality of a product as it is being made. Accomplishing this involves the convergence of multiple ideas, drawing from NMR liquid techniques and solid techniques, of which are both examined in this document.

Chapter 2

Introduction:

NMR Theory Summary

NMR has a beautiful beginning. One December night long ago in 1945, three scientists, Purcell, Torrey and Pound after hours of scanning finally detected a small radio frequency signal. Nuclear spins were detected. [2] Purcell was amazed "in the winter of [his] first experiment... [he looked] on snow with new eyes. There the snow lay around [his] doorstep -great heaps of protons quietly precessing in the Earth's magnetic field. To see the world for a moment as something rich and strange is the private reward of many a discovery." [2]

There is a substantial number of well written works on the subject of NMR. To gain a general understanding, *Spin Dynamics*, by Malcolm H. Levitt gives good insight into the subject. [2] For more common pulse sequences and another view on for useful understanding *Protein MR Spectroscopy Principles and Practice* by John Cavanagh et al. [3] gives a thorough explanation. The first few chapters of this thesis present a short introduction to the most relevant topics necessary to understanding the research topic presented in the chapters.

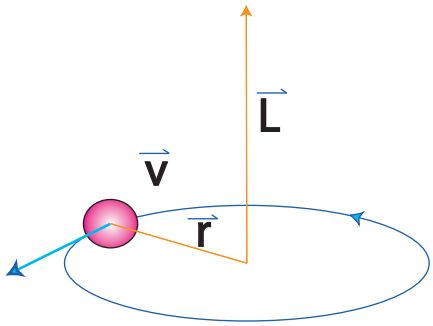

Figure 2.1: *Angular momentum diagram.*

2.1 Angular momentum and spin

NMR is the spectroscopy of nuclear spins when a magnetic field is present. Probing the split nuclear spin energy difference gives rise to spectra similar to Raman or IR spectroscopy. Instead of detecting in the infrared region of frequencies, NMR looks at the radio frequency region. Nuclear spin is conceptually and mathematically treated as momentum. It is therefore important to understand classical momentum (linear and angular) along with quantum mechanical descriptions of momentum.

2.1.1 Classic angular momentum

Momentum is a conserved quantity based on the mass and velocity of an object. The simplest relation for the two quantities is linear momentum, $\vec{\mathbf{p}}$, which is velocity, $\vec{\mathbf{v}}$ times mass, m, $\vec{\mathbf{p}} \equiv m\vec{\mathbf{v}}$. [4] For example, consider one ball striking a second ball; each ball will change velocity, yet the overall momentum is conserved such that $p_1 = p_2$, where p_1 and p_2 are the total momentum before and after the collision.

Now, instead of a ball moving in a straight line consider a point mass being swung around on a rope at a distance, $\vec{\mathbf{r}}$, from the origin. At any one instant the mass has a linear velocity, $\vec{\mathbf{v}}$. This is the speed and direction the mass would have if the rope was released at that instant.

This is its linear momentum, $\overrightarrow{\mathbf{p}}$, but at that instant its angular momentum is $\overrightarrow{\mathbf{L}} = \overrightarrow{\mathbf{r}} \times \overrightarrow{\mathbf{p}}$. Angular momentum is also conserved as the object turns, however, it is perpendicular to the plane of rotation. (See Figure 2.1) [4]

To understand objects with angular momentum examine a spinning top. This top itself is locally stationary; that is, it doesn't move to another location though it is composed of many particles moving circularly. Spinning objects have a frequency of rotation, ω, where the frequency would be related to the linear velocity, $\omega = \overrightarrow{\mathbf{v}}/\overrightarrow{\mathbf{r}}$. (see Figure 2.1) Angular momentum is often put in terms of this frequency, dependence on shape, and distribution of mass through an object of interest such that:

$$\overrightarrow{\mathbf{L}} = m\overrightarrow{\mathbf{r}}^2\omega = \mathbf{I}\omega \tag{2.1}$$

where $m\overrightarrow{\mathbf{r}}^2$ is defined as the moment of inertia, **I**.

For non-uniform distributions of mass **I** is defined as, $\mathbf{I} = \int \mathbf{r}^2 dm$. Many moment of inertias have been previously calculated and can be found in any standard physics books. [4] [5]

2.1.2 Quantum angular momentum

As systems become smaller and smaller quantum mechanical effects become more and more relevant. In quantum mechanics properties such as energy and angular momentum become quantized. [6] [7] This means that there are discrete energy levels as opposed to a classical continuum. The distinguishing feature of quantum mechanical systems is that particles and waves are not distinct entities. This is known as wave-particle duality. Because of this duality a particle of any size has a wave length associated with it, given according to the de Broglie relation, $\lambda = \frac{h}{p}$, where h is the Planck constant, 6.6×10^{-34} J s, and p is the linear momentum

of the object. If every object can be a wave then every object has a wave equation associated with it. The wave equation for any system was proposed by Erwin Schrödinger in 1926 and is known as the Schrödinger equation [8]:

$$-\frac{\hbar^2}{2m}\bigtriangledown^2\psi + V\psi = E\psi \tag{2.2}$$

Here $\hbar$ is equal to $h/2\pi$, ψ is the distribution of the particle through space known as the wavefunction, $i = \sqrt{-1}$, t is time, and $\bigtriangledown$ is known as 'del squared' and is given by:

$$\bigtriangledown^2 = \frac{\delta^2}{\delta x^2} + \frac{\delta^2}{\delta y^2} + \frac{\delta^2}{\delta z^2} \tag{2.3}$$

The left hand of the Schrödinger equation can be generalized to $\mathscr{H}\psi$, where $\mathscr{H}$ is an operator. This operator, $\mathscr{H}$, will take different forms dependent on the system of interest and is known as the Hamiltonian.

The Schrödinger equation reveals fundamental quantum numbers that describe the different possible states (or energy levels) of a quantum mechanical system. Atomic quantum numbers for electrons are: n, l, m_l , s, and m_s. The first three quantum numbers describe the overall energy and shape that an electron orbital can take; the last two describe the electron's spin angular momentum. [9] Similar to electrons' angular momentum, nuclear angular momentum is also quantized and has quantum numbers, S, m_S. Each of these is only allowed to be a distinct integer or half integer value.

For electrons s is $\frac{1}{2}$ and m_s can only take the values$\frac{1}{2}$ and $-\frac{1}{2}$. For nuclei, S can take integer and half integer values $S = 1/2, 1, 3/2, \ldots$ and m_S ranges from $-S$ to S. NMR is focused on the spin angular momentum of the nucleus. Nuclear spin is often designated as I more often than S in NMR. Different locations on a molecule are called sites. For example, CH_3-

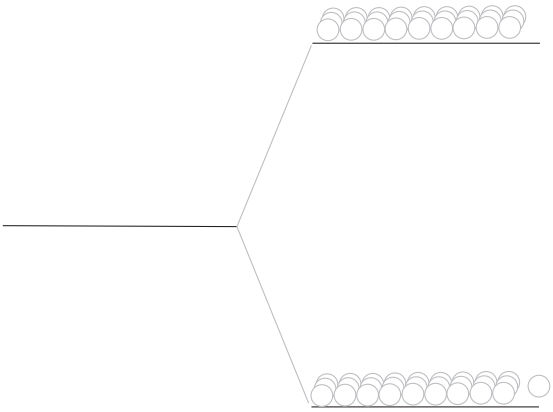

Figure 2.2: *Populations split according to the Boltzmann's distribution into different states. Here the splitting of a spin* $1/2$ *in a magnetic field is shown. The two levels are classified as: up, down,* $|\alpha>$, $|\beta>$, *or* $1/2$, $-1/2$

$CH_2 - COOH$ has 11 different sites by counting each atom. For NMR different chemical and magnetic sites will arise in separate frequencies, known as inequivalent sites. For the example there are only 8 magnetically inequivalent sites. Each inequivalent site can be distinguished using a superscript, e.g. I^i. (For a more comprehensive look at quantum mechanics refer to J.J. Sakurai's explanations in Modern Quantum Mechanics. [6])

2.1.3 Spin angular momentum

Spin angular momentum, often shortened to spin is an intrinsic property of a particle. This means the particle behaves as if it were spinning on its own axis though it's not actually spinning at all. [10]

The atomic nuclear spin energies, m_s, are equivalent until an external field, electric or magnetic, is applied. This means the presence of a magnetic field lifts the degeneracy and splits the nuclear spin energies. This splitting in the magnetic field is the principle on which NMR works. The interaction with the magnetic field is known as the Zeeman interaction.

The difference in m_s energies are $E = \mu \cdot \mathbf{B}$. Where μ, the magnetic dipole moment, will

be discussed in the section 2.1.5. Commonly, the main magnetic field is designated to be along the z direction, $\mathbf{B}_z$ or B^0, leaving a splitting energy of $E = \mu \cdot \mathbf{B}_z$. There are two energy levels for spin $1/2$ with an applied magnetic field.(see Figure 2.2) These can be thought of as with the field or against it. With the field is known as up spins or $|\alpha>$ against the field is known as down or $|\beta>$.

The simplest case is for a spin $1/2$, and is of most interest to the research presented here because all experiments were done on nuclei with spin $1/2$. [2]

2.1.4 Boltzmann distribution

Whenever there are multiple energy levels, there will be a distribution of those states. The difference in this population is determined by the Boltzmann distribution and will determine the maximum signal that can be achieved.

$$\frac{N_m}{N} = \frac{e^{\left(\frac{-E_m}{k_B T}\right)}}{\sum_{m=-l}^{l} e^{\frac{-E_m}{k_B T}}} \tag{2.4}$$

Here N_m is the particular state of interest, k_B is the Boltzmann constant, T is the temperature, and E_m is the energy of that state. At room temperature the difference in population is approximately 1 in 10^6 spins. [2] [3]

2.1.5 Magnetic dipole moment

Substances capable of interacting with magnetic fields have a magnetic momentum. Classically, the magnetic momentum is $\mu = IA$, where here I is the current in a loop and A is the area. For this case magnetic momentum is a quantity which is used in finding torque on loops of cur-

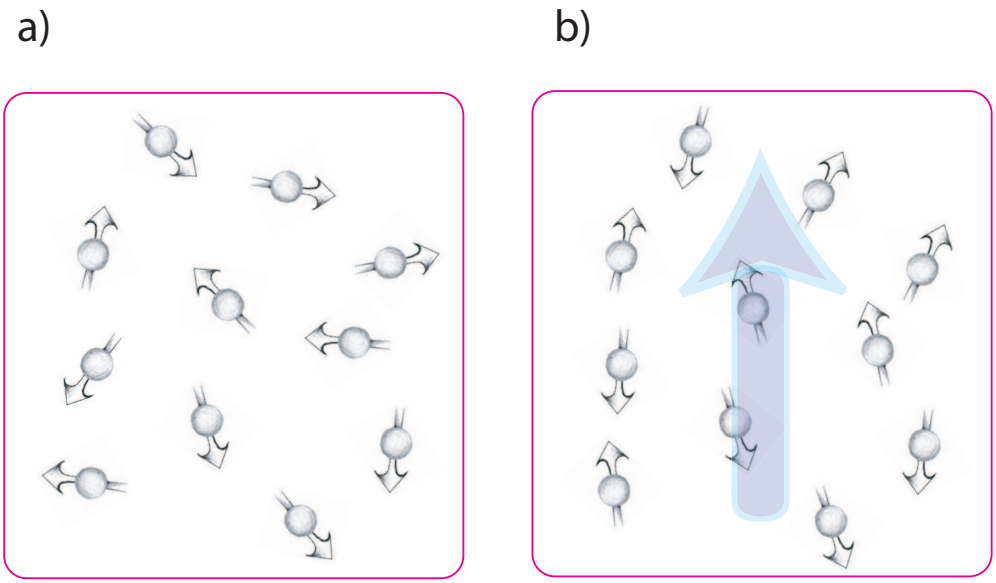

Figure 2.3: a) An ensemble of spins in no magnetic field. The spins are aligned in no particular way. b) When placed in a magnetic field the spins slightly align more towards the field creating a magnetization.

rent. As nuclei have a charge and angular momentum they have a current in some sense, which is over an area thus giving a magnetic moment. Nuclei have magnetic moments proportional by γ the gyromagnetic ratio to their spin, $\mu = \gamma \mathbf{I}$. [3]

2.1.6 Magnetization

A bulk sample contains an ensemble of spins. Quantum mechanically, each ensemble member is a superposition of the up,$|\alpha>$ and down,$|\beta>$ states. However picturing the magnetic moment as a pointing arrow on a ball of spinning charge is also a valid and often more useful picture. (See Figure 2.3)

When a magnetic field is applied to the picture of pointing arrows in figure 2.3 the arrows slightly align with that magnetic field. This is equivalent to the states, $|\alpha>$ and $|\beta>$ distributing according to the Boltzmann equation. This alignment, will cause a small magnetic field called the magnetization. The course and detection of this magnetization, depicted as a single

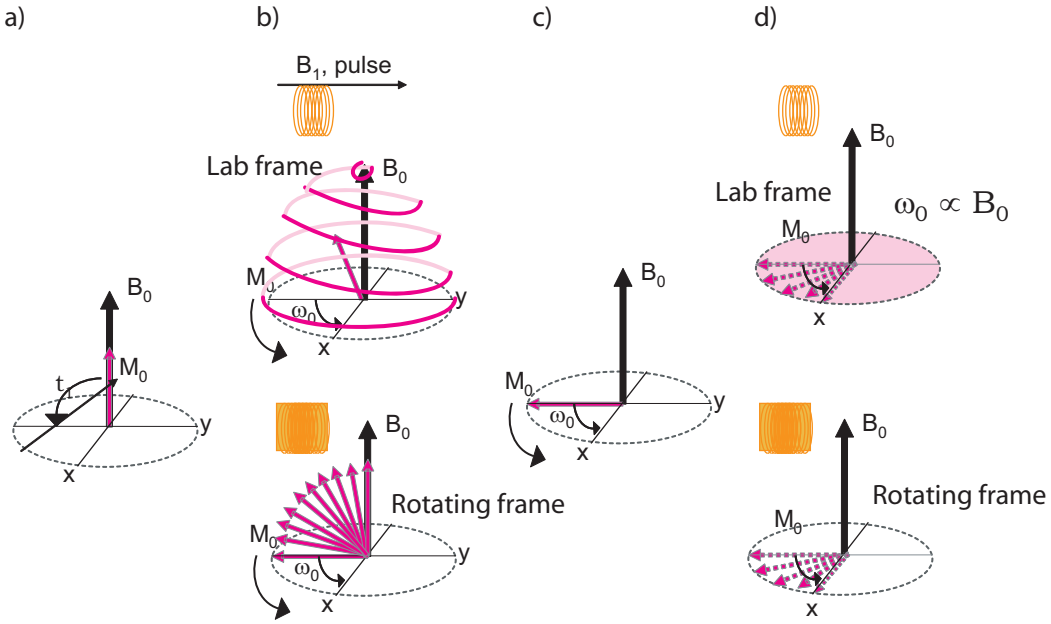

Figure 2.4: a) The magnetization of a sample in a magnetic field. b)A rf pulse generated by a coil is applied to the magnetization and it flips down to the transverse plane. In the lab frame the magnetization spirals down into the *xy* at the Larmor frequency. In rotating frame the magnetization turns down to the *xy* plane. In this frame the coil appears to be moving at the carrier frequency. c)The magnetization has been flipped 90° to the *xy* plane. d) The magnitization precesses at the Larmor frequency in the lab frame, ω_0 which causes a small magnetic field. The precessing magnetic field from the spins is detected by the same coil which excited the system. In the rotating frame the magnetization precesses at the difference between the carrier frequency and the Larmor frequency.

arrow, is the NMR experiment. (see figure 2.4 a)) [2, 3]

2.2 Radio frequency pulse

The difference in population or magnetization can be stimulated using a second magnetic field generated from a coil. The frequency associated with this second field is the Larmor frequency, which corresponds to the splitting energy between the up and down states. This field usually rotates in the radio frequency (rf) regime and is described as $B_{rf} = B_1 \left(cos \left(\omega_{rf} t + \phi \right) \mathbf{i} + sin \left(\omega_{rf} t + \phi \right) \mathbf{j} \right)$. As the magnetization relaxes back to its equilibrium state a signal can be detected by the same coil leading to the NMR signal. This radio frequency field is only active for a short time depending on what kind of experiment is being conducted. Pictorially, it is represented by a solid rectangle and is called the rf (radio frequency) pulse.

In the magnetization picture the rf pulse rotates the magnetization towards the *xy* plane, also known as the transverse plane, causing the magnetization to spiral down. (See Figure 2.4 b)) A pulse which causes the magnetization to end in the *xy* plane is known as a ninety pulse, due to the angle it went through to get there. [2] [3]

2.3 Rotating frame

The apparent mechanics of how something moves depends on the frame of reference. For example, take a ball rolling across a spinning merry-go-round. A person on the ground sees the ball go straight across, however a person on the merry-go-round would see the ball curve. The mechanics of what is happening is the same but the perception of what happens is different depending on the frame of reference.

In NMR a mathematical transformation is used to simplify the system during the rf pulse.

This transformation is into a rotating frame of reference, called the rotating frame. This frame of reference rotates at the radio frequency, called the carrier frequency. The frequency used is close to or exactly the Larmor frequency. This means that instead of the magnetization spiraling down to the *xy* plane when excited, it turns directly down to the *xy* plane. (See Figure 2.4 c))

After the rf pulse, either the rotating frame or the lab frame can be used. In the rotating frame the magnetization precesses at the difference between the carrier frequency and the precession frequency of the spin. If only one nuclear site is in the sample, and the carrier frequency is on resonance with it the magnetization would not move. In the merry-go-round example this would be like someone running along side it. Then the same part of the merry-go-round is next to them at all times. Only one frequency could be exactly on resonance if different nuclear sites are present as they all precess at different frequencies. Through a reverse transformation, the magnetization can be viewed from the lab frame again. In this case the spins all precess at their Larmor frequencies. [2] [3]

2.4 Bloch equations

The equation which describes the course of the magnetization is

$$\frac{d\mathbf{M}(t)}{dt} = \mathbf{M}(t)\,\gamma \times \mathbf{B} \tag{2.5}$$

Here $\mathbf{M}$ is the magnetization with three components, M_x, M_y, M_z. The solution to this is the magnetization precessing around the magnetic field and at a frequency, $\omega = \gamma\mathbf{B}$. Where ω is the Larmor frequency. [3]

The basic form that describes precession of magnetization is $\mathbf{M}(t) = e^{i\omega_0 t}$.

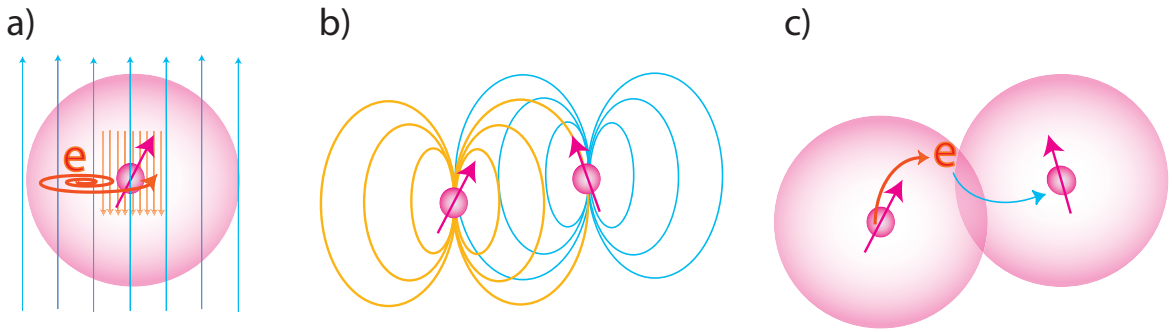

Figure 2.5: a) The chemical shift is caused by the main magnetic field in blue inducing a current in the electrons which causes another field. This field is experienced at the nucleus and shifts the frequency of the NMR signal. b) The dipolar coupling caused by the magnetic field felt by other nuclei. c) The J-coupling is caused by the nucleus of one atom affecting the electrons in a bond which then affect another nuclei.

2.5 Interactions and Hamiltonians

There are several different types of interactions which influence the frequencies for a given site, their resonance frequency, in an NMR signal. The strongest one, the Zeeman effect, is the dependence on the main magnetic field. Other interactions, in order of strongest to weakest, are: quadrupolar interactions (if not zero), dipolar interactions(if not zero), chemical shift, J-coupling, and spin rotation. The quadrupolar and spin-rotation interactions are not relevant to the research described here and are only mentioned here for completeness. [2]

2.5.1 Chemical shift

Chemical shift is the indirect interaction of the main magnetic field with the nuclei through the electrons. The main field induces a current in the electron clouds; this current causes a magnetic field, $\mathbf{B}^{induced}$ at the nucleus changing the magnitude of the field the nuclear site experiences and shifts its resonance frequency. The amplitude of $\mathbf{B}^{induced}$ to a good approximation depends linearly on the main field such that $\mathbf{B}^{induced} = -\sigma\mathbf{B}$. Where σ is the chemical shift shielding tensor. This σ is a second rank shielding tensor as the interaction is spatially dependant on

the orientation of the molecule's electrons and nuclear spins with respect to the magnetic field. The total magnetic field the nuclear site is $B_z + \mathbf{B}^{induced} = (1-\sigma)\mathbf{B}_z$. So then the resonance frequency for that site is $\omega = \gamma(1-\sigma)B_z$. (See Section 2.5.3 for more details on the chemical shift tensor.) [2] [3]

2.5.2 Dipolar interactions

Also known as the dipole-dipole coupling, the dipolar interaction concerns spins interacting with themselves. Each spin is magnetic, thereby each spin creates a field which influences neighboring spins. The interactions are mutual: one influences the other and vice versa through space. Since it is directly from spin to spin, this interaction is also called the direct dipole-dipole coupling. [2]

2.5.3 J coupling

When two nuclei are coupled with the help of the bonding electron between them it is known as the indirect coupling. This is an important interaction since the direct coupling (see section 4.2.4) is averaged to 0 in isotropic liquids. This means that the spin-spin coupling can still be seen in a spectra, and that the chemical bonds are still being probed in the experiment. [2]

Hamiltonians

Every NMR interaction can be described by an appropriate Hamiltonian. For NMR, only the nuclear Hamiltonians which describe the above interactions are of interest most of the time. The Hamiltonians are used in the Schrödinger equation, $i\hbar\frac{d\psi(t)}{dt} = \mathscr{H}\psi(t)$ and can be used to theoretically describe the observable quantities of a system. Hamiltonians are described in

terms of spin operators. Spin operators are the representation of the spin angular momentum and are denoted, $\mathbf{I}_x$, $\mathbf{I}_y$, and $\mathbf{I}_z$. These have a cyclic commutation, $[\mathbf{I}_x, \mathbf{I}_y] = i\mathbf{I}_z$.

For high-field NMR experiments the spin interactions are dominated by the large Zeeman effect along B_0. The full nuclear Hamiltonians are not needed for most calculations because of this dominating interaction. Each term which does not commute with the Zeeman interaction is eliminated. This truncation of the Hamiltonian is known as the secular approximation. The secular Hamiltonians for chemical shift, dipolar coupling, and j-coupling are organized into table 2.1. [2]

Table 2.1: Hamiltonian table.

	Solids		Liquids		
			Intramolecular		
			Isotropic	Anisotropic	
Chemical shift: Indirect magnetic interaction of the external mag field & nuclear spins through electrons $B_j^{loc} = B^0 + B_j^{induced}$ indicates local e^- environment effect in spectrum: shifts line down stream and spreads out multiple lines $\hat{\mathscr{H}}_j^{cs} \approx -\gamma_j \delta_{zz}^j(\Theta) B^0 I_{jz}$	$\hat{\mathscr{H}}_j^{cs}(\Theta) = \gamma_j B^0 \delta_{zz}^j(\Theta) I_{jz}$		$\hat{\mathscr{H}}_j^{cs\ iso} = -\gamma_j B^0 \delta_j^{iso} I_{jz}$, $\omega_j^0 = \gamma_j B^0(1 + \delta_j^{iso})$ withdrawn $e^- \rightarrow$ increased δ	$\hat{\mathscr{H}}_j^{cs} = -\gamma_j \overline{\delta_{zz}^j(\Theta)} B^0 I_{jz}$; $\overline{\delta_{zz}^j(\Theta)} = \int d\Theta \delta_{zz}^j(\Theta) P(\Theta)$	
Dipole - Dipole: Direct magnetic interactions of nuclear spins with each other; splits line in spectrum $\hat{\mathscr{H}}_{jk}^{DD,full} = b_{jk}(3(\hat{\mathbf{I}}_j \cdot \mathbf{e}_{jk})(\hat{\mathbf{I}}_k \cdot \mathbf{e}_{jk}) - \hat{\mathbf{I}}_j \cdot \hat{\mathbf{I}}_k)$ $b_{jk} = -\frac{\mu_0}{4\pi} \frac{\gamma_j \gamma_k \bar{h}}{r_{jk}^3}$	Homonuclear $\hat{\mathscr{H}}_{jk}^{DD}(\Theta_{jk}) = d_{jk}(3\hat{I}_{jz}\hat{I}_{kz} - \hat{\mathbf{I}}_j \cdot \hat{\mathbf{I}}_k)$ $d_{jk} = b_{jk}\frac{1}{2}\left(3\cos^2\Theta_{jk} - 1\right)$ Θ is the angle between the vector connecting the spins and the magnetic field	Heteronuclear $\hat{\mathscr{H}}_{jk}^{DD}(\Theta_{jk}) = d_{jk} 2\hat{I}_{jz}\hat{I}_{kz}$ $d_{jk} = b_{jk}\frac{1}{2}\left(3\cos^2\Theta_{jk} - 1\right)$	All orientations are equally probable, so $\int_0^\pi d\Theta \sin\Theta(3\cos^2\Theta - 1) = 0$ $\hat{\mathscr{H}}_{jk}^{DD} \approx 0$	Homonuclear $\hat{\mathscr{H}}_{jk}^{DD}(\Theta_{jk}) = d_{jk}(3\hat{I}_{jz}\hat{I}_{kz} - \hat{\mathbf{I}}_j \cdot \hat{\mathbf{I}}_k)$ $d_{jk} = b_{jk}\frac{1}{2}\overline{(3\cos^2\Theta_{jk} - 1)}$	Heteronuclear $\hat{\mathscr{H}}_{jk}^{DD}(\Theta_{jk}) = d_{jk} 2\hat{I}_{jz}\hat{I}_{kz}$ $d_{jk} = b_{jk}\frac{1}{2}\overline{(3\cos^2\Theta_{jk} - 1)}$
J-coupling: indirect spin-spin coupling, indirect dipole-dipole coupling $\hat{\mathscr{H}}_{jk}^{iso} = 2\pi J_{jk}\hat{\mathbf{I}}_j \cdot \hat{\mathbf{I}} + k$ J_{jk} is the isotropic J-coupling $J_{jk} = \frac{1}{3}(J_{xx}^{jk} + J_{yy}^{jk} + J_{zz}^{jk})$	$\hat{\mathscr{H}}_{jk}^{J} = 2\pi J_{jk}\hat{\mathbf{I}}_j \cdot \hat{\mathbf{I}}_k$ + J-anisotropy	$\hat{\mathscr{H}}_{jk}^{J} = 2\pi J_{jk}\hat{I}_{jz}\hat{I}_{kz}$ + J-anisotropy	Homonuclear $\hat{\mathscr{H}}_{jk}^{J} = 2\pi J_{jk}\hat{\mathbf{I}}_j \cdot \hat{\mathbf{I}}_k$ Heteronuclear $\hat{\mathscr{H}}_{jk}^{J} = 2\pi J_{jk}\hat{I}_{jz}\hat{I}_{kz}$	$\hat{\mathscr{H}}_{jk}^{J} = 2\pi J_{jk}\hat{\mathbf{I}}_j \cdot \hat{\mathbf{I}}_k$ + J-anisotropy	$\hat{\mathscr{H}}_{jk}^{J} = 2\pi J_{jk}\hat{I}_{jz}\hat{I}_{kz}$ + J-anisotropy

Table 2.2: Chemical shift spherical tensor entries

	$A_q^{(k)}$		$T_{-q}^{(k)}$
$A_0^{(0)}$	$-\frac{\sigma_{xx}+\sigma_{yy}+\sigma_{zz}}{\sqrt{3}} = -\frac{Tr[\sigma]}{\sqrt{3}}$	$T_0^{(0)}$	$-\frac{I_xB_x+I_yB_y+I_zB_z}{\sqrt{3}}$
$A_0^{(1)}$	$\frac{-i(\sigma_{yx}+\sigma_{xy})}{\sqrt{2}}$	$T_0^{(1)}$	$\frac{-i(I_yB_x-I_xB_y)}{\sqrt{2}}$
$A_0^{(2)}$	$\frac{-\sigma_{xx}-\sigma_{yy}+2\sigma_{zz}}{\sqrt{6}}$	$T_0^{(2)}$	$\frac{-I_xB_x-I_yB_y+2I_zB_z}{\sqrt{6}}$
$A_{\pm1}^{(1)}$	$\frac{-\sigma_{zx}-\sigma_{xz}\pm i(\sigma_{zy}-\sigma_{yz})}{2}$	$T_{\pm1}^{(1)}$	$\frac{I_zB_x-I_xB_z\pm i(I_zB_y-I_yB_z)}{2}$
$A_{\pm1}^{(2)}$	$\frac{\mp\sigma_{zx}\mp\sigma_{zz}+i(-\sigma_{zy}-\sigma_{yz})}{2}$	$T_{\pm1}^{(2)}$	$\frac{\mp I_zB_x\pm I_xB_z+i(-I_zB_y-I_yB_z)}{2}$
$A_{\pm2}^{(2)}$	$\frac{\sigma_{xx}-\sigma_{yy}\pm i(\sigma_{yx}+\sigma_{yz})}{2}$	$T_{\pm2}^{(2)}$	$\frac{I_xB_x-I_yB_y\pm i(I_xB_y-I_yB_x)}{2}$

These interactions are all second order tensors, meaning that they are represented by a 3 by 3 matrix. Each tensor interaction could be split into a spatial/orbital part and a spin part. This more explicitly written out for an interaction's Hamiltonian is:

$$\mathscr{H}_{int} = \mathbf{A}(lab)\cdot\mathbf{T}(lab) = \sum_{k=0}^{2}\sum_{q=-k}^{+k}(-1)^q A_q^{(k)}(lab)\,T_{-q}^{(k)}(lab) \tag{2.6}$$

Sometimes a more convenient notation for quantum mechanical analysis of NMR is the spherical tensors notation. (See table 2.2 for chemical shift spherical tensors)

2.5.4 Isotropic and Anisotropic interactions

Each interaction has a spatial dependence on the magnetic field. The spatially dependent part is called the anisotropic interaction while the spatially independent part is called the isotropic interaction. An anisotropic interaction is dependent on the orientation of the chemical site while a isotropic interaction is independent of it. The anisotropy is also motion dependent, rapid motion from either molecular tumbling or sample spinning (See Section(4.2.4), can

average the interaction to zero. On the other hand the isotropic interactions appear in every spectrum. A spectrum that only shows isotropic interactions is called an isotropic spectrum. A spectrum showing anisotropic interactions is called an anisotropic spectrum. The isotropic spectra usually have sharp, distinguishable peaks in general. The isotropic spectra are the easiest to understand and give scientist the most useful data. The information in anisotropic spectra is considered to be an overload of information from the spins and gives limited insight. Anisotropic spectra consist of broad, indistinguishable overlapping peaks (when there is more than one site) in general. The particular shape of an anisotropic spectrum depends on which interaction the anisotropy is arising from. It could be as simple as a wide Lorenzian or Gaussian, or as complex as a powder pattern (from the chemical shift anisotropy) as shown in Figure 4.7.

In liquids the rapid motion of the molecules averages out the anisotropic interactions. If a sample has any general alignment there will be anisotropies. Some examples of aligned samples are: solids, liquid crystals, tissues, bicells, and semi-solids.

The anisotropies are the second rank tensor interactions in the Hamiltonian. These interactions in high field NMR can be generalized to having a second order Lagrandre polynomial, $P_2(\cos\theta) = 1/2\left(1-3\cos^2\theta\right)$, dependence with their orientation to the field. Section 4.2.4 shows the origin of this dependence. Because of this simple dependence anisotropies are often mechanically averaged out by fast sample spinning at the angle of 54.74°, where $1/2\left(1-3\cos^2\right) = 0$. Another, way to average them is to use specialized rf pulses. [11]

2.6 Relaxation

After a system is excited it will return to its equilibrium state. The equilibrium state is described by the Boltzmann distribution. The way in which an excited state gets to its equilibrium state is referred to as relaxation. The NMR system has two separate relaxation processes. The first

is the build up of magnetization along the main magnetic field to the z direction and is called T_1, or spin-lattice relaxation. The second is the decrease of magnetization from the xy plane after a rf pulse. It's called T_2, or spin-spin relaxation. The Block equation including relaxation is as follows:

$$\frac{d\mathbf{M}(t)}{dt} = \frac{d}{dt}\begin{bmatrix} M_x(t) \\ M_y(t) \\ M_z(t) \end{bmatrix} = \begin{bmatrix} \gamma(M_y(t)B_z(t) - M_z(t)B_y(t)) - R_2M_x(t) \\ \gamma(M_z(t)B_x(t) - M_x(t)B_z(t)) - R_2M_y(t) \\ \gamma(M_x(t)B_y(t) - M_y(t)B_x(t)) - R_1(M_z(t) - M_0) \end{bmatrix} \tag{2.7}$$

2.6.1 Mechanisms of relaxation

Relaxation is caused by the magnetic field fluctuating at the nucleus of interest. The fluctuation is caused by changes from dipole-dipole interactions and by the chemical shift anisotropy as the molecules tumble, even in liquids, which may seem surprising because the interaction has averaged to zero through the molecular motion. An average, however, is not representative of all times. On very short time scales these interactions still influence the system and therefore cause relaxation. (See section 4.2.4) For those spins greater than $1/2$ the quadrupolar interaction will be the largest contributor.

Chapter 3

NMR Methodology

The basic equipment needed to conduct a NMR experiment includes the magnet, the spectrometer and the probe. This chapter will focus on what these are and how to use them in the lab.

3.1 Magnets

3.1.1 Superconducting magnets

A current flowing through a wire generates a magnetic field, $dB = k\frac{Ids\times\hat{\mathbf{r}}}{r^2}$(Biot-Savart law). This is the basic principle behind the NMR coil which generates the r.f. and superconducting magnets. When wire is wrapped into a coil the center field in the center is very homogeneous to the order of parts per million, ppm. This field can be maintained as long as the current is flowing. In a superconductor the resistance is as close to 0 as is physically possible. This is accomplished by placing the superconductor in liquid helium, as a closed circuit so the current will not be lost. These are the basic ideas of the superconductor used as the main magnet field

in the majority of NMR experiments. [3]

3.1.2 Permanent magnets

For some NMR experiments, such as rotating field NMR(See chapter 5), a permanent magnet is more convenient than a superconductor. They are cheaper since they do not need cryogens to maintain their magnetization and they are smaller so they are more readily portable. Permanent magnets are made out of materials which [10] have strong paramagnetic substances and thus always create a magnetic field.

3.1.3 Shimming

It is desirable to have as homogeneous as possible magnet for NMR. To improve homogeneity secondary small magnets, called shims, are placed inside the bore. The shims used are based off of the spherical harmonics expansion of magnetic fields because they obey Maxwell's equations and the Laplace equation, which are stated explicitly in Chapter 6. [12]

Conventional shims are orthogonal coils which surround the sweet spot. The current through the coils creates a field which either adds or subtracts from the main magnetic field. Shimming can be automated or done 'by hand' by changing the current values going through the coils. The spectrometer software gives the option to change each of the harmonic orders separately; though, the traditional shim stack cannot produce pure harmonics. When shimming, the effectiveness of one shim order will depend on the strength of the others to some extent. Each harmonic order needs to be tried and retried until the best linewidth is obtained.

The strongest field inhomogeneities are most commonly along the direction of the main field, z. Therefor, when shimming the 'axial' shims, (z, z^2, z^3, z^4) are usually a good place to start. Higher orders than fourth are less effective and sometimes not effective at all. [3]

For axial shimming the most effective orders are x, y, low orders, and ones mixed with z. The shimming process is slow and will take many repititions of shimming axial, then radial, and back and forth. Some spectrometer software doesn't separate the two so it would be better to shim the linear gradients first and then progress to higher orders. In most high resolution systems, linewidths well below 0.1 ppm can be reached. Conveniently, there are auto shimming options. These are a good start for shimming, but could get stuck in a local minimum so some manual shimming is always advantageous.

3.2 Spectrometer

The spectrometer makes NMR happen. All the supporting electronics can be overwhelming to know, but the basics parts, what they do, and a general knowledge of how they work is an obtainable goal.

3.2.1 Transmitter

The transmitter precedes the probe and sample and is responsible for the pulse sequence, timing, phasing, and amplification making the high power monochromatic radio frequency pulse. Most spectrometers have more than one transmitter,a seperate one for each nucleus to be pulsed on during the experiment. [2, 3]

Pulse programmer

There are two computers which control the spectrometer. The first is the user computer and the second is a computer on the spectrometer. The user computer uploads a pulse program to the spectrometer computer which controls the timing, amplitude, and phases of the r.f. pulses. [2,

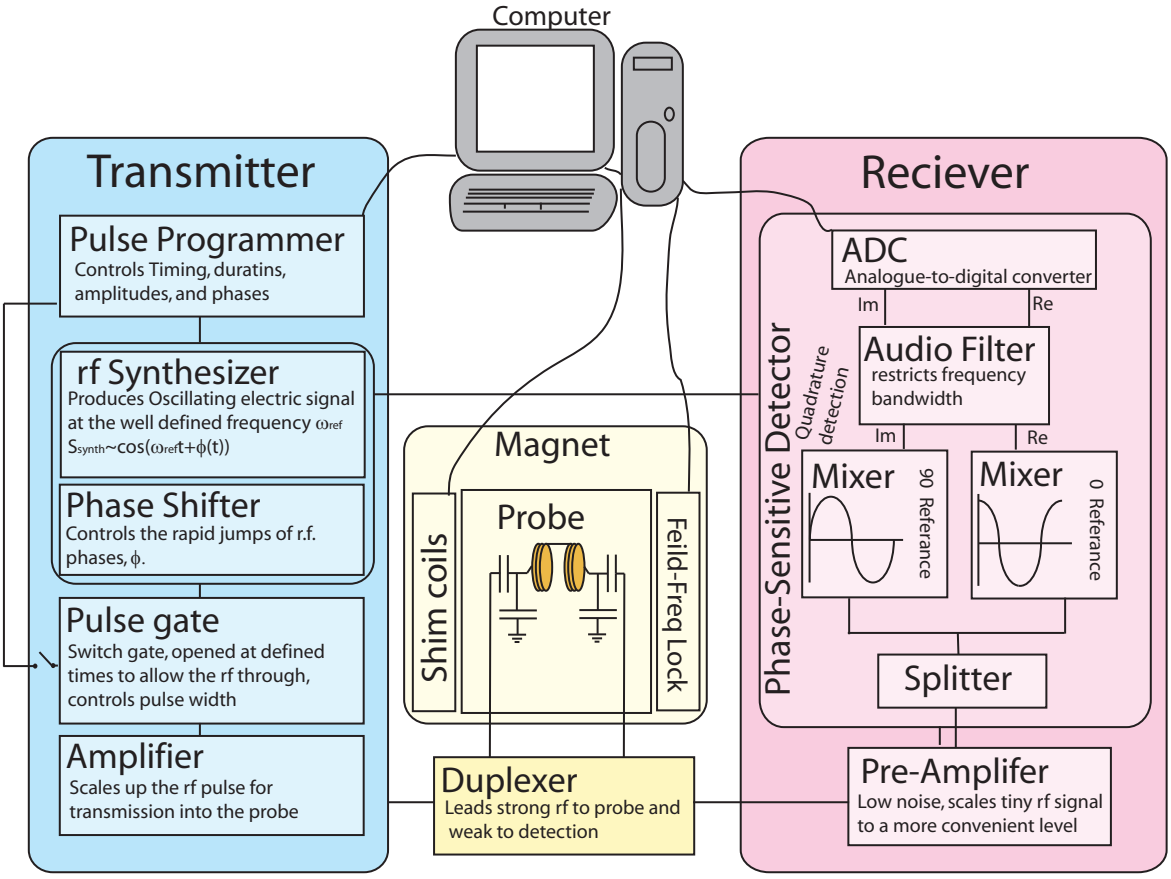

Figure 3.1: The spectrometer.

3]

Radio frequency synthesizer and Phase Shifter

The r.f. synthesizer makes a standard oscillating electronic signal, which is a radio frequency of frequency Ω_{ref}. The signal can be written as the following oscillation:

$$S_{synthesized} \approx A\cos\left(\Omega_{ref}t + \phi\left(t\right)\right) \tag{3.1}$$

where ϕ is the phase and t is the time and A is the amplitude.

The phase shifter controls the rapid jumps of the r.f. phase, ϕ. This hardware has stored very precisely calculated values for cos and sin to give the pulse. The synthesized r.f. is used for mixing down the signal to a usable frequency for the hardware. [2, 3]

Pulse gate

Signal from the r.f. synthesizer is continuous and always on. The gate, controlled by the pulse programmer, is a switch which can be quickly opened and closed allowing the r.f. to travel to the rest of the system. [2, 3]

Amplifier

The gated signal then goes through an amplifier to increase the size of B_1, the r.f. amplitude as the ninety time is dependent on that. In liquids, this is in the range of tens of watts; for solids up to one kilowatt is sometimes needed. [2, 3]

3.2.2 Duplexer

The next step, is for the high power radio frequency to go to the probe which will be discussed in more detail below. Having one coil for excitation and detection, which is the most common set up, means that the high power r.f. coming in, and the small current from the spins will be going through the same circuitry. The receiver which detects the small signal cannot receive the high power r.f. without damaging the system. If on the other hand, the signal returns to the transmitter then the signal would not be detected. The duplexer allows high power from the transmitter into the probe and restricts it from going to the receiver while allowing the low power current from the spins to go to the receiver and not back to the transmitter. This is done with a creative use of cables and diodes. [2, 3]

3.2.3 Receiver

The receiver receives the small current (the free induction decay(FID)), from the probe, amplifies it, mixes the signal down in frequency, converts it to digital data, and sends it to the computer. [2, 3]

Pre-amplifier

The signal which comes from the duplexer is too small to digitize in the electronics as is, so it is amplified. The pre-amplifier is optimized to introduce as little noise as possible while doing the first stage of this amplification. [2, 3]

Phase-sensitive detector

The course of events in the phase sensitive detectors can be seen in the receiver section in Figure 3.1. After amplification the signal is split into two parts. Then in the mixer the signal's frequency is scaled down and one is phased ninety degrees off from the other. The noise in the signal is then reduced as it goes through an audio filter and finally is converted to digital data for use in the user computer. This is the order in which events happen but the reason for the parts as they are is more easily explained by going through in the reverse order. [2, 3]

The analog signal coming from the probe needs to be converted to digital data. This is done with the analog to digital converter(ADC). Before that can happen, the signal needs to be scaled down to a frequency which the ADC can handle. The NMR signal, which can range from low MHz to several hundred MHz, is too fast for the ADC. Some new ADCs can handle hundreds of MHz, but it is not common. As such the signal needs to be mixed down to a useable frequency, usually less than 1 MHz. A reference frequency, ω_{ref} is subtracted from the NMR frequency, ω_0. This frequency is known as the carrier frequency:

$$\Omega^0 = \omega_0 - \omega_{ref}. \tag{3.2}$$

If a single detector is used to observe the NMR signal received, only a cosine or a sine is observed. This causes problems when the offset frequency is placed in the middle of the resonance frequencies. This means that some frequencies are higher and others are lower than the offset frequency. With only a cosine or sine modulated FID, the sign of a peak can not be determined. This will leave a signal at both Ω_0 and $-\Omega_0$. Quadrature detection, or splitting the signal and mixing one half with a cosine and the other half with a sine is the solution to this problem. [2, 3]

3.3 Probes

The probe is the most customized part of the NMR system. Each probe has its own special purpose. Some probes are specifically for imaging, while others are for flow experiments, and some just for solids. A scientist's collection of probes will determine the variety of experiments she can do.

The probe has many important functions and parts. The first function that it has is to hold and place the sample in the sweet spot of the magnet. The next function the probe has is to excite, or encode, the spins of the sample. The final function a probe has is to detect the oscillation of the spins.

3.3.1 Supports

The structure of a probe can take many different shapes, but it always accomplishes the same thing. The probe base holds the probe to the magnet. The stability of the probe is very important. Mechanical vibrations can cause noise in a spectrum. The holding mechanism can also allow the coil to be adjusted to the sweet spot in the magnet.

The body of the probe holds the essential electronics of the probe: the capacitors and coil. It also houses any special attributes of the probe like a gradient stack or a stepping motor.

The top of the probe is where all the action happens, usually. The probe can be built to be bottom loaded also. It houses the sample holder (a stator for solids) and coil for all experiments. The stator holds the sample in place. [13] For solid state probes the stator also has an air system set up which spins the sample. The coil can take many different forms but is what excites and detects the spins in traditional NMR systems. Sometimes, the coil itself is referred to as the probe. There are specialized systems where more than one coil is used or a coil is not used at

all for NMR detection. [14, 15] These methods are unconventional and were not used for this research so only traditional methods of detection are focused on.

3.3.2 Electronics

As stated above the coil is the most important part of the probe as it excites and detects the NMR signal. To do this its resonance frequency needs to match the frequency of the spins of interest. The circuit for the probe is made with the coil, and variable capacitors making a RLC (resistance, inductor, and capacitor) circuit. [13]

There are several different designs of coils: solenoid, split solenoid, saddle, bird cage, and surface. [16, 17, 18] Each coil can be tuned easily to two different frequencies and possibly more with specialized electronics. Each frequency has a channel on the spectrometer associated with it. That is, a separate transmitter and receiver. It is common to have triple resonance probes with two coils. The second coil often has a forth resonance specifically used to lock on to a deuterium signal to compensate for any field drift.

A simplistic double resonance circuit is shown in Figure 3.1. On each side of the coil are two variable capacitors referred to as match and tune, where the tune capacitor is connected to ground. The frequency, ω of the coil is:

$$\omega = \sqrt{\frac{1}{LC}}, \tag{3.3}$$

where L is the inductance and C is the total capacitance. The effectiveness of the probe head is determined by the quality factor,

$$Q = \omega L/R, \tag{3.4}$$

where R is the resistance. [2, 3] The quality factor evaluates the rate at which energy dissipates at specific frequencies. [10] To maximize the power transfer the impedance, Z, needs to be matched in the probe, [2]

$$Z = R + i\left[\omega L - 1/\left(\omega C\right)\right], \tag{3.5}$$

to that of the spectrometer, usually 50 ohm. [13]

3.3.3 Samples: tubes and rotors

Samples themselves come in all shapes and sizes. For NMR, liquids are easily placed in a tube. Solids are placed into rotors which are further discussed in section 9.3 Each sample needs to be considered in its own right: elongated samples will not always fit into a MAS probe and unconventional methods need to be used to obtain NMR spectra from them, as discussed in Chapter 7. Whereas NMR to observe chemical reactions needs a special container like a microfluidic chip [19] or specialized tubes that are used to accommodate flow into a biological sample. [20]

Chapter 4

Pulse sequences

4.1 General NMR experiments

The NMR experiment is often used for chemical analysis. This means chemical composition can be determined for a simple molecule with a simple experiment taking but moments or a complicated molecule with a series of elaborate experiments that can take up a whole PhD thesis.

4.1.1 One Pulse Experiment

At the root of every NMR experiment is the ability to control the angle which the magnetization flips. This angle is determined by the time the rf pulse is on. The time in which the magnetization ends in xy plane is called the ninety, 90°, time. This simply means the time it takes for the magnitization to flip 90° degrees. Similarly there is a 180° time. This 90° time is important becuase maximum signal is acquired with it. The 180° is important because it changes the sign of the magnetization. A simple NMR experiment excites magnetization with a 90° degree pulse

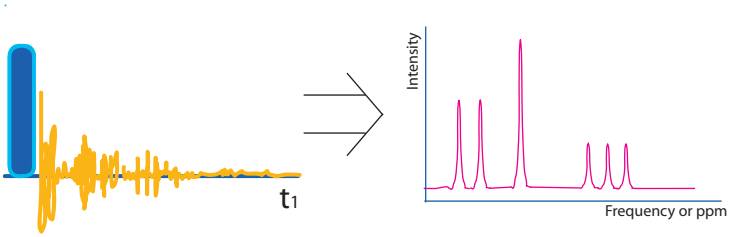

Figure 4.1: *A ninety pulse diagram.*

and then collects the FID (free induction decay), $S(t) = M_0 e^{i\Omega t} = M_0(\cos\Omega + \sin\Omega)$. There are two sets of data are taken with sine and a cosine reference signals, called quadruture detection, in order to phase the spectra. This data is then Fourier transformed, $S(\Omega) = \int_0^\infty s(t) e^{-i\Omega t} dt$ from the time domain to the frequency domain. Here different chemical shifts are readily viewable. (See Figure 4.1)

A single rf pulse where the time of the pulse is varied in an array, called a nutation curve, is used to determine the 90° time and the 180° time. These are the key elements in most NMR experiments and this calibration of pulse must be done before every experiment as in Figure 4.2. [3]

4.1.2 Multi-dimensional NMR

There are many factors which affect the final spectrum which could leave it very complex. One could be a similar chemical shift for two groups on a molecule. A one dimensional experiment is simply not always enough to obtain conclusive data. In a two dimensional, or if necessary a three dimensional, experiment new insight can be found. For example, this can resolve two resonances at the same frequency. The multi dimensional experiment increments the time between multiple pulses producing a second time domain. In these spectra, one dimension is correlated with the other. The peak position depends on the evolution from each period.

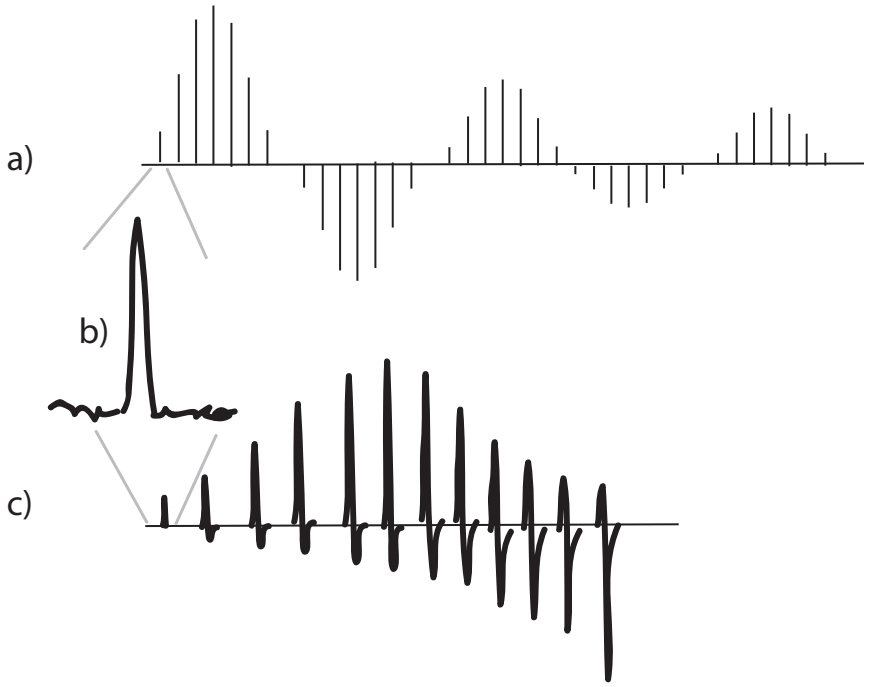

Figure 4.2: *a) The 90° and 180° time are calibrated using a one pulse experiment where the duration of the rf is arrayed. Stacking the data sets next to each other the 90° time can be read off as the peak with the most intensity while the 180 time is the where there is no signal. As the array is some what periodic it makes sense to compare the 90° time to the 450° and 810° to see how effective the probe is, that is how much power is lost using longer pulses. b) In order to read off the 90 time correctly the first spectra in the array needs to be phased such that the peak is all absorptive. c) Sometimes the ninety pulse is obscured by non-uniform excitation due to B_1 inhomogeneity. This will cause what looks like a phasing error in the nutation curve. This can be improved by signal averaging or by using a smaller sample.*

The cosine and sine modulated FID are:

$$S_c(t_1,t_2) = \cos(\Omega_1 t_1)\, e^{i\Omega_2 t_2} \tag{4.1}$$

$$S_s(t_1,t_2) = \sin(\Omega_1 t_1)\, e^{i\Omega_2 t_2} \tag{4.2}$$

These are double Fourier transformed to obtain the spectrum.

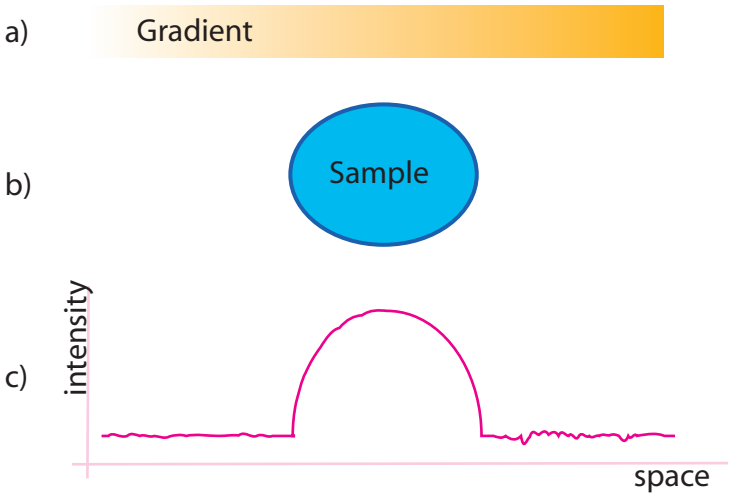

Figure 4.3: *a) To image an object a gradient magnetic field is used. b) The sample. c) The image.*

4.1.3 Imaging

One of the more powerful tools that has emerged from NMR is NMRI, nuclear magnetic resonance imaging, or more classically known as MRI as the word " nuclear" scares off patients. MRI works on the basic princle that the frequency of a spin is directly proportional to the magnetic field it senses. In this way a gradient can be added along one, two, or three axis in order to give a spatial dependence of the frequency. It is best if the gradient is much larger than any interaction in the sample. [3]

4.2 Other Pulse sequences

4.2.1 Hahn and Chemical Shift echo

The magnetic field may not be perfect or the ring down time of the coil maybe long. In this case, it is good to be able to refocus the magnetization. Field inhomogeneities are problematic in spectroscopy and imaging in that they obscure the useful information. The inhomogeneities

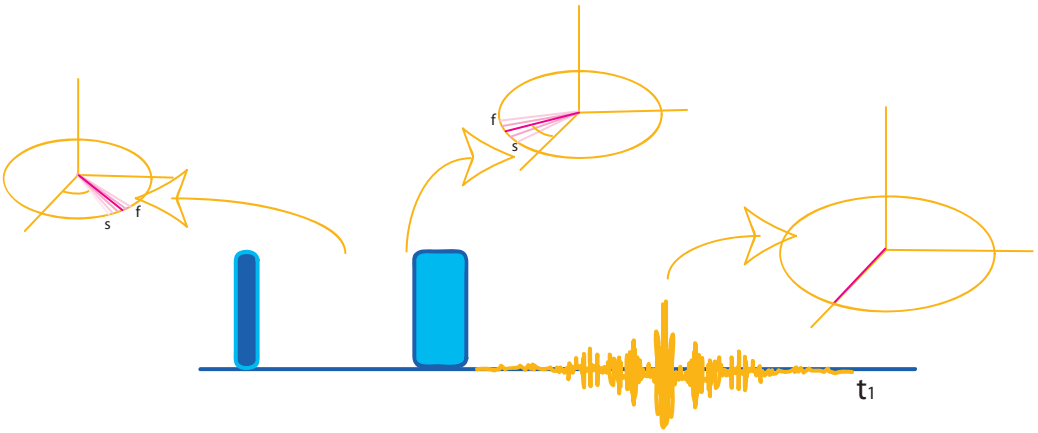

Figure 4.4: *A Hahn echo pulse diagram. Here s stands for"slow' spins while f is for 'fast'.*

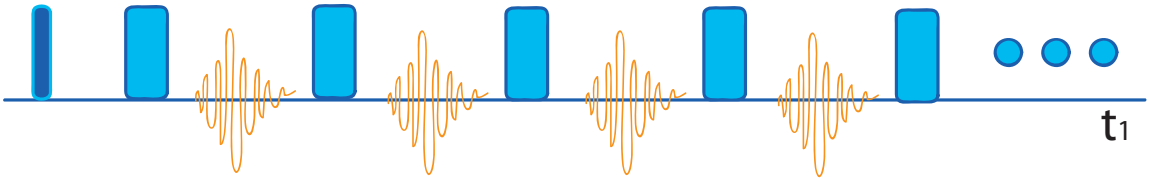

Figure 4.5: *CPMG pulse sequence*

broaden lines due to chemical shift's dependence on the magnetic field strength. A Hahn echo refocuses the broadening by effectively causing a time reversal. In figure 4.4 an echo sequence is shown. The magnetization is first tipped into the *xy* plane and then allowed to precess for some time, Δt. During this time the magnetization begins to spread out. Some of the magnetization precesses faster (designated 'fast') than the average and some slower (designated 'slow'). The magnetization then undergoes a 180 degree pulse. This flips it around the axis putting it back into the *xy* plane, however the fast and slow magnetization have now switched places. After an other time period of Δt the magnetization comes back to its original location as the fast magetization catches back up to the slow. Observation of this event appears as an echo. That is the FID grows and then decays.

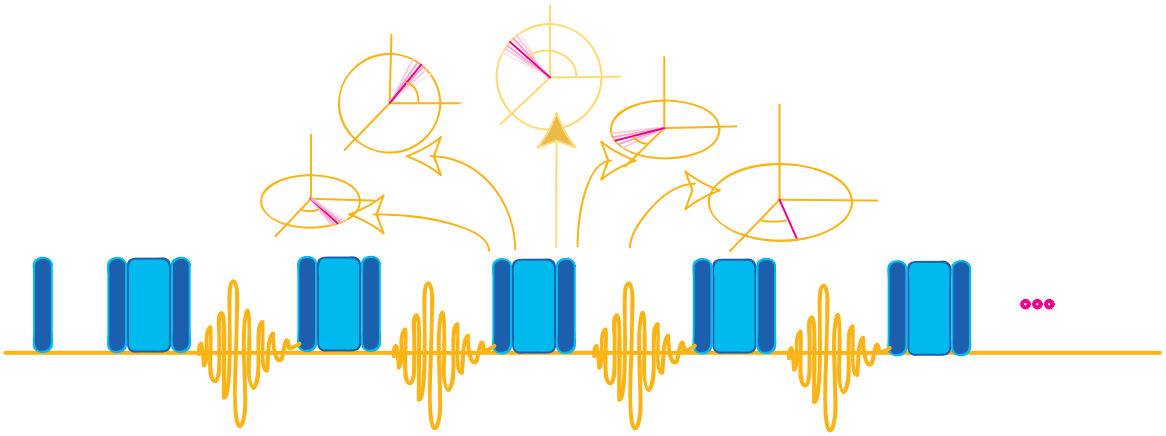

Figure 4.6: *Ex-situ z-rotation pulse sequence.*

4.2.2 CPMG

An extension of the Hahn echo is to repeat the echo and acquire an FID in between each pair of pulses. Then the echoes can be summed together to give the signal to noise of several experiments in the time of one. This can be processed by Fourier transforming with either the echo and doing zero and first order phasing, or by cutting off half of the FID and Fourier transforming that. The former makes reading off the center frequency of a particular site of interest difficult and nearly impossible if the carrier frequency is far off. Due to that, the experiments in Chapter 4 were done with CSechoes(chemical shift) instead of CPMGs. [3]

4.2.3 *Ex-situ*

If the magnetization is left to undergo free precession again after any of these pulses it will dephase. In this manner the broadening of the spectra is not really improved. To refocus and maintain that focus an experiment must be done point-by-point with several focusing pulses. [21] To obtain chemical shift the CPMG cannot be used as its echo peak amplitude set is just an exponential decay and will give no sine or cosine modulation. A point-by-point FID needs to be done in a special manner. These sequences, contains z-rotation pulses or

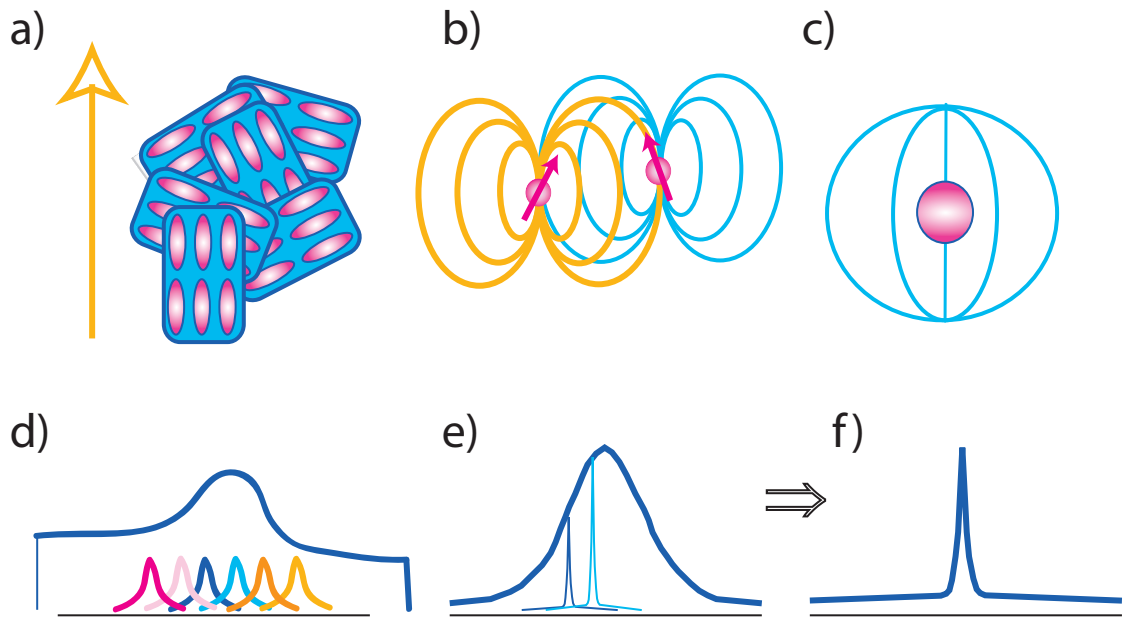

Figure 4.7: *a)Chemical shift anisotropy. b)Dipolar Coupling c) Magnetic Susceptibility d) Powder patterns arise from solid sample which have crystals with many orientations e) Other anisotropies cause broad lines. f) With MAS spinning the anisotropies are zeroed leaving only the Zeeman interaction, isotropic Chemical shift, and J-coupling.*

adiabatic double passages and have been done in previous work.(See Figure 4.6) [1]

4.2.4 MAS

In oriented samples, for example solids, the anisotropic part of the Hamiltonian is not averaged out by motional tumbling. [2] In these cases to obtain the isotropic spectra one must artificially average out the anisotropic Hamiltonian. Most common is to spin the sample faster than the anisotropy at 54.7 degrees, commonly called the magic angle. This is called magic angle spinning (MAS). Most anisotropic interactions under magic angle spinning average out to the isotropic spectra: chemical shift anisotropy, dipole dipole interactions, magnetic susceptibility, and first order quadrupole. These all take the form of a second order Lagrandre polynomial, $P_2 \cos\theta_R = 1/2\left(1 - 3cos^2\theta_R\right)$ as will be shown below.

The DD coupling, magnetic susceptibility, and quadrupole will all average out to zero under

MAS. The chemical shift anisotropy, figure 4.7 a), can be averaged out while still leaving the isotropic chemical shift spectra. The chemical shift anisotropy is an interaction based on the sample's orientation with the magnetic field. As the orientation of a crystal changes so does the chemical shift frequency. In this way a powder, or a powder sample with all single crystal orientations, will give a broad spectrum.(See Figure 4.7 d)) This broadening depends on the chemical shift tensor with the specific shape depending on the values of σ_{11}, σ_{22}, and σ_{33}.

The following examines the spherical tensor treatment of spinning a sample. The general Hamiltonian from section 2.5.3 is:

$$\mathscr{H}_{int} = \mathbf{A}(lab) \cdot \mathbf{T}(lab) = \sum_{k=0}^{2} \sum_{q=-k}^{+k} (-1)^q A_q^{(k)}(lab) T_{-q}^{(k)}(lab) \tag{4.3}$$

In MAS the system under goes a rotation, of frequency ω_R at the angle θ_R. In the lab frame this would be a difficult calculation; it is easier to convert the Hamiltonian to the rotor frame. Thereby it is easier to use the rotor's reference frame which is spinning using the rotation operator and its element's the Wigner matrices, as can be found in many standard text. [6, 22]

$$LAB - - - (\omega_R t, \theta_R, 0) - - - > ROTOR \tag{4.4}$$

This leaves the Hamiltonian in the form:

$$\mathscr{H}_{int} = \mathbf{A}(lab) \cdot \mathbf{T}(lab) = \sum_{k=0}^{2} \sum_{q=-k}^{+k} (-1)^q \left(\sum_{m=-k}^{+k} D_{mq}^{(k)}(-\omega_R t, \theta_R, 0) A_m^{(k)}(rotor) \right) T_{-q}^{(k)}(lab) \tag{4.5}$$

Substitution of the Wigner matrix elements,

$$D_{mq}^{(k)}(\alpha\beta\gamma) = e^{-i(m\alpha+q\gamma)} d_{mq}^{(k)}(\beta) \tag{4.6}$$

gives:

$$\mathscr{H}_{int} = \mathbf{A}(lab)\cdot\mathbf{T}(lab) = \sum_{k=0}^{2}\sum_{q=-k}^{+k}\sum_{m=-k}^{+k}(-1)^q e^{i(m\omega_R t)} d_{mq}^{(k)}(\theta_R) A_m^{(k)}(rotor) T_{-q}^{(k)}(lab) \tag{4.7}$$

The secular appromimation can be used here for systems with large magnetic fields, having large Zeeman interaction, the internal spin interaction can be neglected as they are small. Practically this means that q=0:

$$\mathscr{H}_{int} = \mathbf{A}(lab)\cdot\mathbf{T}(lab) = \sum_{k=0}^{2}\sum_{m=-k}^{+k} e^{i(m\omega_R t)} d_{m0}^{(k)}(\theta_R) A_m(k)(rotor) T_0^{(k)}(lab) = \mathscr{H}_{int}^{(0)} + \mathscr{H}_{int}^{(1)} + \mathscr{H}_{int}^{(2)} \tag{4.8}$$

The second order Hamiltonian is of particular interest. The zeroth order is the isotropic interaction and is zero for all the interactions but for the chemical shift. The first order will equal zero for all interactions. At this point $d_{m0}^{(k)}(\theta_R)$ and $T_0^{(k)}(lab)$ can be substituted in for specific interactions. After $A_m(k)(rotor)$ is averaged over a rotor period:

$$\overline{A_0^{(2)}(rotor)} = \frac{1}{T}\int_0^T dt A_0^{(2)}(rotor)(t) \tag{4.9}$$

All are averaged to 0 except for the d_{00} term, $1/2(3\cos\theta_R - 1)$. When θ_R is set to 54.74, this term is equal to zero and the anisotropies are averaged out. [22]

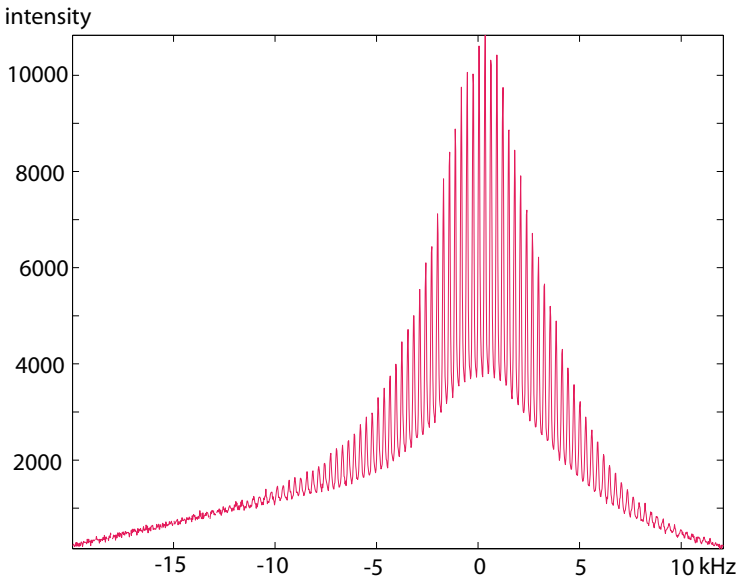

Figure 4.8: *A slow spinning, 250Hz, sample of water and beads. The anisotropy is cause by the magnetic susceptibility of the beads.*

4.2.5 MAT

When spinning slower than the anisotropy in a system, the spectrum no longer collapses to the isotropic spectrum, but has spinning side bands at the frequency of spinning.(See Figure 4.8) [23] The side band intensities are determined by the envelope of the static spectrum. Side-bands are usually undesired since the spectra can get very complex with them even if a few chemical shifts are involved. [24] A magic angle turing(MAT) pulse sequence is useful for dealing with spinning sidebands in two ways. First it can recover the isotropic spectrum from a slowly spinning sample and second it correlates the isotropic spectrum to the anisotropic spectrum.(See Figure 4.10. a))

MAT sequences work by having rotor synchronized pulses. The time of one rotor rotation is T.(See figure 4.9) To be rotor synchronized in the pulse sequence there are consistent (at the same time in each scan) pulses at 120 degree intervals of a rotor rotation period. Between those pulses are the incremented ones for the acquisition in the second dimension. For calculating the response the resonance frequency is considered a function of the position,$\gamma(t)$. As such

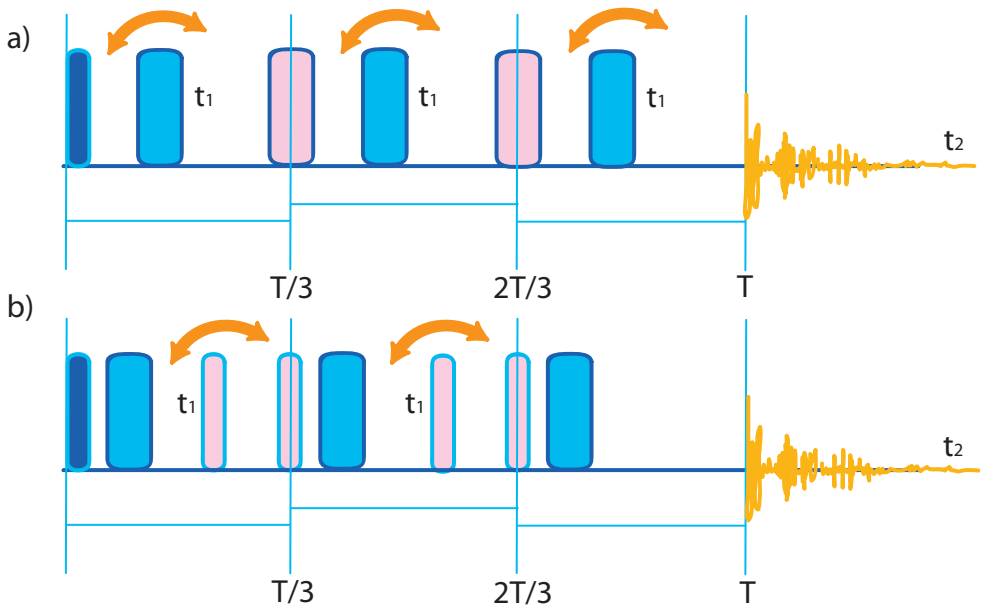

Figure 4.9: *MAT pulse sequences diagram. a) An early version of the MAT. [23] One 90° pulse is followed by five 180 pulses. Two of the pulses are rotor synchronized while the other three are time incremented to acquire the second dimension. b) A more robust MAT sequence dubbed the triple echo. For the p-MAT sequence this one is going to be used. Here there is a ninety excitation pulse followed by a series of 180° and 90° pulses. The 180° and two of the 90° pulses are rotor synchronized, while two of the 90° pulses are time incremented for acquiring the second dimension.*

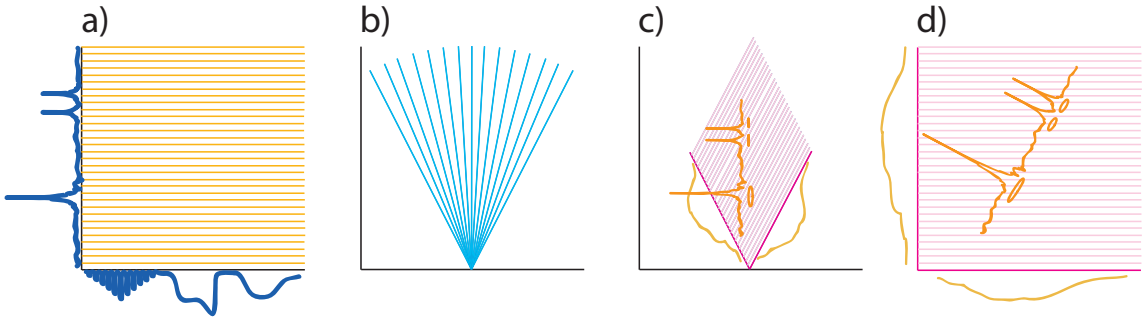

Figure 4.10: *a) An isotropic vs. anisotropic spectra taken incrementally by directly detecting the anisotropic and indirectly the isotropic. This can be considered as the full isotropic vs anisotropic 'space'. The anisotropy could be spinning sidebands, the full powder pattern, or an arbitrary anisotropy. This can be acquired with a pulse sequence like MAT. b) The isotropic vs. anisotropic spectra acquired through diagonals in the correlation 'space'. This is done in a VACSY experiment. Acquiring this way the entire isotropic vs anisotropic 'space' is only acquired if all angles are used. c) Incrementing time domain of one angle and detecting at a second a portion of the isotropic vs anisotropic 'space' is observed. This is the basic [rincple of the p-MAS pulse sequence. d) When processing the data acquired from a p-MAS sequence the data set will be square not rectangular. The isotropic spetra is not on either axis but on a shearing line.*

to calculate the full evolution the integral over the time period need to be taken. There are three periods of spin precession, Φ_i will be taken as the total angle of precession during the *i*th period. The total precession angle is the sum of the Φ_i:

$$\Phi_1 = \int_0^{t_1/3} \omega(\gamma(t))\, dt \tag{4.10}$$

$$\Phi_2 = \int_0^{T/3+t_1/3} \omega(\gamma(t))\, dt \tag{4.11}$$

$$\Phi_3 = \int_0^{2T/3+t_1/3} \omega(\gamma(t))\, dt \tag{4.12}$$

$$\Phi_1 + \Phi_2 + \Phi_3 = \int_0^{t_1/3} 3\omega_{iso} dt = \omega_{iso} t_1 \tag{4.13}$$

For a properly phased spectrum the MAT has to have a cosine and sine, e.g. $\cos(\Phi_1 + \Phi_2 + \Phi_3)$ and $\sin(\Phi_1 + \Phi_2 + \Phi_3)$. This is not as straightforward as phasing the receiver as there are three separate times, during $\Phi_1, \Phi_2, and \Phi_3$, which phase is accumulated. This means the three precession periods need to sum up to a sine or cosine modulated data set. In order to do that, four different scans need to be taken varying the phases of the three precession periods. [25, 26, 27]

$$\begin{aligned} cos(\phi_1+\phi_2+\phi_3) =& cos(\phi_1)cos(\phi_2)cos(\phi_3) && (4.14)\\ & - sin(\phi_1)sin(\phi_2)cos(\phi_3) && (4.15)\\ & - sin(\phi_1)cos(\phi_2)sin(\phi_3) && (4.16)\\ & - cos(\phi_1)sin(\phi_2)sin(\phi_3) && (4.17) \end{aligned}$$

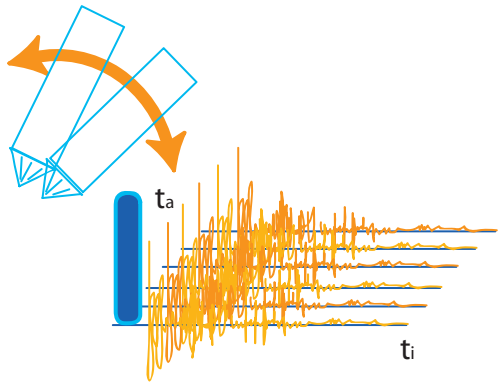

Figure 4.11: *VACSY pulse sequence. Each successive FID is taken at a different angle,* θ_R

$$sin(\phi_1+\phi_2+\phi_3) = sin(\phi_1)cos(\phi_2)cos(\phi_3) \quad (4.18)$$
$$+ cos(\phi_1)sin(\phi_2)cos(\phi_3) \quad (4.19)$$
$$+ cos(\phi_1)cos(\phi_2)sin(\phi_3) \quad (4.20)$$
$$- sin(\phi_1)sin(\phi_2)sin(\phi_3) \quad (4.21)$$

4.2.6 VACSY dynamic angle probe

VACSY (variable angle COSY), like MAT, also correlates the anisotropic spectrum to the isotropic spectrum. [28] In this experiment the time domain is not incremented, but the rotation angle is incremented with respect to the field.(See Figure 4.11) This experiment does a circular sweep of the isotropic correlated anisotropic spectrum 'space' instead of a vertical.(See Figure 4.10b)) [29] The VASCY experiment recovers the anisotropic spectrum from a sample that is rapidly spinning. The interaction Hamiltonian the spins are under going can be considered as the isotropic, $\mathscr{H}_{iso}$ plus the anisotropic,$\mathscr{H}_{aniso}$. Using the result from the MAS iteration of equation 4.7, the anisotropy is dependent on $P_2(\cos\theta_R)$. This means that a Hamiltonian can be written as:

$$\mathscr{H}_0(\theta_R) = \mathscr{H}_{iso} + P_2\cos(\theta_R)\mathscr{H}_{aniso} \quad (4.22)$$

It follows from this that the precession frequency is:

$$\omega \approx \omega_i + P_2 \cos(\theta_R) \cdot \omega_a(\theta, \phi) \tag{4.23}$$

Where ω_i is the isotropic chemical shift, ω_a the anisotropic chemical shift, and the Euler angles from the crystal's principle axis system to a fixed frame on the rotor, (θ, ϕ).

The signal from the experiment is:

$$S(\theta_R, t) = \int\int I(\omega_a, \omega_i) e^{i[\omega_a \cdot P_2(\cos\theta_R)t + \omega_i \cdot t]} \times d\omega_a d\omega_i \tag{4.24}$$

Where

$$I(\omega_a, \omega_i) = \int\int S(t_a, t_i) e^{-i(\omega_a \cdot t_a + \omega_i \cdot t_i)} dt_a dt_i \tag{4.25}$$

is the correlated spectrum. If

$$t_a = P_2(\cos\theta_R)\, t \tag{4.26}$$

and

$$t_i = t \tag{4.27}$$

are substituted into 4.24 then it is the signal for the correlated spectra. [28]

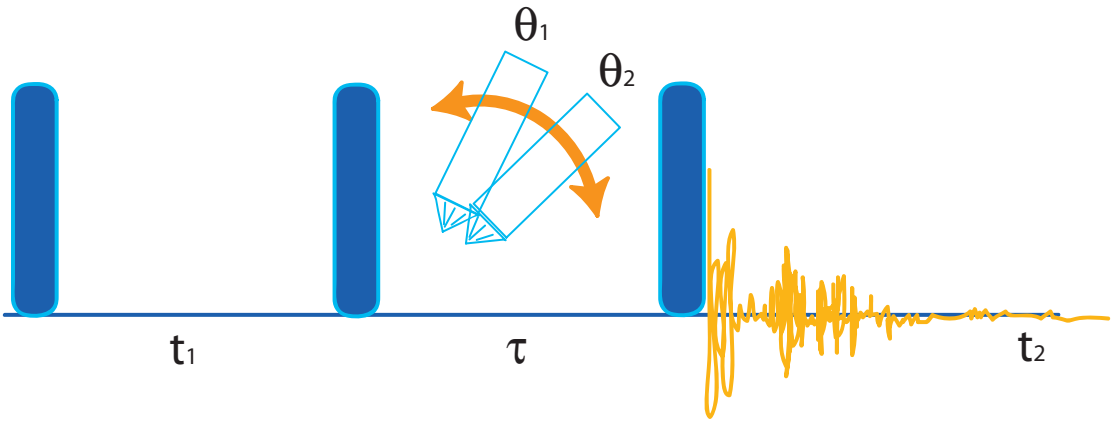

Figure 4.12: *A p-mas pulse diagram.*

$$S(t_a, t_i) = \int\int I(\omega_a, \omega_i)\, e^{i(\omega_a \cdot t_a + \omega_i \cdot t_i)} d\omega_a d\omega_i \tag{4.28}$$

4.2.7 p-MAS

Projected-magic angle spinning (p-MAS) is derived from the same idea which the VASCY pulse works on. Its motivation, similar to VACSY, is to recover information(isotropic spectrum) from samples which cannot be spun at the magic angle. The p-MAS instead of having to use all angles only needs two for isotropic spectrum recovery. [30] These experiments create the same data set as VACSY but incorporate a second time domain to do it. This is done by incrementing the time domain of one of the angles and collecting at the second as in Figure 4.12. A diamond shaped area of the isotropic anisotropic spectrum is carved out with the p-MAS experiment, figure 4.10 c), however the Fourier transformed data is still processed as a square spectra, 4.10 d). This means that the isotropic spectra appears on a shearing line and is scaled. The scaling factor λ is:

$$\lambda = \frac{P_2(cos\theta_{R1}) - P_2(cos\theta_{R2})}{P_2(cos\theta_{R1}) + P_2(cos\theta_{R2})} \tag{4.29}$$

4.2.8 p-MAT

It is conceivable to put the p-MAS and MAT pulse sequence together, dubbed p-MAT, to recover isotropic and anisotropic data from a slow spinning system and small angles. (See chapter 8)

Chapter 5

Rotating Field NMR: project motivation

5.1 Introduction

The next step in NMR technology is portability. A magnet, probe, and spectrometer that can be taken to the sample are currently being developed. With this instrument the sample does not need to be taken or placed into the magnet. This portability could be expressed in various ways. A magnet could be placed on a laboratory bench top where spectra could be taken from a beaker. An environmental scientist could take a portable device and take a reading from tree bark without removing a sample. The system may even be developed into a wall sized unit that could take an MRI of a person just standing in front of it. Such systems would have countless uses.

In designing a one-sided portable NMR system, it would be advantageous to be able to examine materials with anisotropies, and not just isotropic materials. While some anisotropies give additional useful information they also obscure useful information. Other material than

solids also have anisotropic couplings, for example tissue, rocks, foods, etc. The portable NMR system could be used to track changes in diseases. Recovering isotropic information is of particular interest to oil companies, in their samples magnetic susceptibilities obscure chemical shiftr in their oil spectra. In the food industry every product that leaves a factory could be quickly examined. The possibilities are really endless.

The standard way of achieving anisotropy removal is to spin the sample. (See Section 4.2.4) With a portable system spinning the sample is counter to the purpose of a noninvasive system. However, the sample can remain undisturbed if there is a spinning magnetic field created. However the physical requirements for building such a field spinning apparatus kept it from being a common technique. The first field spinning experiment was complete in 2002. [31] This showed a reduction in spectral line width of Xe. However, a field spinning experiment that reveals chemical shift has still not been done.

5.2 Rotating Magnet

In order to successfully conduct a rotating field experiment, an apparatus would have to be developed that creates a spinning magnetic field. Construction of such a device can be difficult. In previous work the rotating field was created with 3 orthogonal coils. [31] These experiments showed linewidth improvements but were unable to show chemical shift since the fields that were created were too weak, however, electrical coils and permanent magnets could create the necessary field strength.

5.2.1 Magnet parts

Electrocoil and permanent magnets both have their advantages and disadvantages. Electrocoil magnets can be made stronger with either high currents or a small wrapped radius. Strong

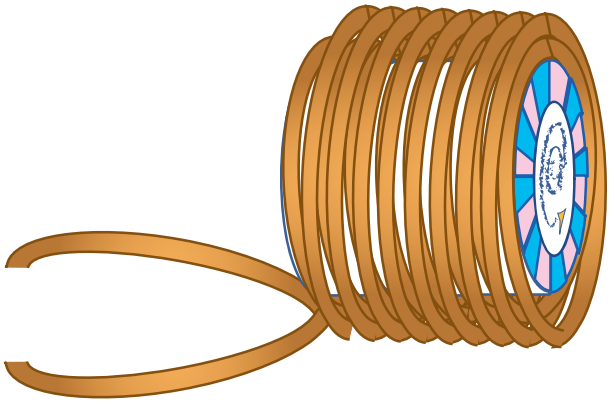

Figure 5.1: *The permanent magnet inside of the electrocoil. The field strength of the permanent magnet is 0.5T with a proton frequency of 21.4 MHz. The magic angle would be when the electrocoil produced a field of 0.35T giving a total field of 0.62T and a proton frequency of 26.2MHz*

currents have the disadvantage of needing expensive power generators, current stabilizers, and consequently cause high electricity bills. A smaller radius can also be problematic in that the sample size is then restricted. Permanent magnets, however, give strong fields on their own, and have no associated operation expenses. They need to be carefully constructed to obtain a homogeneous field. An additional disadvantage is that permanent magnets suffer from the drift effects of temperature. (Discussed in further detail below.) The strength of the magnetic field will change depending on the temperature of the magnet. This is because the over all magnetic field arises from the magnetic moments of the material of which it is made. The magnetic moment's alignment has a Boltzmann distribution and thus changes in temperature changes cause small changes in the field strength.

5.2.2 Magic Angle

One of the challenging parts of rotating magnets is to set the magic angle. If a solely permanent magnet system is used, adjusting the field to the magic angle would take a complex mechanical setup that is hard to design, construct, and use. However, the permanent magnet is advantageous relative to an electromagnet method because it requires less power and is cheaper. The

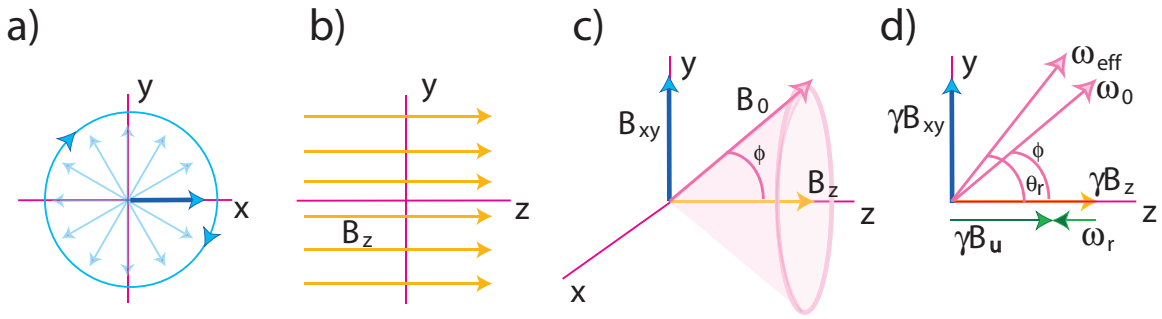

Figure 5.2: *a) A magnet field which rotates in the xy plane (from the permanent magnet in the built system). This field is mechanically rotated. b) A second magnetic field perpendicular, along the z axis, to the first field, (from the electrocoil in the built system). c) The field in the xy plane and z axis add together to make a field at an angle ϕ from the z axis. When the field in the xy plane rotates the sum of the two field carves out a cone, making a rotating field. d) Diagram defining the relevant angles and frequencies.*

permanent magnet system could be set to the magic angle by having a single magnet at the magic angle, relative to the axis of rotation, and developing a way to rotate it properly. This method would require a way to fine tune the angle at which it spins. An alternative would be to use more than one permanent magnet. One magnet could rotate while a second stationary magnet produces a perpendicular field. The sum of the two fields could be used to obtain the magic angle.(See Figure 5.2.) However this system would also be difficult to adjust.

The compromise between these problems for a rotating field experiments is a permanent Halbach array with an electrocoil wrapped around it. This system was physically built and tested. The permanent magnet mechanically is rotated with a motor while the electrocoil produces a perpendicular permanent fields as in figure 5.1. The Halbach's magnetic field is designated to be in the *xy* plane and the electrocoil's is on the *z* axis, figure 5.2. As the electrocoil is turned on the direction of the sum of the two field gradually approaches to the magic angle. At this point the permanent magnet can be spun to remove anisotropies. One of the advantages of having a system in which any angle between zero and the magic angle can be achieved is that an experiment with any angle could be performed.

Since there is great difficulty involved in achieving the magic angle it may be advantageous

to find a way around it. For example, using a pulse sequence like p-MAS would remove the need to be at the magic angle. This greatly reduces the operating expense since energy requirement levels are reduced.

5.2.3 Spinning the magnet

The achievable rate of rotaion for the rotating field also needs to be considered. Speed can be controlled by either changing the current in an electrocoil system or mechanically rotating a permanent magnet though neither can compete with a rotor which can spin up to 80kHz. For the built system the permantent magnet is spun. Where as in the first experiments the current in electrocoils were changed. [31] However if the magnet field is spun slowly then spinning side bands arise. This is a perfect use for an MAT sequence! A MAT sequence, see section 4.2.5, recovers the isotropic spectra from in slow spining conditions.

5.3 Theory

Rotating the magnetic field is essentially equivalent to rotating the sample, which means that they can be mathematically treated the same as long as the adiabatic condition is maintained. In an adiabatic system the nuclear spins' alignment is able to follow the movement of the field. This is obeyed as long as the field rotates much more slowly than the Larmor frequency. If the rotation speed approaches the Larmor frequency the response of the system becomes difficult to predict. As the Larmor frequency for the built system is 21.4 MHz and the permanent magnet's motor's mechanical rotation speed maximum cannot exceed 50Hz, the adiabatic condition is kept.

In this magnet set up the rotating magnetic field is in the *xy* plane while a permanent field is placed on the *z* axis. The magnetic field would then be [32]:

$$B(t) = B_{xy}\left[\cos(\omega_r t)\,\hat{i} + \sin(\omega_r t)\,\hat{j}\right] + B_z\hat{k} \tag{5.1}$$

Then the Hamiltonian for this magnetic field, using $\mathscr{H} = \gamma\mathbf{IB}$, is:

$$\mathscr{H} = \gamma B_{xy}\left[\cos(\omega_r t)\,\mathbf{I}_x + \sin(\omega_r t)\,\mathbf{I}_y\right] + \gamma B_z\mathbf{I}_z \tag{5.2}$$

The general tensor interaction, using λ to designate a specific interaction, Hamiltonian (equation 2.6)is:

$$\mathscr{H}_\lambda = \sum_{k=0}^{2}\sum_{q=-k}^{k}(-1)^q A_{k,q}^{\lambda}\mathbf{T}_{k,-q} \tag{5.3}$$

As in MAS(Section 4.2.4) a change in coordinates to the rotation frame is needed. This constitutes two transformations for this system, $V_1(t) = e^{i\omega_r t\mathbf{I}_z}$, to the interaction rotating frame and $V_2(t) = e^{i\theta\mathbf{I}_y}$, with $\theta = \arctan\frac{\gamma B_{xy}}{\gamma B_z - \omega_r}$, into the tilted frame. Then the above Hamiltonian, equation 5.2, will be diagonal and time independent:

$$\mathscr{H}_2 = V_2V_1(t)\,\mathscr{H})t)V_1^{-1}V_2^{-1} = \omega_{eff}\mathbf{I}_z \tag{5.4}$$

The effective Larmor frequency becomes:

$$\omega_{eff} = \sqrt{(\gamma B_z - \omega_r)^2 + (\gamma B_{xy})^2} \tag{5.5}$$

The transformations, V_1 and V_2, for the anisotropic interaction are then:

$$\mathscr{H}_{int} = \mathbf{A}(lab)\cdot\mathbf{T}(lab) = \sum_{k=0}^{2}\sum_{q=-k}^{+k}(-1)^q\left(\sum_{m=-k}^{+k}D_{mq}^{(k)}\left(-\omega_R t,\theta_R,-\omega_{eff}\right)A_m^{(k)}(rotation)\right)T_{-q}^{(k)}(lab) \tag{5.6}$$

Substitution of the Wigner Matrix elements,

$$D_{mq}^{(k)}\left(-\omega_R,\theta_R,-\omega_{eff}t\right) = e^{-i\left(m\omega_R+q\omega_{eff}\right)}d_{mq}^{(k)}(\theta_R) \tag{5.7}$$

gives:

$$\mathscr{H}_{int} = \mathbf{A}(lab)\cdot\mathbf{T}(lab) = \sum_{k=0}^{2}\sum_{q=-k}^{+k}\sum_{m=-k}^{+k}(-1)^q e^{\left(-im\omega_R+q\omega_{eff}\right)}d_{mq}^{(k)}(\theta_R)A_m^{(k)}(rotation)T_{-q}^{(k)}(lab) \tag{5.8}$$

Using the secular approximation this becomes

$$\mathscr{H}_{int} = \mathbf{A}(lab)\cdot\mathbf{T}(lab) = \sum_{k=0}^{2}\sum_{m=-k}^{+k}e^{-im\omega_R}d_{m0}^{(k)}(\theta_R)A_m^{(k)}(rotation)T_0^{(k)}(lab) \tag{5.9}$$

which is the same as equation 4.8 and can be treated in exactly the same way. This means when the field rotates at the magic angle the anisotropies will average out. [22, 32]

5.3.1 Magnet drift

One of the problems in using a permanent magnet is the field dependence on temperature. A small, even ppm, fluctuation in the main field's frequency will cause the spectra to broaden. In the above Halbach array the drift over several hours approaches 200ppm, though over 30 min

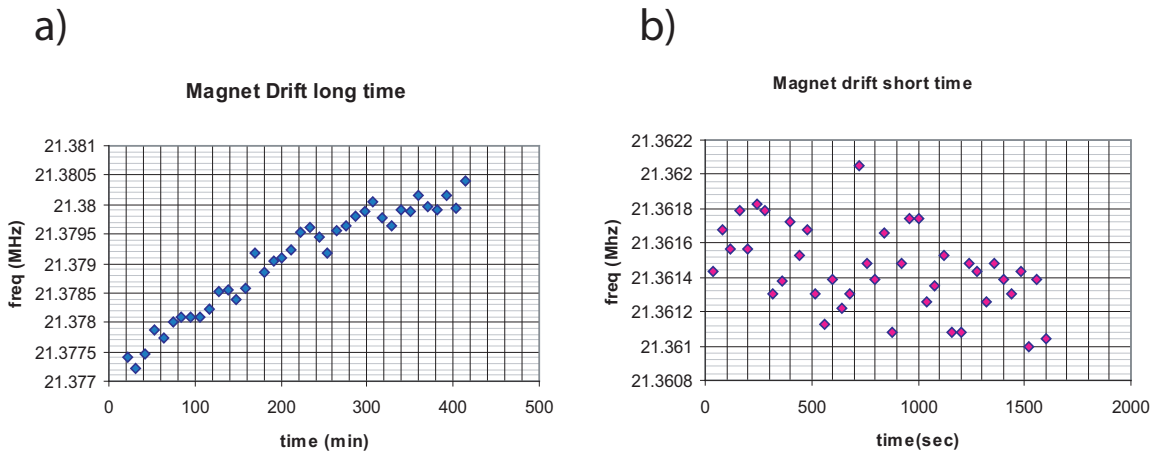

Figure 5.3: *a)The permanent magnet's drift over several hours. b) the permanent magnet's drift over an hour*

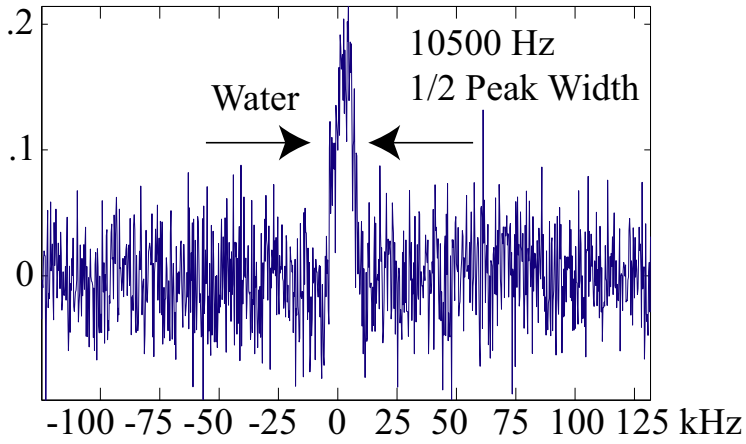

Figure 5.4: *A spectrum of water from the permanent magnet. The peak width is unsuitable for spectroscopy even for species with large chemical shift.*

the drift is much smaller at 50ppm, as shown in figure 5.3. The magnet was found to be most stable after sunset because the outside temperature would has smaller fluctuations.

5.3.2 Permanent field inhomogenieties and Electrocoil inhomogenieties

The biggest problem with a permanent magnet or electrocoil system is dealing with the field inhomogenieties. The rotating field's permanent magnet had inhomogenieties of upwards 500ppm even while using a micro coil to minimize inhomogenieties. In the better regions

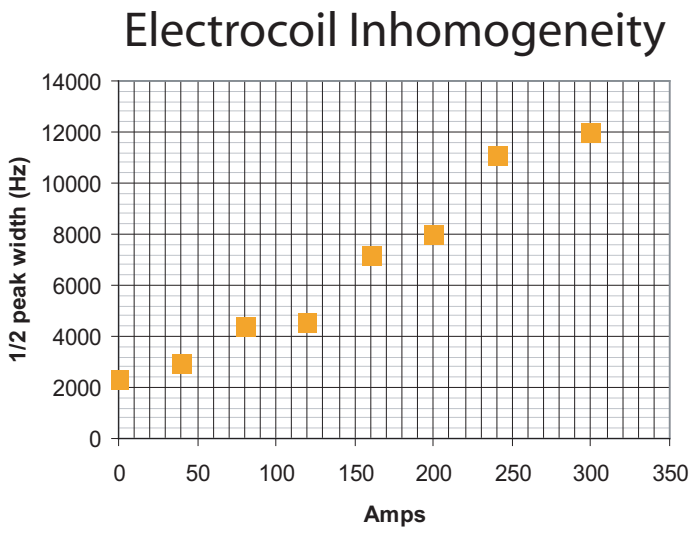

Figure 5.5: *After shimming the permanent magnet the electrocoil ruins the better field homogeneity. At levels far below the magic angle the inhomogenieties are upward of 10,000 Hz.*

of the magnet 40ppm inhomogenieties were easily seen. In the sweet spot, the most homogeneous spot, the inhomogeniety was 20ppm. One can conceivably shim the system using a shim stack that rotates with the magnet.(See chapter 6) [33] This was accomplished for the magnet however the rotating field experiment was hindered by the inhomogenieties of the electrocoil. After shimming the permanent magnet to achieve a 6 to 9 fold homogeneity improvement the electromagnet reintroduced inhomogenieties of at least 400ppm at about $1/2$ the current required to achieve the magic angle.

5.3.3 Suggested experiments

Though a full rotating experiment cannot be done with the described electrocoil inhomogenieties, it is conceivable to do a two-dimensional anisotropy average for a proof of principle experiment. Here the anisotropy would need to be only two-dimensional. This could be in a sample with long rods such as carbon nanotubes or fibers. This experiment is still technically difficult since the probe's coil need to be at the axis of rotation. As the permanent magnet

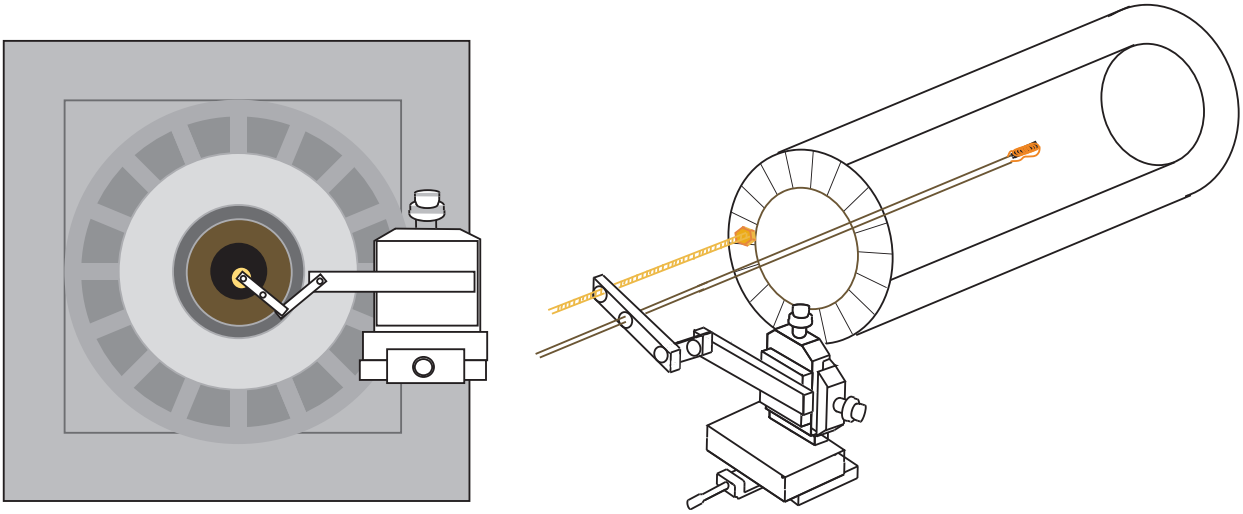

Figure 5.6: *Possible way to rotate probe with the permanent magnet. The probe is attached to the rotating permanent magnet in some sort of slip system where the probe's coil is always oriented in the same direction in the lab frame. The probe is held to the positioning system by a lever arm which can be set rigidly to the same position when the magnet is not spinning.*

rotates different magnetic field stregth rotating into the probe's coil causing the spins to evolve under the different magnetic strengths which produces broader spectrum than when there is no rotation. Therefore, even if a chemical shift can be observed on a static field it maybe obscured by the inhomogenieties of rotation. A solution to this may be to rotate the probe's coil along with the magnet, while keeping the orientation of the probe's coil fix in the lab frame. This would require a special mechanical system as suggested in figure 5.6

Chapter 6

Multipole Shimming of Permanent Magnets Using Harmonic Corrector Ring

6.1 Introduction

Magnet shimming is an essential part of NMR spectroscopy. Removing inhomogeneities arising from magnet design and construction should be done to the best extent possible in order to improve resolution of spectroscopic peaks. If left uncorrected, field inhomogeneities obscure the chemical shielding information needed to provide structural detail. This is particularly relevant when designing a portable NMR apparatus. These small scale magnets are fabricated using a small number of permanent magnet (PM) blocks or coils. The resulting field is highly inhomogeneous by NMR standards. Based on our experience, a 16-element Halbach array designed to create a dipole field can easily exhibit inhomogeneities upwards of 500 parts per million (ppm) over cubic millimeter volumes, which is unacceptable for high-resolution spec-

troscopy. Though more homogeneous arrays have been created showing inhomogeneities of 100 ppm and even as low as 20 ppm [34, 35] there is still a need for shimming systems.

Magnetic fields, and consequently their inhomogeneities, obey Maxwell's equations. Therefore, a shimming scheme capable of producing an arbitrary 3-D perturbation field can in principle null, that is cancel out, any conceivable preexisting inhomogeneity. The standard method of shimming an NMR magnet utilizes an expansion of the magnetic field in spherical harmonics. Since the magnetic scalar potential obeys the Laplace equation $\nabla^2\Phi_M = 0$ and the magnetic field is the gradient of this potential $\mathbf{H} = -\nabla\Phi_M$, differentiation of the Laplace equation reveals that each component of the magnetic field also obeys the Laplace equation. In particular, $\nabla^2 H_z = 0$. This permits an expansion of the field in terms of spherical harmonics [12]:

$$\begin{aligned} H_z(\mathbf{r}) - H_z(0) = &\sum_{l=1}^{\infty}\left(\frac{4\pi}{2l+1}\right)^{1/2} r^l \sum_{m=-l}^{+l} a_{lm}Y_{lm}(\Theta,\Phi) \\ =&a_{10}z - \Re a_{11}\sqrt{2}x + \Im a_{11}\sqrt{2}y \\ &+ a_{20}\frac{2z^2-r^2}{2} + \Re a_{22}\sqrt{\frac{3}{2}}(x^2-y^2) \\ &+ \sqrt{6}(\Im a_{21}yz - \Re a_{21}xz - \Im a_{22}xy) + \ldots \end{aligned} \tag{6.1}$$

where $a_{l,-m} = (-1)^m a^*_{lm}$, thus making the field real-valued. Because H_z is much larger than the transverse components, H_x or H_y, they are truncated by H_z and therefore negligible. Hence, to a good approximation, H_z determines the Larmor frequency. The task of the shimming system is to vary the currents in shim coils, which amounts to varying the coefficients $\Re a_{lm}$ or $\Im a_{lm}$.

Similarly, spherical harmonics can be used when the shims are Halbach-type arrays instead of coils, however the solution and execution are of slightly different form. Halbach-type arrangements can provide one-sided fluxes which show a remarkable degree of uniformity inside a ring and nearly zero flux outside [36]. This means the usable shimming field can be relatively large; in fact, almost as large as the shimming aperture itself. Additionally, the absence of

flux outside the aperture does not perturb the magnet creating the external field. While shim coils can achieve considerable homogeneity over the bore Halbach-type shimming can have its advantages in smaller systems. When designing small scale portable magnets with small bores, it is crucial that the shimming system does not occupy too much space inside the bore of the magnet, as this would severely limit the usable region. For such systems, a Halbach-type arrangement of permantent magnets can yield gradient field strengths strong enough for shimming purposes and still be compact, thus leaving enough room for experiments. Furthermore, Halbach arrays eliminate the need for a power supply, which can be important in portable ex-situ and rotating field type systems. Fulfilling the need for shimming systems suited for rotating field NMR systems [37, 38] would be technically challenging in connecting and controlling electro-coil shims as the shimming coils would need to rotate with the field. However permanent magnets supply a perfect solution as they have no leads which would tangle as the bore rotates.

To overcome difficulties, in the contexts of portable and/or rotating field NMR systems, a “one shot" shimming system where one maps the field and compensates for each order of inhomogeneity in the field is presented in this chapter. Shimming with this method can be done previous to an experiment, using field mapping, or it can be done only once, as part of the magnet design phase.

The novelty of our method lies in its use of harmonic corrector rings [39] which are rings composed of concentric permanent magnet rods (magnetic dipoles) whose overall and relative orientations can be used to adjust the field strength, orientation, and multipole order. In our case, the rods are substituted by adjacent pairs of small disc permanent magnets (PMs) which approximate magnetic dipoles. This chapter demonstrates the method’s implementation in generating quadrupolar fields to correct inhomogeneities. Any number of additional rings can be added to correct arbitrary multipole orders simultaneously.

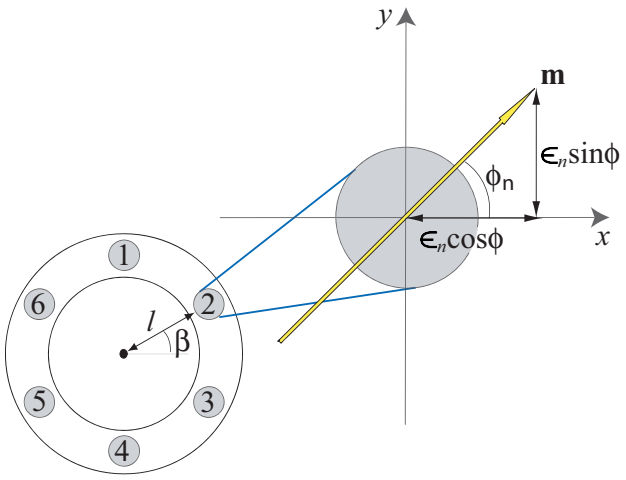

Figure 6.1: *The magnets 1 to 6 have β_n values* $(2n-1)\pi/6$.

6.2 Theory

6.2.1 General multipole correction

Magnets can be arranged in a ring to produce a field of a chosen order, N, by selecting their overall and relative orientations to each other. Assembled this way they can be used to correct for an inhomogeneity in an already existing magnetic field. In order to null a multipole term of order N, using a single ring of equally spaced magnets as in Figure 6.1, the orientation of the nth magnet is given by [39]:

$$\phi_n = (N+1)\beta_n + \phi_{init} \tag{6.2}$$

where n can be 1 to n(the number of magnets), β_n is the angle of the location of the nth magnet on the ring and ϕ_{init} is an angle defined by the orientation of the required multipole, both with respect to the x-axis. In general, the magnetic dipole moment of the nth magnet is given by $\mathbf{m}_n = \varepsilon_n(\cos\phi_n, \sin\phi_n, 0)$, where ε_n is the magnitude of the dipole moment. The latter is related to the dimensions of the magnet according to the volume integral of the magnetization

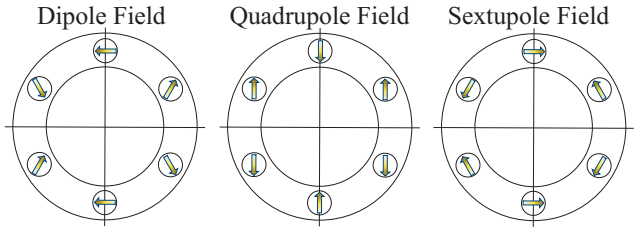

Figure 6.2: *A ring of 6 magnets oriented to produce a dipole, quadrupole, and sextupole field. These orientations are based on Equation 6.2. The quadrupole arrangement can be used to null a gradient in a strong magnetic field; to control the strength of the gradient, additional rings are necessary.*

or remanent field $\varepsilon_n = \|_V \int \mathbf{M}(\mathbf{r}) d^3\mathbf{r}\|$.

Figure 6.2 shows a ring of six magnets oriented to produce dipolar, quadrupolar and sextupolar magnetic fields in this manner.

6.2.2 Quadrupolar correction

Our analysis will concentrate on the quadrupolar case, though extension to higher orders is straightforward (See Section 6.6.1). In this case, $N = 2$ and ϕ_{init} is the orientation of the H_x component of the quadrupole. Using β_n values defined for a six-magnet ring in Figure 6.1 and applying these values to Equation 6.2, gives:

$$\phi_o = \phi_e + \pi = \phi_{init} + \frac{3\pi}{2} \tag{6.3}$$

where ϕ_o is the orientation of odd-numbered magnets and ϕ_e is the orientation of the even-numbered magnets. Thus, going round the circle, the orientation of neighboring magnets differs by π. In order to control the magnitude and orientation of the quadrupole, the contribution of each magnet and magnet ring to the overall magnetic field was analyzed.

If the dimensions of a magnet are small in comparison to the distance to a point, **r**, at which

a field measurement is being made, then the magnet can be approximated as a point dipole. The magnetic field of a point dipole at **r**, the position vector of the measurement point relative to the position of the dipole, is given by:

$$\mathbf{H}(\mathbf{r}) = \frac{1}{4\pi r^3}\left[3(\mathbf{m}\cdot\hat{\mathbf{r}})\hat{\mathbf{r}} - \mathbf{m}\right] \tag{6.4}$$

where $\mathbf{H} \equiv (H_x, H_y, H_z)$ is the magnetic field at **r**, the position vector of the measurement point relative to the position of the dipole. Differentiation of this expression with respect to **r** gives the field gradient due to the point dipole:

$$\nabla\mathbf{H} \equiv \frac{d\mathbf{H}}{d\mathbf{r}} = \frac{3}{4\pi r^4}\left[\mathbf{m}\hat{\mathbf{r}} + \hat{\mathbf{r}}\mathbf{m} + (\mathbf{m}\cdot\hat{\mathbf{r}})\mathbf{I} - 5(\mathbf{m}\cdot\hat{\mathbf{r}})(\hat{\mathbf{r}}\hat{\mathbf{r}})\right] \tag{6.5}$$

where **I** is the identity tensor and the notation **uv** indicates a tensor (dyadic) product of **u** and **v**.

In our experiments, the *x* axis was designated as main magnetic field direction, while the *z* direction was along the longitudinal axis of the magnet bore. Truncation of H_y and H_z, as described in the introduction, means that the relevant tensor component for our experiments is $\nabla H_x \equiv dH_x/d\mathbf{r}$.

The analysis is now restrict to points along the *z* axis, as shown in Figure 6.3a), where *r*, the magnitude of **r**, is the same for all magnets on a given ring. It is also assumed that the value for the magnet strength, ε_n, is the same for all magnets. In the case of a single ring of six magnets, the gradient of H_x is given by substitution of the values of **m** and **r** from Table 6.1 into Equation 6.5:

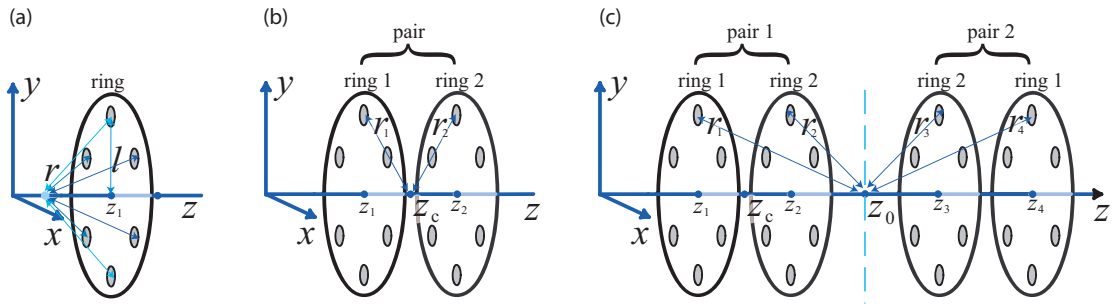

Figure 6.3: *Spatial arrangement of the ring pairs. The analysis is limited to points along the z-axis, which runs through the center of the two ring pairs. (a) Single ring of magnets: each of the six magnets are the same distance from the z axis and to the point* **r** *of interest. (b) Two corrector rings: on each ring the distance to the z axis is equal, but the magnets on each ring have a different distance to the point of interest* **r** *except at the center point* z_c*, where the distances are equal. (c) Four corrector rings or two pairs of corrector rings: the magnets on ring 1 have the same angles as ring 4 and so do the magnets on rings 2 and 3, thus making the system symmetric.*

Table 6.1: The position and magnetic dipole moment vectors for the magnets shown in Figure 6.1. The ring is determined by the index on z.

	$\mathbf{r}$			$\mathbf{m}/\varepsilon$		
	r_x	r_y	r_z	m_x	m_y	m_z
1	0	$-l$	$-z_i$	$\cos\theta$	$\sin\theta$	0
2	$-\sqrt{3}l/2$	$-l/2$	$-z_i$	$\cos(\theta+\pi)$	$\sin(\theta+\pi)$	0
3	$-\sqrt{3}l/2$	$l/2$	$-z_i$	$\cos\theta$	$\sin\theta$	0
4	0	l	$-z_i$	$\cos(\theta+\pi)$	$\sin(\theta+\pi)$	0
5	$\sqrt{3}l/2$	$l/2$	$-z_i$	$\cos\theta$	$\sin\theta$	0
6	$\sqrt{3}l/2$	$-l/2$	$-z_i$	$\cos(\theta+\pi)$	$\sin(\theta+\pi)$	0

$$\frac{dH_x}{d\mathbf{r}} = -\frac{45\varepsilon_n}{8\pi}\frac{l^3}{r^7}\begin{pmatrix} \sin\phi_o \\ \cos\phi_o \\ 0 \end{pmatrix} \tag{6.6}$$

where l is the radius of the ring of dipoles. Thus a single ring of magnets enables control of the orientation but not the magnitude of the field gradient. To null a quadrupolar term of arbitrary magnitude, a second corrector ring is required (Figure 6.3 b). The gradient is given by the sum of the contributions from each ring,

$$\frac{dH_x}{d\mathbf{r}} = -\frac{45\varepsilon_n}{8\pi}l^3\left[\frac{1}{r_1^7}\begin{pmatrix} \sin\phi_{o1} \\ \cos\phi_{o1} \\ 0 \end{pmatrix} + \frac{1}{r_2^7}\begin{pmatrix} \sin\phi_{o2} \\ \cos\phi_{o2} \\ 0 \end{pmatrix}\right] \tag{6.7}$$

where r_i (i = 1,2) is the distance from the magnets on the ith ring to the point of interest and ϕ_{oi} is the value of odd numbered magnets for the ith ring.

A small limitation to consider when choosing the strength of magnets used for shimming was found. The gradient has l^3/r^7 dependence. Thus a probe having a finite length in the z dimension will experience a variation in $dH_x/d\mathbf{r}$, even if centered at Z_c, the center point between two paired rings. This new inhomogeneity can be minimized by making r as large as possible. Hence, the probe's coil must be centered away from Z_c, though this reduces the overall magnitude of gradient that can be produced by the ring pair. The situation is improved with the incorporation of an identical second ring pair symmetrically opposite to the first, as shown in Figure 6.3 c). This doubles the available gradient magnitude, whilst further reducing the z-dependence of the H_x gradient. The field gradient at Z_0, the point between the two ring pairs is then simply twice Equation 6.7.

The ideal case for this system is one where the magnets in Ring 1 and 2 would literally occupy the same space. In this case our rings would be capable of correcting for any field error within the PMs strength in *xy* up to order 5. It should be noted that Equation 6.7 implies that there is a minimum gradient magnitude that a given ring pair can correct for. This occurs when $\phi_{o1} = \phi_{o2} + \pi$. To obtain lower magnitude gradients r must be increased by separating the two ring pairs along the *z*-axis or PMs of smaller strength should be used.

Nulling higher order harmonics can also be done using this system along with using multiple sets of shimming rings for simultaneously nulling multiple orders of harmonics. The corrections for second order and third order inhomogeneities are provided in Section 6.6.1. The PM shims can in principle be used to reduce a *z* gradient simultaneously with an *xy* plane gradient through a vectorial superposition of magnet orientations which would individually null the errors in the *xy* plane and *z* axis.

6.3 Methods

The magnet is a 16-element NdFeB Halbach array as shown in Figure 6.4. The elements are arrayed in four layers to produce a dipole field. The array has a mass of approximately 5 kg with an outer diameter of 100 mm and a usable bore diameter of 41 mm. The resulting field strength was 0.5 T, or a proton resonance frequency of 21.4 MHz.

Typical inhomogeneities over a volume of 0.1 mm^3 at the center of the magnet, are approximately 10,500 Hz (450 ppm)(see Figure 6.7 c). Two types of magnetic inhomogeneities can arise in a magnetic system. One, those produced by the inherent discretization and symmetries of the magnet design. Two, those due to the accuracy of design execution and level of tolerace in fabrication. The magnet described above was designed to have an intrinsic inhomogeneity limit of 20 ppm in a field region of 1 mm^3. The homogeneity was not achieved due to the

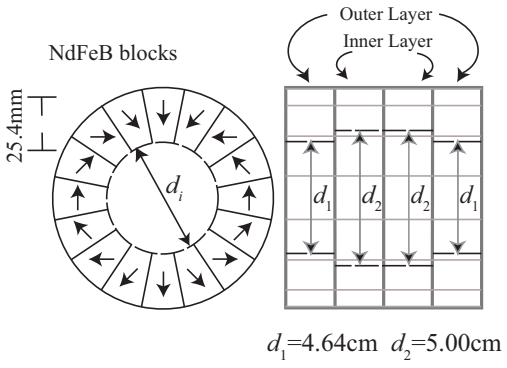

Figure 6.4: *The Halbach array, with four rings having 16 NbFeB elements oriented into a dipole configuration. The outer layers have a radius of 23.2 mm while the inner layers have a radius of 25.0 mm. The strength of the permanent magnet dipole field is about 0.5 T (proton resonance frequency approx. 21.4 MHz*

pieces in the Halbach array not having perfectly matched fields, and not being placed perfectly together. Basically the limitation is the in the precision of construction. However, even at the 20 ppm level of homogeneity the field would still benefit from shimming. A third broadening specific in NMR is the field drift, which is discussed at more length in section 6.4.2.

The shimming experiments were performed on water and fluorinated compounds using a Chemagnetics Infinity 400 spectrometer. Due to the significant inhomogeneity in the field, and to bypass the probe coil ring down time, a single spin echo readout was used to measure the center frequency and linewidth of the peak.

Field measurements, for the first attempts made at mapping the field see section 6.6.2, were made using a home built probe which consisted of a solenoidal microcoil of length 2 mm and inner diameter 350 μm, using copper wire of width 50 μm, wrapped around a capillary tube of outer diameter 350 μm and inner diameter 250 μm. It was a single resonance probe with the tuning circuit located out side of the magnet. This allowed the coil to be on a thin rod which could be moved via a positioning system for accurate field mapping (See Figure 6.6). The tube was filled with $MnCl_2$ doped water, to keep the T_1 relaxation time under 1 second in order to speed up the acquisition time typically to under 2 minutes.

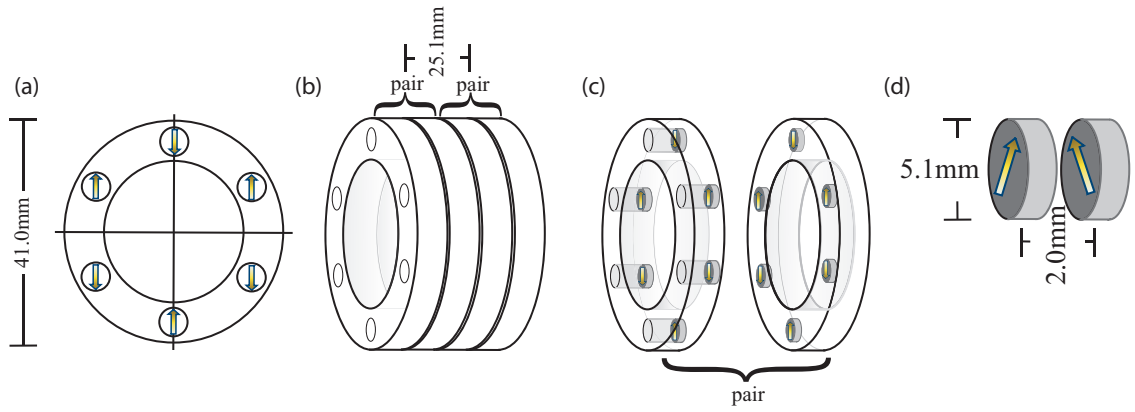

Figure 6.5: *(a)A face-on view of a single shim ring. Within each ring the PM are equally spaced at angles separated by 60 degrees around the diameter. (b) The two pairs of shims rings used to null a field. The casings for the permanent magnets are white Delrin. The center-to-center of each pair is 25.1 mm. However if the strength of the magnets is too high additional spacers could be added. (c) A single pair of the shims. Within each pair one has the magnet at the base of the casing while the other has them at the top making them adjacent. (d) Each PM has a diameter of 5.1 mm. The centers of permanent magnets pairs are only 2 mm apart, making them close enough to almost null the other's field when placed in opposition.*

The harmonics correcting device consists of four azimuthally evenly spaced cylindric PMs mounted into rings of Delrin, as shown in Figure 6.5. The PMs are small cylinders of NdFeB with radius 2.5 mm and length 2 mm. Each PM can be rotated in the *xy* plane but is prevented from rotation into the *z* direction. Each ring of PMs is directly adjacent to another ring (Figure 6.5b and c), in the *z* axis, creating two pairs. The distance between the two ring pairs can be increased by adding spacers. This reduces the magnitude of the correction gradient, as described at the end of section 6.2.2. Further issues concerning the rings can be found in Section 6.6.3.

Magnetic field maps were constructed from the proton resonance frequency of water (Figure 6.7a and b) with the mapping coil oriented parallel to the *z*-axis in order to obtain the smallest possible voxel size in the *xy* plane. The probe was positioned using a translational stage, as shown in Figure 6.6, which had a positioning precision of 0.01 mm in all three dimensions.

Using a map of the *xy* plane of the magnetic field at the Z_0 position, the dominant inhomogeneity in the magnetic field was determined to be quadrupolar, $n = 2$. The values of dH_x/dx

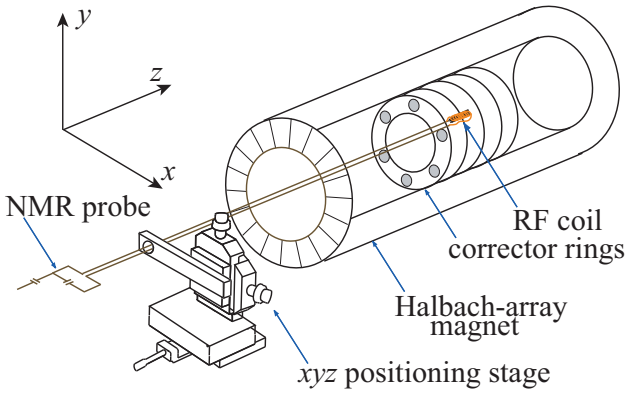

Figure 6.6: *Total overview of the experimental system showing the PM shim rings within the 16-element Halbach-array magnet. The probe coil is placed close to the shim ring's center and can be precisely positioned using a translational system, allowing for mapping an area of interest in the Halbach-array magnet. Our tuning and matching capacitors are located outside of the magnet so that the coil can have free movement inside the bore of the magnet. The positioner is affixed to the outside of the permanent magnet to ensure that the position is reproducible. Each platform within the positioner has a precision of 0.01 mm.*

and dH_x/dy were determined and used to solve Equation 9.3 for the angles ϕ_{o1} and ϕ_{o2}. The angles ϕ_{e1} and ϕ_{e2} were calculated from Equation 6.3 and the PMs were manually oriented into their respective directions.

6.4 Results and discussion

6.4.1 Experimental

Figure 6.7a and b are maps of the H_x component of the magnetic field before and after placement of the shim rings. The shim rings compensated for a gradient of approximately 2.78 G/mm at 300 degrees with respect to the positive *x* axis.

In further experiments the nullification of the *xy* plane, first derivative, gradient was accompanied by a significant improvement in NMR linewidth. In the center region of the magnet, before shimming, linewidths were as great as 12,000 Hz. Figure 6.7 c) and d) demonstrate

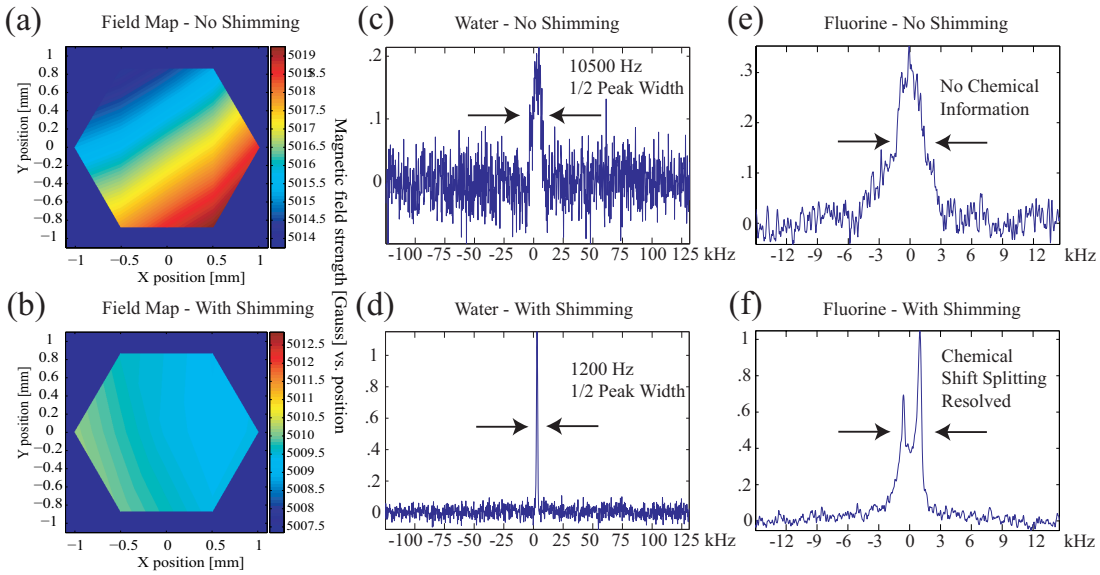

Figure 6.7: *(a) A field map of the center region of the magnet. Points were taken at even intervals around the circumference of a circle of radius 1 mm, and further data points were taken within the circle. The gradient was determined to be approximately 2.78 G/mm with an orientation of 300 degrees. (b) A field map of the same region following shimming. The gradient was successfully nullified. (c) Spectrum of $MnCl_2$ doped water without shimming after 128 scans. The half peak width is 10,500 Hz (450 ppm). (d) Spectrum of $MnCl_2$ doped water after shimming after 128 scans. The half peak width is 1,200 Hz (56 ppm). This is an 8.75 improvement in linewidth. (e) Spectrum of a mixture of hexa-fluorobenzene and perfluorinated polyether without shimming after 128 scans. No chemical information can be seen. (f) Spectrum of a mixture of hexa-fluorobenzene and perfluorinated polyether with shimming after 128 scans. The chemical shift difference is clearly resolved.*

the spectroscopic improvement on a water sample. The nullification of the gradient led to a concomitant reduction in half peak width from 10,500 Hz (450 ppm) to 1,200Hz (56 ppm), or an improvement of about 8.75:1. Following the "one-shot" shimming process, linewidth improvements of 7.5:1 were commonplace, whilst improvements of up to 9:1 were sometimes observed. In other experiments, the linewidths of two ^{19}F species were improved to reveal a chemical shift splitting that could otherwise not be resolved, as demonstrated in Figure 6.7 e) and f).

Our multi-element Halbach magnet typically exhibited drifts in the gradient of the (main) static field on the order of $\pm$ 0.05 G/mm and $\pm$ 5 $^\circ$ over the course of a day, due to the poor temperature control in the room ($19-22^\circ C$ over 24 hours). As for any permanent magnet, adequate temperature stabilization is required.

Further improvements in linewidth can be made by identifying higher-order inhomogeneities following shimming, and adding additional shim rings to correct for them. Such additional corrections were not necessary in order to resolve the ^{19}F chemical shift in a mixture containing two fluorinated compounds. For higher resolution spectroscopy such as proton NMR, where the whole chemical shift range is 10 ppm, this method would be necessary.

6.4.2 Error analysis

The shimming magnets are themselves a source of uncertainty due to the lack of precision knowledge of the easy-axis(direction of the remanent field) orientation and field strength of each PM. The variations in these properties are due to unavoidable inaccuracies in the fabrication process. However, in principle these errors could also be nulled with the system itself. Adjustments of the PM after further inquiries into each PMs properties and further iterations of the mapping, shimming system would eventually allow the system to shim out its own inhomogenieties.

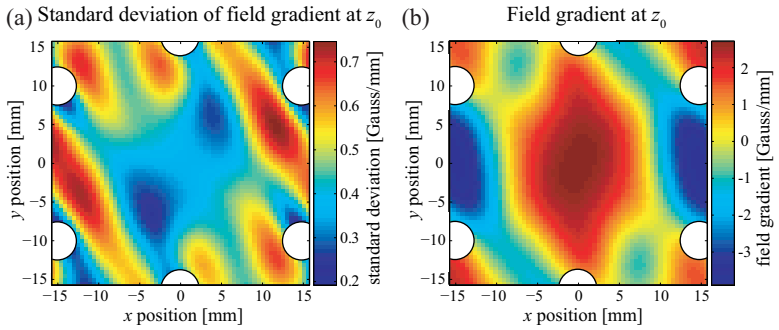

Figure 6.8: *The xy coordinates of the PMs, at z_i are projected on the plane of the field map at Z_0, and are indicated by the white circles. The PMs were oriented so that the gradient should be in the + x direction with a magnitude of 2.78 G/mm. (a) Map of the standard deviation of the gradient over the 100 simulations. This map gives a measure of the response of the field gradient to variation in PM orientations and strengths. The standard deviation of the gradient, 2.78 G/mm, in the center region is under 0.4 G/mm. (b) Map of the dH_x/dx component of the mean gradient, with no error in the magnet strengths and orientations. The area where the gradient is within 20 % of the desired gradient at the center comprises a region of about 1/5 the total width of the shim ring.*

The response of this shimming method to these inaccuracies was analyzed through computer simulation. The computer program used the charge sheet model described by Schlueter et al. [40] to calculate the magnetic field due to the PMs. The PM field strength standard deviation was estimated to be 20 percent while the error in the orientations of the magnets was estimated to be 3 degrees (standard deviation). This variation was included as a random value added or subtracted from the strengths and orientations of the PMs. One hundred simulations were run and the data are displayed in Figure 6.8. From this, it is concludes that, within the center of a harmonic corrector ring, a large portion of the area can be used to provide desired gradient corrections.

For a shimming method to be useful, the gradient from the shim must be uniform across the spatial extent of the coil. These data imply that the region within center of the magnet has a tolerable variability in its field gradient. This region could be made larger by increasing the accuracy of magnet orientation and improving the consistency of the surface fields of the magnets.

6.5 Conclusion

It has been shown that harmonic corrector rings can be used to shim the field of a permanent magnet, leading to NMR linewidth improvements of up to an order of magnitude. Nullification of the quadrupolar inhomogeneity has been demonstrated and the methodology for higher-order harmonics correction using further sets of rings has been outlined.

The method has been shown to be robust in response to inherent uncertainties in the strength and orientation of the PMs. Adjustment of the angle and magnitude of the applied correction gradient is simple, allowing for quick response to drift in the magnetic field. The method could be further sped up by automation of the magnet reorientations.

The low-cost, simplicity, and flexibility of this shimming device make it a useful tool in the development of magnets where field homogeneity is important but shimming coils are unsuitable. In particular, the large size of the usable shimmed region in comparison to the overall size of the corrector rings makes this shimming method particularly convenient for use in small portable NMR systems.

6.6 APPENDIX

6.6.1 Higher order gradients

In general, a ring of n equally spaced permanent magnets can be used to null up to a harmonic of order $n-1$. Thus the corrector rings described in this paper could be used to null an inhomogeneity of up to a decapole. The analytical expressions for the second and third derivatives of the field are:

Table 6.2: The magnet positions, magnetic sextupole vector, and octupole moment vector for the magnets of Figure 6.1. The ring is determined by the index on z.

	$\mathbf{r}$			$\mathbf{m}/\varepsilon$ n=3			$\mathbf{m}/\varepsilon$ n=4		
	r_x	r_y	r_z	m_x	m_y	m_z	m_x	m_y	m_z
1	0	$-l$	$-z_i$	$\cos\theta$	$\sin(\theta+\pi)$	0	$\cos\theta$	$\sin\theta$	0
2	$-\sqrt{3}l/2$	$-l/2$	$-z_i$	$\cos(\theta+4/3\pi)$	$\sin(\theta+4/3\pi)$	0	$\cos(\theta+5/3\pi)$	$\sin(\theta+5/3\pi)$	0
3	$-\sqrt{3}l/2$	$l/2$	$-z_i$	$\cos(\theta+8/3\pi)$	$\sin(\theta+8/3\pi)$	0	$\cos(\theta+10/3\pi)$	$\sin(\theta+10/3\pi)$	0
4	0	l	$-z_i$	$\cos\theta$	$\sin\theta$	0	$\cos(\theta+5\pi)$	$\sin(\theta+5\pi)$	0
5	$\sqrt{3}l/2$	$l/2$	$-z_i$	$\cos(\theta+4/3\pi)$	$\sin(\theta+20/3\pi)$	0	$\cos(\theta+4/3\pi)$	$\sin(\theta+20/3\pi)$	0
6	$\sqrt{3}l/2$	$-l/2$	$-z_i$	$\cos(\theta+8/3\pi)$	$\sin(\theta+25/3\pi)$	0	$\cos(\theta+4/3\pi)$	$\sin(\theta+25/3\pi)$	0

$$\frac{d^2\mathbf{H}}{d\mathbf{r}^2} = \frac{15}{4\pi r^5}\left[\frac{1}{5}[2\mathbf{Im}+\mathbf{mI}] - \hat{\mathbf{r}}\mathbf{m}\hat{\mathbf{r}} - \hat{\mathbf{r}}\hat{\mathbf{r}}\mathbf{m} - \mathbf{m}\hat{\mathbf{r}}\hat{\mathbf{r}} - (\mathbf{m}\cdot\hat{\mathbf{r}})[2\mathbf{I}\hat{\mathbf{r}}+\hat{\mathbf{r}}\mathbf{I}] + 7(\mathbf{m}\cdot\mathbf{r})\hat{\mathbf{r}}\hat{\mathbf{r}}\hat{\mathbf{r}}\right] \tag{6.8}$$

and

$$\begin{aligned}\frac{d^3\mathbf{H}}{d\mathbf{r}^3} = \frac{15}{4\pi r^6}\Big[7\Big(&\mathbf{m}\hat{\mathbf{r}}\hat{\mathbf{r}}\hat{\mathbf{r}} + \hat{\mathbf{r}}\mathbf{m}\hat{\mathbf{r}}\hat{\mathbf{r}} + \hat{\mathbf{r}}\hat{\mathbf{r}}\mathbf{m}\hat{\mathbf{r}} + \hat{\mathbf{r}}\hat{\mathbf{r}}\hat{\mathbf{r}}\mathbf{m} \\ &- 9(\mathbf{m}\cdot\hat{\mathbf{r}})\hat{\mathbf{r}}\hat{\mathbf{r}}\hat{\mathbf{r}} + (\mathbf{m}\cdot\hat{\mathbf{r}})(3\hat{\mathbf{r}}\mathbf{I}\hat{\mathbf{r}} + 2\mathbf{I}\hat{\mathbf{r}}\hat{\mathbf{r}} + \hat{\mathbf{r}}\hat{\mathbf{r}}\mathbf{I})\Big) \\ &- 3(\mathbf{I}\hat{\mathbf{r}}\mathbf{m} + \mathbf{I}\hat{\mathbf{m}}\mathbf{r} + (\mathbf{m}\cdot\hat{\mathbf{r}})\mathbf{II}) - 2(\hat{\mathbf{r}}\mathbf{Im} + \mathbf{mI}\hat{\mathbf{r}}) - (\mathbf{m}\hat{\mathbf{r}}\mathbf{I} + \hat{\mathbf{r}}\mathbf{mI})\Big].\end{aligned} \tag{6.9}$$

Substitution of the terms for the dipole positions from Table 6.2 and orientations calculated in Equation 6.2 yields usable expressions for the second and third derivatives, given in Tables 6.3 and 6.4.

Table 6.3: Non-vanishing tensor components of the second derivative $d^2H_x/d^2\mathbf{r}$ calculated from equation 6.8 through substitution of **r** and **m** from Table II. Summation over ϕ_n gives the solution for multiple rings.

indexing		*term*
i	j	times $\frac{45l^2\varepsilon_n}{16\pi r^9}$
1	1	$-3\left(7l^2-6r^2\right)\cos\phi_n$
1	2	$\left(7l^2-10r^2\right)\sin\phi_n$
2	1	$\left(7l^2-2r^2\right)\sin\phi_n$
2	2	$-\left(7l^2-6r^2\right)\cos\phi_n$
3	3	$4\left(7l^2-6r^2\right)\cos\phi_n$

Table 6.4: Non-vanishing tensor components of the third derivative $d^3H_x/d^3\mathbf{r}$ calculated from equation 6.9 through substitution of **r** and **m** from Table II. Summation over ϕ_n gives the solution for multiple rings.

indexing			*term*
i	j	k	times $\frac{315\varepsilon_n l\sin\phi_n}{16\pi r^{12}}$
1	1	1	$3\left(9l^4+208r^5/63-4l^2r^2\left(2+r\right)\right)$
1	2	2	$l^2\left(9l^2-4r^3\right)$
1	3	3	$4\left(9l^4+2r^5-l^2r^2\left(9+2r\right)\right)$
2	1	2	$9l^4+160r^5/21-4l^2r^2\left(3+r\right)$
2	2	1	$9l^4+16r^5/7-4l^2r^2\left(3+r\right)$
3	1	3	$4\left(9l^4-2l^2r^2\left(6+r\right)+4r^4\left(1+5r/21\right)\right)$
3	3	1	$4\left(-9l^4-10r^5/7+2l^2r^2\left(3+r\right)\right)$

6.6.2 First probe and field mapping

The first mapping was done with a home built probe, in which the stator had slots built into it at designated distances and the coil was able to be moved from slot to slot as shown in Figure

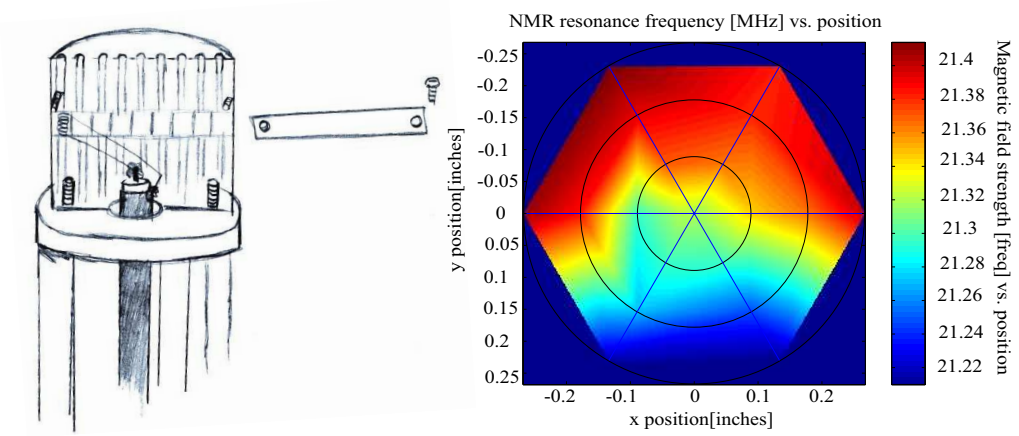

Figure 6.9: *a)The first probe design to map the inhomogeneities of the field. Slots were .083" apart. b) A field map taken with this system. Though a quadrupolar field could be seen from it, the map was unreliable.*

6.9. The Halbach magnet would then be turned 60°, using the marks on the outside plate to determine a 60° angle increment. The first field mapped gradients from this system didn't come out as a clean quadrupole. The orders of inhomogeneity could not be determined. This was for several reasons; at the time it required between 1024 averages and 4096 averages to see the spectra, which meant the frequency could have significantly drifted over the experiment's time. In the following system, refining of the coil and probe reduced the number of scans needed for usable data to between 16 and 32. The second problem was that the center slot position was not necessarily at the center of the Halbach array, and there was no way to determine how far off it was from the center. Mapping the center is the most important since that is the most desirable area to do an experiment. The center of the magnet is the most important to a rotating experiment becasue of the compounding effects inhomogenieties have during roation. If the coil is placed on the magnets axis of rotation there is no broadening from the field inhomogeneities as the magnet rotates, but the further is is away from the center of rotation it will experience more field inhomogenieties. Since the map is take by rotating the magnet and probe coil's location to the axis of rotation in unknown then the true direction of the gradient is unknown. The third problem encountered was that the coil was considerably smaller than the slots. Attempts to place the coil in the center of a slot were made, but the precise placement

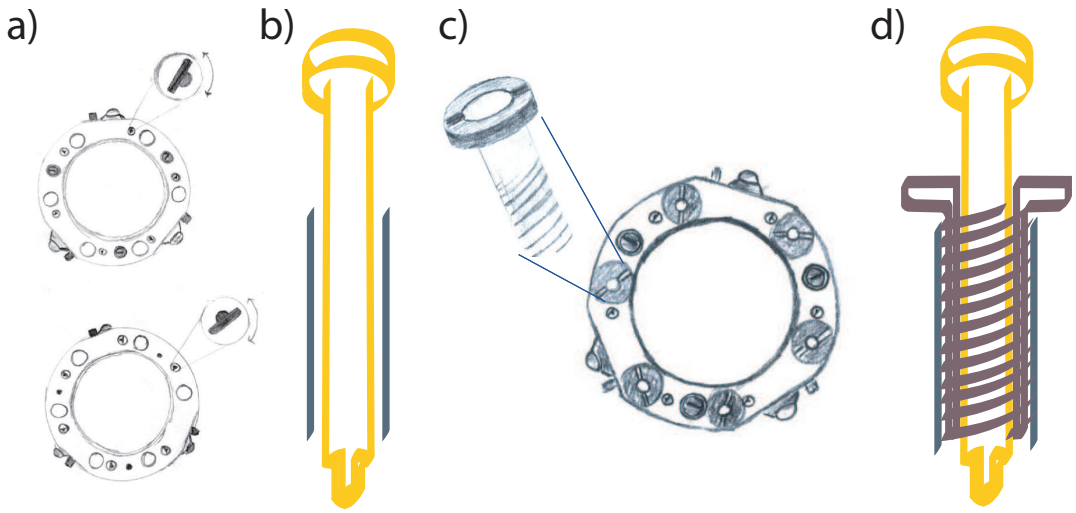

Figure 6.10: *(a)The original Delrin container, with three screws keeping the top and botton part together. Six access holes were made so that each PM on each ring could be turned while in the magnet. On the sides of the containers are locking mechanisms used to maintain the shims orientation to magnet while it spins. (b)A specialized screw with a moon shaped tip was used to turn the magnets. This was useful in distinguishing between the the north and south pole on the magnets. The screw slipping through the Delrin pieces to set the PMs. (c) Since the magnets were slipping severely we needed to tighten the two parts of Delrin holding them in place. The six wholes used to access the magnets were used since there was no other space on the piece. (d) We designed the screws to have a whole in its center such that the screw could still access the PMs while in the Halbach array.*

was impossible to accomplish. This system could not produce reliable map so a more precise positioning system and a new probe were developed.

6.6.3 PM containers

The pieces have passage holes which allow the PMs to be turned while the shims are stacked in the magnet. Different rings can be accessed by lining up the outer rings passage holes. The original pieces were made out of phenolic. However the material was too brittle and snapped under the pressure needed to keep the PMs from slipping. The final material was chosen to be Delrin but possibilities for future designs are aluminum, brass, or other non-magnetic metal. The more rigid material helps keep the PM from slipping when in the Halbach magnet. Metals can be machined thinner which would let magnets in a pair get closer, allowing a pair to be

better nulled.

Since in the Delrin the PMs were slipping new screws had to be made which went into the passage hole designed to turn the PMS while in the Halbach array. As seen in Figure 6.10 these screws were specially designed to allow turning of the PMs to still remain.

Chapter 7

Projected Magic Angle Spinning

7.1 Introduction

Monitoring metabolites in tissues to detect changes in cellular function due to disease has been done by high resolution proton NMR. [41, 42, 43, 44, 45] However, resolving useful NMR spectra with a static sample of tissue can often be difficult because of inherently broad linewidths. The NMR linewidth is broad, causing spectral overlap, mainly due to local field gradients arising from the variations in local magnetic susceptibilities. This anisotropic interaction as discussed in section 4.2.4 can be time averaged away with the rapid spinning of the sample at the magic angle (MAS), which transforms as a second order Legendre polynomial, $P_2(\cos\theta_R)$. This interaction is fully eliminated when $P_2(\cos\theta_R)$ is equal to zero, that is, when the rotor is at the magic angle of 54.74 degrees with respect to the main magnetic field, B_0.

MAS is used for studying diverse materials such as proteins, inorganic solids, polymers, and macromolecular crystals. The rotational speeds in MAS can be as high as 80kHz. On the other hand, slow spinning techniques are essential for a variety of experiments including rotating field NMR (Chapter 5), intact organ studies, and living animal studies. [46] Pulse se-

quences such as 1D- Total Sideband Suppression(1D-TOSS) [47] and 2D-Phase Altered Sideband Suppression (2D-PASS) [48] have been used to study excised human tissue. [44] [49] These recover the isotropic spectrum at slow spinning speeds through rotor synchronization of the pulses. Other sequences like Magic Angle Hopping (MAH) [50],which uses three distinct stationary positions, and Magic Angle Turning (MAT) [51] [52] [53] have been used to take spectra of metabolites in tissue and organs for both excised tissues [54] and a living mouse. [46]

Slow spinning speed is an arbitrary term, but generally implies that the sample rotates significantly more slowly than the time scale of the anisotropy. When spinning slower than the anisotropy, sidebands emerge at the rotor's spinning frequency. This makes the effective signal-to-noise smaller. Yet, pulse sequences for slow spinning samples can be advantageous relative to the MAS analog because they not only recover the isotropic spectra without fast spinning speeds but also correlate the isotropic and anisotropic interactions together in a 2D spectrum. This retains important information otherwise lost. The first dimension is the manifold of sidebands under the stationary powder pattern envelope while the second is the isotropic spectrum.

Techniques other than slow spinning have been developed which give the isotropic spectrum correlated to the anisotropic spectrum. These include techniques of variable angle correlated spectroscopy(VACSY). From this technique, which uses many angles incremented in small steps, another technique was developed, projected-Magic Angle Spinning. (See sections 4.2.6 and 4.2.7) The p-MAS pulse sequence needs only two angles to obtain a high-resolution spectrum which has both anisotropic and isotropic information. The separation of angles needed for a useful spectrum has a practical limit. The angles can both be significantly smaller than the Magic Angle, but too close to zero will result in no signal. The p-MAS method produces scaled isotropic spectra, but is useful for samples which can not be set to the magic angle, for example an enlongated sample.

In this preliminary study the spinning speeds are faster than could be used on a living crea-

ture, but it shows that p-MAS can produce high-resolution spectra for elongated samples, or tissues from nonliving organisms. For living organisms a similar experiment could be used with a rotating field magnet as living organisms are difficult to rotate. This experiment woulde use both the p-MAS pusle sequence and slow spinning techniques like magic angle turning (MAT) which combine to make the projected magic angle turning (p-MAT). This pulse sequence and supporting hardware, which is under development, are discussed in chapter 8. Because of the technical difficulties associated with p-MAT this proof of principle experiment was used to show that the isotropic spectrum from tissue can be resolved for a projected data set. Initially this was tested using a model system of water beads and oil. [38] The results presented here suggest that the tissue broadening is spatially correlated as the results from the model system had suggested. This provides motivation to further pursue development of the p-MAT sequence.

7.2 Theory

The Hamiltonian for a sample with an anisotropic broadening which is spun faster than the relevant anisotropy is the sum of the isotropic and anisotropic parts:

$$H_0(\theta) = H_{iso} + P_2(\cos\theta) H_{aniso} \tag{7.1}$$

The pulse sequence for p-MAS is shown in Figure 7.1. This experiment has two evolution time periods: the first evolution is indirectly detected by incrementing time t_1 at θ_{R1}, and the second is detected directly during t_2 at θ_{R2}. While the angle is changed (typically 10-50 ms), the magnetization is stored along the z axis with a 90° pulse, then restored with another 90° pulse. The experiment itself correlates two anisotropic dimensions with the spectral width determined for on each dimension by $P_2(\cos\theta_{R1})$ and $P_2(\cos\theta_{R2})$, respectively. The isotropic spectra is

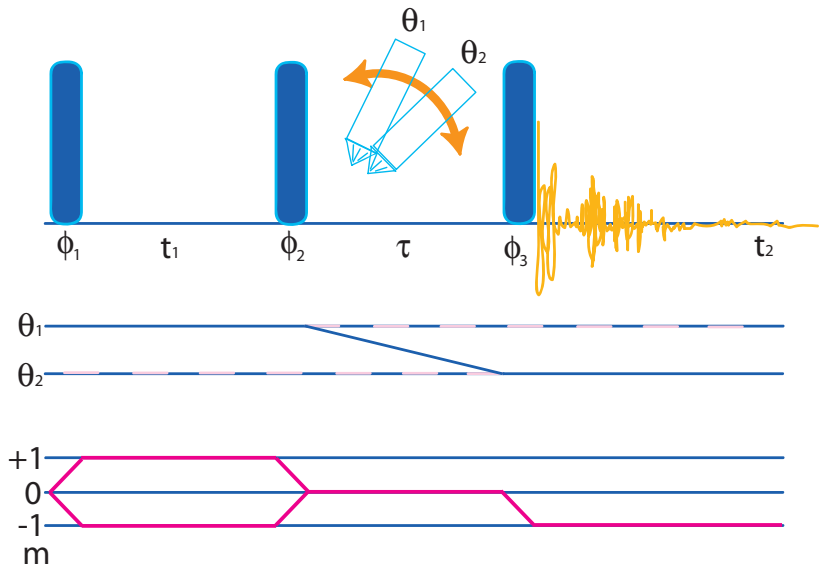

Figure 7.1: *A p-MAS pulse sequence allows recovery of isotropic spectra from anisotropic samples using spinning angles other than the magic angle. The 2-D NMR experiment consists of a 90° pulse which places the magnetization in the transverse plane, a second 90° pulse which stores the magnetization as the sample switches angles, and a third 90° which places the magnetization back into the transverse plane for detection at the second angle. Phase cycling selects the desired coherence pathway.*

recovered from a shearing line determined by the values of θ_{R1} and θ_{R2}. That spectrum is scaled-down by a ratio, the chemical shift scaling factor, λ, based on the angles chosen:

$$\lambda = \frac{P_2(cos\theta_{R1}) - P_2(cos\theta_{R2})}{P_2(cos\theta_{R1}) + P_2(cos\theta_{R2})} \tag{7.2}$$

The beneficial range of angles is confined by the chemical shift scaling factor, λ, which depends on the spinning angles and the difference in the spinning angles. The benificial range is wider that would be first thought as the residual linewidths do not scale with angle. A plot of the scaling factor for different paired spinning angles, and a constant inherent linewidth, smaller than the induced broadening, is showing in Figure 7.2. The scaling factor from angles close to zero can be very small as it depends on both the absolute values of the angles and the difference between the two p-MAS angles, which may seem to impair the usefulness of the technique. Fortunately, the residual linewidth caused by inhomogeneous interactions is

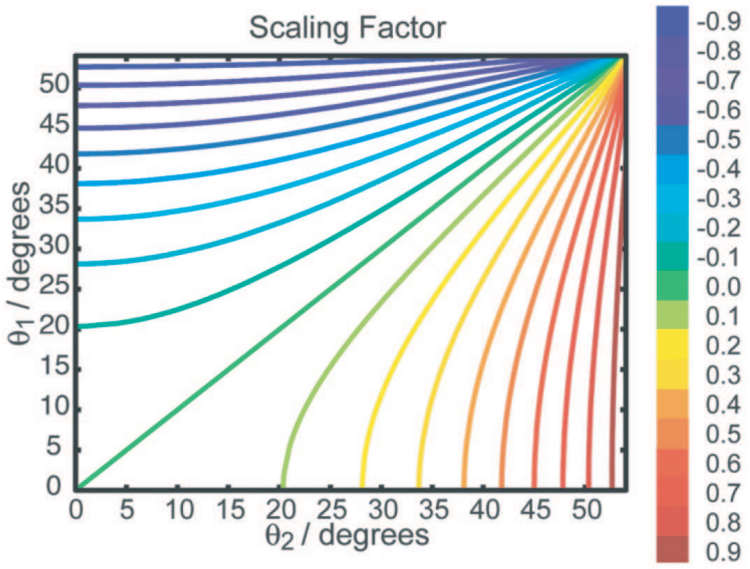

Figure 7.2: *The reconstructed isotropic chemical shift scaling factors as functions of two different spinning angles*

also scaled, actually maintaining the usefulness of the technique. The true limiting factor for choice of angles, in the p-MAS experiment, is the homogeneous broadening mechanisms, like T_2, which do not scale, relative to the chemical shift differences, that maybe inherently small. Once the scaled chemical shift difference is on the order of the homogenious broadening the peaks will not be resolved.

The theoretical minimum linewidth obtainable in the projection from p-MAS depends on the level to which the frequencies present are correlated. When there are perfectly correlated interactions the projection experiment gives the isotropic spectrum. [55] An example of a highly correlated interaction is the chemical shift changes caused by susceptibility differences. An example of a highly uncorrelated interaction is the chemical shift changes induced by sample disorder. [56]

For tissue samples, linewidths are broadened by differences in magnetic susceptibilities of the cellular structure, mostly by the lipid bilayer of the cell walls. The direct dipolar (DD) coupling minimumly contributes to line broadening as the majority of the cell is still a solution and the molecules have high mobility. [57] Despite these speeds, measurements of residual DD

couplings have been observed for metabolites in *in vivo* tissue samples in studying muscle fiber ordering effects. [57, 58] The DD coupling in the sample for this study though are averaged out at the spinning speeds which are used. An interesting possibility use for p-MAS in the future would be to correlate the DD couplings to the isotropic spectra. For this preliminary study, p-MAS is used to evaluate the practicality of eliminating anisotropic interactions for biological tissue samples by spinning two different bovine tissue samples at small angles compared to the magic angle.

7.3 Methods

Bovine muscle and liver were acquired by taking a 45 min walk down College Ave. to the Andronico's and then taking a nice 45 min walk back to campus, during which the walkie was proposed to by a bum on the street. The muscle and liver samples were "double deuturated" by soaking them in a solution of 50 mM NaCl D_2O for 10 hours and then refreshing the solution and soaking for another 10 hours. The samples were deuterated to remove the strong proton water signal and signal from other exchangeable protons. The NaCl solution more closely resembled the natural environment of a cell than pure D_2O, thus stabilizing the sample during proton deutrium exchange. The proton exchange method was used instead of a water suppression pulse sequence to simplify the experiment, however, in the future water addition of suppression pulse sequences will be desired. This will be important for *in vivo* experiments since they cannot be 'twice deuturated' beforehand as it would kill the subject.

These samples were packed inside a 4mm Varian Pencil MAS rotor, with specially made Kel-F, o-ring spacers shown in Figure 9.5. The spacers were there to prevent the sample from drying out. [59] Packed this way, the sample maintains spectral resolution for several days.

NMR proton, ^1H, spectra were taken on a Chemagnetics (Varian) Infinity spectrometer with

a Larmor resonance frequency of 500MHz. The probe is a substantially-modified Varian 4mm HX switched angle probe. A split solenoid is used to prevent variability in the B_1 field and makes the 90° time independent of spinning angle. Similar coil designs were used in other recent experiments. [60] This type of coil produces a constant B_1 field, perpendicular to the B_0 field, a method different from a traditional solenoid wound parallel to the spinning axis of the sample. As sensitivity is not a limiting factor, the sample, using the spacers, was restricted to a small region in the coil to get homogeneous excitation, as shown in Section 4.1.1. One-dimensional static (non-spinning) and MAS spectra were acquired using a standard one-pulse experiment, with a B_1 frequency of 50kHz, and a standard 90, 270, 0, 180 phase cycle. Acquisition length for the static spectra was 8192 points, with a spectral width of 20kHz, and 16 scans for muscle while 64 scans for liver. Acquisition for the MAS spectra was 8192 points, a spectral width of 20kHz and 30 kHz, a spinning frequency of 1.74kHz and 6kHz, and 4 scans and 64 scans taken for muscle and liver respectively. The chemical shifts were assigned by designating water's resonances as 4.7ppm.

For p-MAS, depicted in Figure 7.4 [38], a two-dimensional data set was collected. Frequency sign discrimination in both dimensions was achieved with phase cycling. The angles, θ_{R1} and θ_{R2}, for both samples were 4.5 degrees and 26 degrees, respectfully. The time to switch the angle was 50 ms. The accuracy of switching to the same angle is estimated to be close to 0.1 degrees. The muscle sample was spun at 2 kHz while the liver was spun at 6 kHz. For both samples the indirect dimension($f1$) had 256 points and the direct dimension($f2$) 2048 points. There were 16 scans acquired for each point in the indirect dimension. The isotropic spectrum was recovered during data processing after shearing the data set and projecting the spectrum onto the axis.

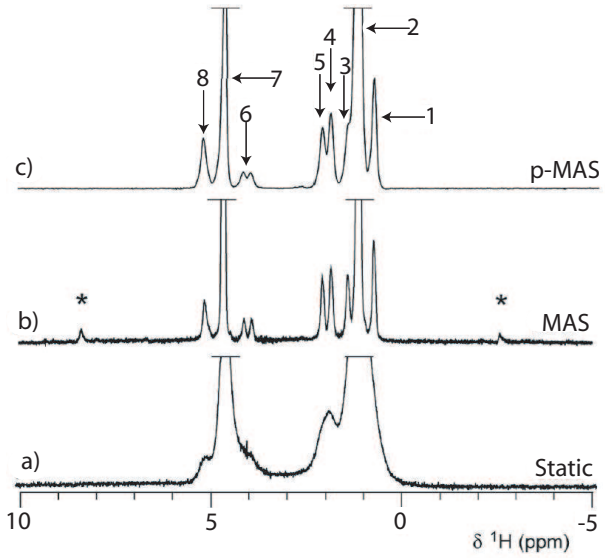

Figure 7.3: *a) The static bovine muscle spectrum. b) The MAS(1.7 kHz rotor spinning frequency) bovine muscle spectrum. The spinning sidebands are designated with an asterisk (*). c) Projection from the p-MAS spectrum of bovine muscle. The partial assignments are 1:(0.8ppm) triglyceride terminal -C***H***$_3$, or neutral amino acid -C***H***$_3$ 2: (1.2ppm) Triglyceride -CH_2-C***H***$_2$-CH_2 lactate, threonine -C***H***$_3$ 3: (1.5ppm) not assigned 4: (1.9ppm) triglyceride -CH=CH-C***H***$_2$-CH_2 5: (2.1ppm) triglyceride -CH_2-C***H***$_2$-CO 6: (4.0ppm, 4.2ppm) triglyceride -CH=CH-C***H***$_2$-CH_2, triglyceride -CH_2-C***H***$_2$-CO 7: (4.7ppm) water 8:(5.2ppm) phosphocreatine N-C***H***$_3$.*

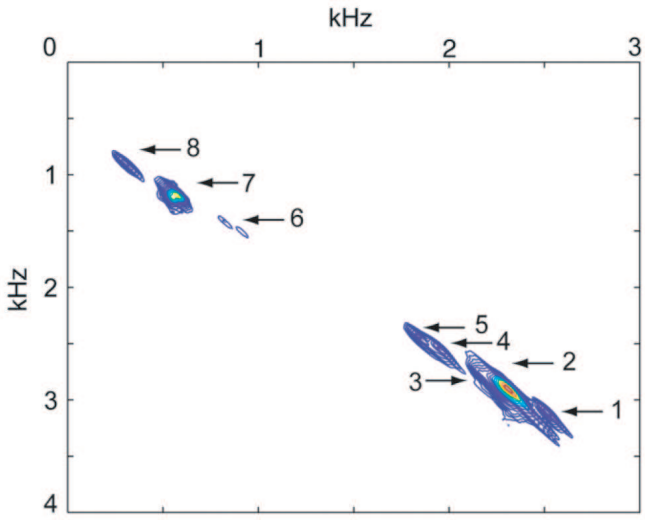

Figure 7.4: *The p-MAS pulse sequence gives two-dimensional correlated spectra between the anisotropic line shapes dependent on $P_2(\cos\theta_R)$ of $\theta_R 1$ and $\theta_R 2$. Even though the direct and indirect linewidths are broad the isotropic spectra can be obtained on a shearing line. The slope of this is determined by the angles $\theta_R 1$ and $\theta_R 2$. The spectrum is plotted in kHz instead of ppm because of the chemical shift scaling. The spectrum has 20 contour levels and is plotted on an exponential scale in order to accommodate the large range of intensities observed in different peaks.*

7.4 Results and Discussion

The data collected from bovine muscle are in Figure 7.3. The static spectrum in Figure 7.3 a) shows a strong water signal at 4.7ppm, the triglyceride methylene protons at 1.2ppm, and some poorly resolved resonances for other species. The MAS spectra in Figure 7.3 b) shows several more resonances. The assignments known from previously published work [54, 61] are presented in the figure caption. Figure 7.3 c) shows the appropriately projected p-MAS spectrum after a shearing transformation and re-scaling to the isotropic spectrum, using λ. This spectra contains the same information that the MAS does.

The two-dimensional p-MAS spectrum is shown in Figure 7.4 to show the type of data obtained in this experiment pre-shearing. Broad lines are seen in both the direct and indirect dimension in the 2D spectrum, but the isotropic spectrum can be reconstructed along a shearing line determined by the two angles used. The resonances assigned in the 1D spectrum are

all distinguishable in the 2D p-MAS spectrum. The residual linewidths in the p-MAS projection are slightly larger than the MAS spectrum's residual linewidths. This is due to truncation, caused by not acquiring the time domain FID until it reaches zero signal, in the indirect dimension. These effects can be minimized by using methods to predict the rest of the FID such as linear prediction or maximum entropy. These processing techniques do not show the true capacity of the pulse sequence's usefulness and can not be justly used in a proof of princple experiment. The downside of the p-MAS is that it is inherently a two-dimensional method meaning that the time to acquire it greatly exceeds the time for a one-dimensional spectrum. In most two-dimensional experiments the indirect dimension's quality is sacrificed, meaning truncated, to minimize the acquisition time. However, the objective with this experiment is not to replace MAS but allow experiment that would otherwise not be possible to be done such as in the case of an elongated sample that can not be spun at the magic angle in the bore or in a rotating magnet set up.

The data for the bovine liver is shown in Figure 7.5. The static spectrum shows a large water signal at 4.7ppm, and a broad resonance composed of the indistinguishable resonances from individual metabolites. The MAS spectrum, Figure 7.5 b), shows more detail than the static spectrum. Figure 7.5 c) shows more closely the region between 0-4ppm in which distinct resonances can be assigned based on previous studies, given in the caption. [54, 62] The projected spectrum, Figure 7.5 d), shows the same resonances which are in the MAS spectrum. The linewidth in the MAS and p-MAS for the liver are comparable indicating that the indirect dimension FID was not truncated. As the liver has a shorter T_2^*, which means that the signal approaches zero faster and has inherently larger linewidths. This could be attributed to the higher concentration of paramagnetic compounds in this type of organ, or to its morphology.

An additional mechanism of linewidth broadening besides magnetic susceptibility is molecular diffusion. In an ideal MAS experiment, each spin returns to the exact same place at the end of each rotation period. Molecular diffusion causes the spins to be displaced from their

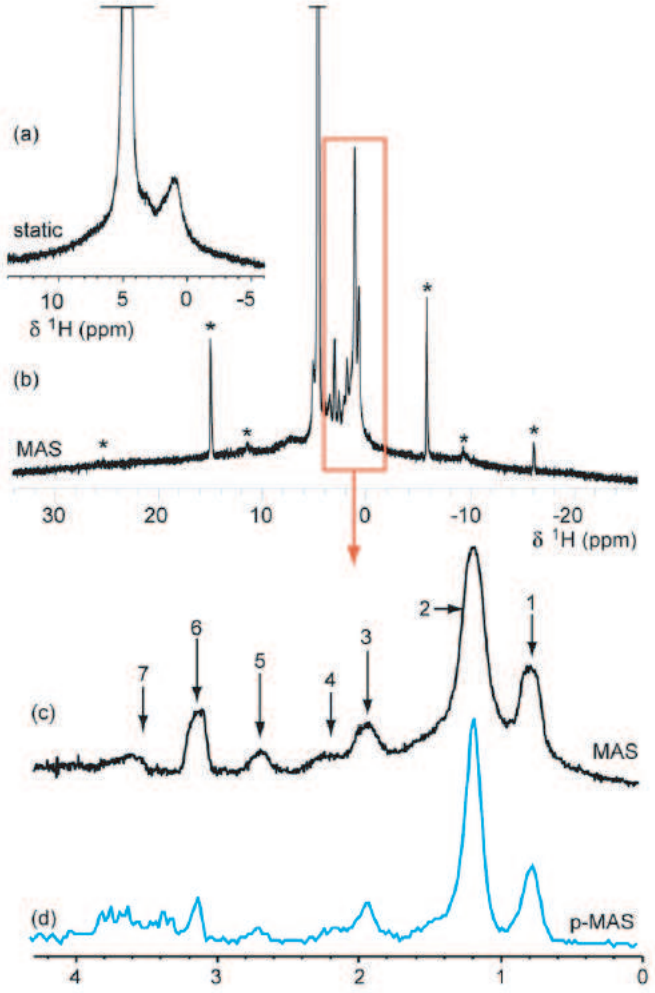

Figure 7.5: *a) The static bovine liver spectrum. A large water signal is observed and a small triglyceride signal. b) The MAS(6kHz rotor spinning frequency) bovine liver spectrum. The spinning sidebands are designated with an asterisk (*). c) The metabolite region of the MAS spectra. The partial assignments are 1:(0.8ppm) triglyceride terminal -C***H***$_3$, or neutral amino acid -C***H***$_3$ 2: (1.2ppm) Triglyceride -CH$_2$-C***H***$_2$-CH$_2$ lactate, threonine -C***H***$_3$ 3: (1.9ppm) triglyceride -CH=CH-C***H***$_2$-CH$_2$ 4: (2.2ppm) triglyceride -CH$_2$-C***H***$_2$-CO 5:(2.7ppm) triglyceride -CH=CH-C***H***$_2$-CH=CH- 6:(3.1ppm) choline, phosphocholine and β-glucose -C***H***$_3$ 7:(3.5-3.8ppm) glucose and glycogen 8: (4.7ppm) water 9: (5.2ppm) phosphocreatine N-C***H***$_3$. d) Projection from the p-MAS spectrum of bovine liver.*

previous location. Furthermore as the spin diffuses to a different tissue location which has a different magnetic susceptibility or chemical shift environment it undergoes decoherence. The important time scale for this interaction is the time scale of a rotor rotation. For speeds used in this experiment the diffusion broadening is probably not a source of line broadening. Diffusion for spinning speeds greater than 100Hz have contributions which scale as $\frac{1}{F_r^2}$, where F_r is the rotor frequency in Hz. For this experiment, the relevant diffusion linewidth broadening happens during the hopping time, τ. It is desirable to reduce this effect in the p-MAS experiment so faster switching times could be useful.

7.5 Conclusions

The p-MAS technique produces spectra that are functionally equivalent to conventional MAS spectra for tissue samples. Metabolites' resonances are separated by the p-MAS spectra from that of water in muscle and liver tissue samples. The potential use of p-MAS for less invasive *in vivo* biological tissue studies was demonstrated. There is a possibility of improvement with water suppression in addition to the p-MAS sequence, or by detecting other nuclei with greater chemical shift differences such as ^{13}C or ^{31}P in future experiments.

The p-MAS technique allows the user to choose the angle based on sample geometry or experimental setup factors only limited by the chemical shift scaling inherent to the p-MAS method. This method should be useful in cases where the sample cannot be spun at the magic angle, for example an elongated samples where it has to be spun at smaller angles to fit into the magnet bore. This is also a proof of principle that a rotating field experiment where the field angle is switched between two small angles could be used on biological samples. Discussion of rotating field NMR can be found in Chapter 5. [37] Improvement and implementation of a p-MAS sequences will be necessary to a commercially practical rotating field system because of either the large power requirements to rotate a magnetic field or the use of power to produce

the magic angle in an electrocoil. The p-MAS techniques may be the deciding factor in making rotating field experiments possible and practical by giving them the necessary sensitivity and resolution.

Chapter 8

progress towards

Projected Magic Angle Turning

8.1 Introduction

In the previous chapters the removal of anisotropies through magic angle spinning has been discussed extensively. The possibility of spinning the magnetic field instead of the sample was also discussed, Chapter 5. Magic angle spinning is useful in its ability to remove anisotropies but is restricted by having to be at the magic angle and having to spin faster than the anisotropy. Other angles than the magic angle can be used if the p-MAS pulse sequence is used, Chapter 7. Anisotropies are removed for slow spinning systems when a pulse sequence like MAT, PASS, or TOSS is used. [63]

The construction of a pulse sequence that is a combination of the p-MAS sequence and the slow spinning sequences could be of particular value to some experiments. The rotating field experiment could benefit greatly from such a pulse sequence. Other uses are for samples that are destroyed under fast rotation and that align to the magnetic field like some liquid

crystals. [64]

The specific slow sequence chosen depends on the speeds a specific experiment can handle. The TOSS and PASS pulse sequence give very good data around 1kHz and decent down to about 250 Hz while MAT is better for experiments 250Hz and below. [63] For the interest of this project where rotating field NMR is the main goal, the MAT sequence is most ideal since the mechanical rotation speed for such a system is slower than 250Hz. Specifically for the system that was built and described in Chapter 5, a permanent magnet that can rotated up to 50Hz. The combination of the p-MAS and MAT pulse sequences is called p-MAT. Another interesting sequence that the MAT could be combined with is the VACSY. [28] This would give similar data to the p-MAT and could be taken with the same instrumentation.

8.2 Theory

The theory for p-MAT, like the sequence itself, is a combination of the theory for MAT and p-MAS. The same interactions are of interest in this experiment as in the p-MAS and have the Hamiltonian:

$$H_0(\theta) = H_{iso} + P_2(\cos\theta) H_{aniso}. \tag{8.1}$$

The anisotropy in the p-MAT sequence is averaged out by the rotor synchronized pulses rather than fast spinning; therefore, the MAT is indirectly causing the same interaction as MAS. When adding the MAT to the p-MAS sequence it's important to keep in mind that the fast spinning of MAS is present during both the t_1 and t_2 dimensions. Therefore, the MAT sequence needs to be added to both the t_1 and t_2 sections to make the p-MAT pulse sequence work, shown in Figure 8.1.

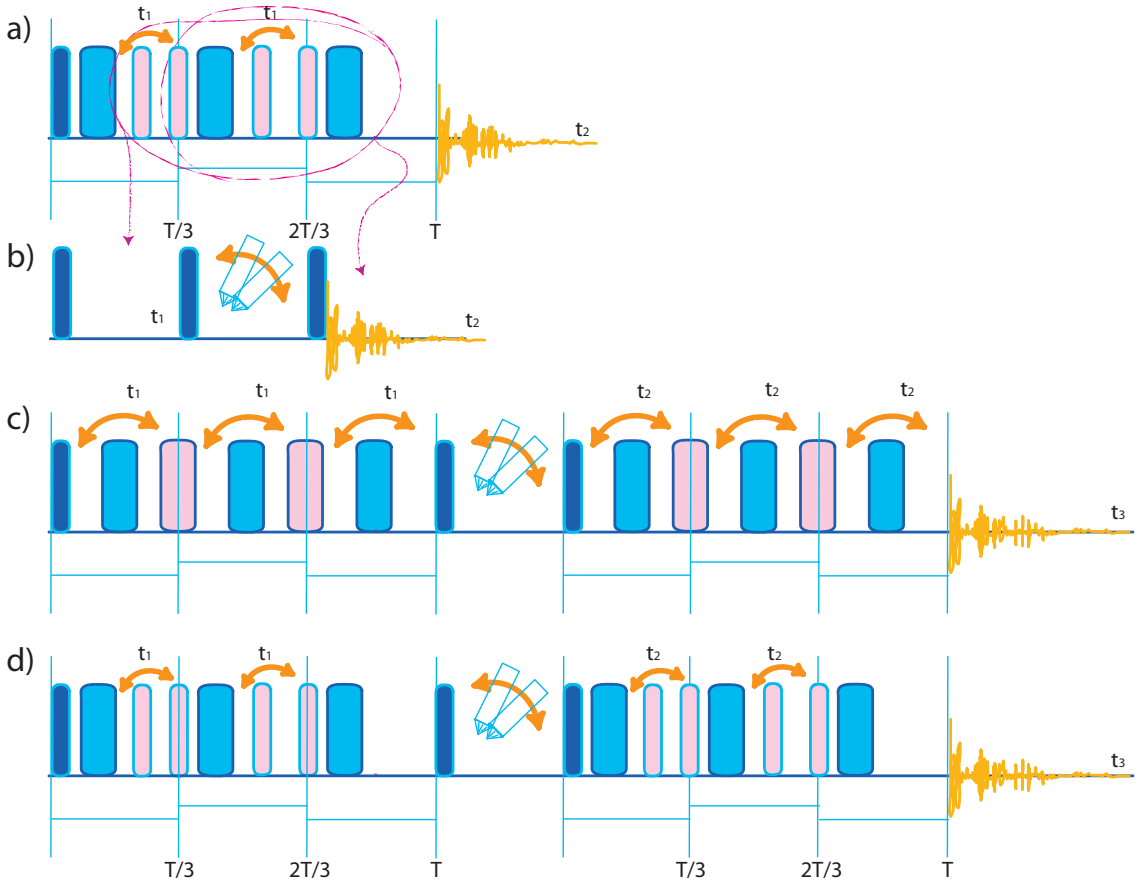

Figure 8.1: *a)The MAT sequence, for spinning slowly b)The p-MAS sequence, for spinning away from the magic angle. c) A possible p-MAT pulse sequence uses the MAT sequence in 4.9 a). This sequence is a little bit simpler than 4.9 b) but not as robust as some MAT sequences. d)Another possible p-MAT pulse sequence uses the triple echo MAT from 4.9b).*

The p-MAT ezperiment is three-dimensional. The first time period is incremented by the timing of the 180° in the first MAT sequence. This interaction occurs at the angle θ_{R1} and the dimension's width will be determined by $P_2(\cos\theta_{R1})$. The magnetization is then stored along z, as in the p-MAS, while the sample hops to a second angle. The second time period is incremented by the timing of the 180° in the second MAT sequence. This interaction occurs at the angle θ_{R2} and the dimension's width will be determined by $P_2(\cos\theta_{R2})$. The last dimension will give the spinning sideband pattern and the width is again determined by $P_2(\cos\theta_{R2})$.

The MAT data is recovered from a shearing plane which is determined by the angles θ_{R1} and θ_{R2}. From the MAT data, the isotropic spectrum can be recovered. The MAT data will be scaled, and consequently the isotropic spectrum also:

$$\lambda = \frac{P_2(cos\theta_{R1}) - P_2(cos\theta_{R2})}{P_2(cos\theta_{R1}) + P_2(cos\theta_{R2})} \tag{8.2}$$

.

The experimental parameters, angles chosen, of the p-MAT will have the same restrictions on the beneficial range as the p-MAS.

8.3 Probe Building

The basic parts of a probe are discussed in Section 3.3. The vital parts of making a p-MAT probe are to have a probe which can switch angles and stably spin the sample at slow speeds.

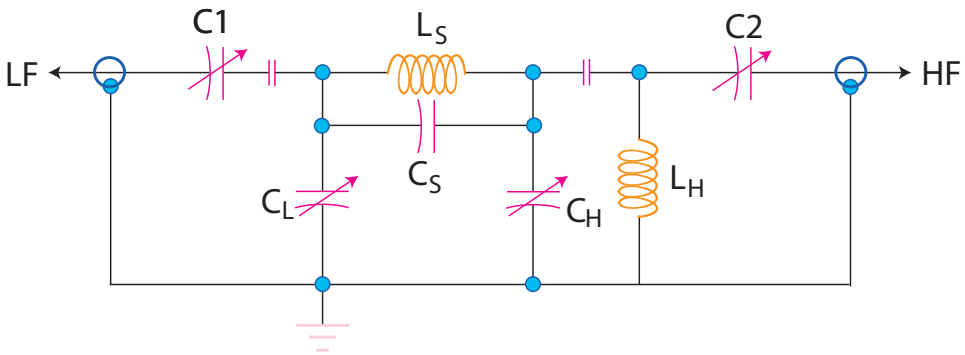

Figure 8.2: *The schematic for a typical double resonance probe. [13] Four variable capacitors are used, two for each channel, C1, C_L, C2, C_H. A channel is retuned by changing out the non-variable capacitors. The non-variable capacitors are soldered between the variable capacitors of each channel. This changes the over all capacitance with our having the exchange out the variable capacitors. The circuit above has a possible capacitor, C_S, between the high and low frequency channels, however for the p-MAT probe tuning this was not necessary. There is a second inductor in the circuit which determines which channel is favored.*

8.3.1 Remaking a probe

The original probe for this experiment was a two channel, Varian, commercial, probe. It was originally modified to do some slow spinning *ex situ* experiments. [31] To do the p-MAT experiment the probe needed to undergo some serious reconstruction, including a new stator and coil. The proton frequency which was chosen for the experiment was 300MHz even though for the previous experiment a proton frequency of 180MHz was used. This probe was retuned by soldering different non-variable capacitors to the variable capacitors to gain a proton frequency. The electronics' schematic for this probe is in Figure 8.2. The frequency was chosen for better chemical shift difference and for easier tuning as a new coil would be easily tuned to 300MHz with the available capacitors. The divider between the stator and the electronics needed to be reconstructed to run an experiment at 300Mhz as the 180MHz system is wide bore. A pictorial diagram of the probe is shown in Figure 8.3.

After the divider was machined and the probe was tuned to the proper frequency it was tested for signal and the signal's efficiency. As calculated from the nutation curve by comparing the peak to peak intensity of the first to the third peak, Figure 8.5, the probe efficiency was

Figure 8.3: *A MAT probe.*

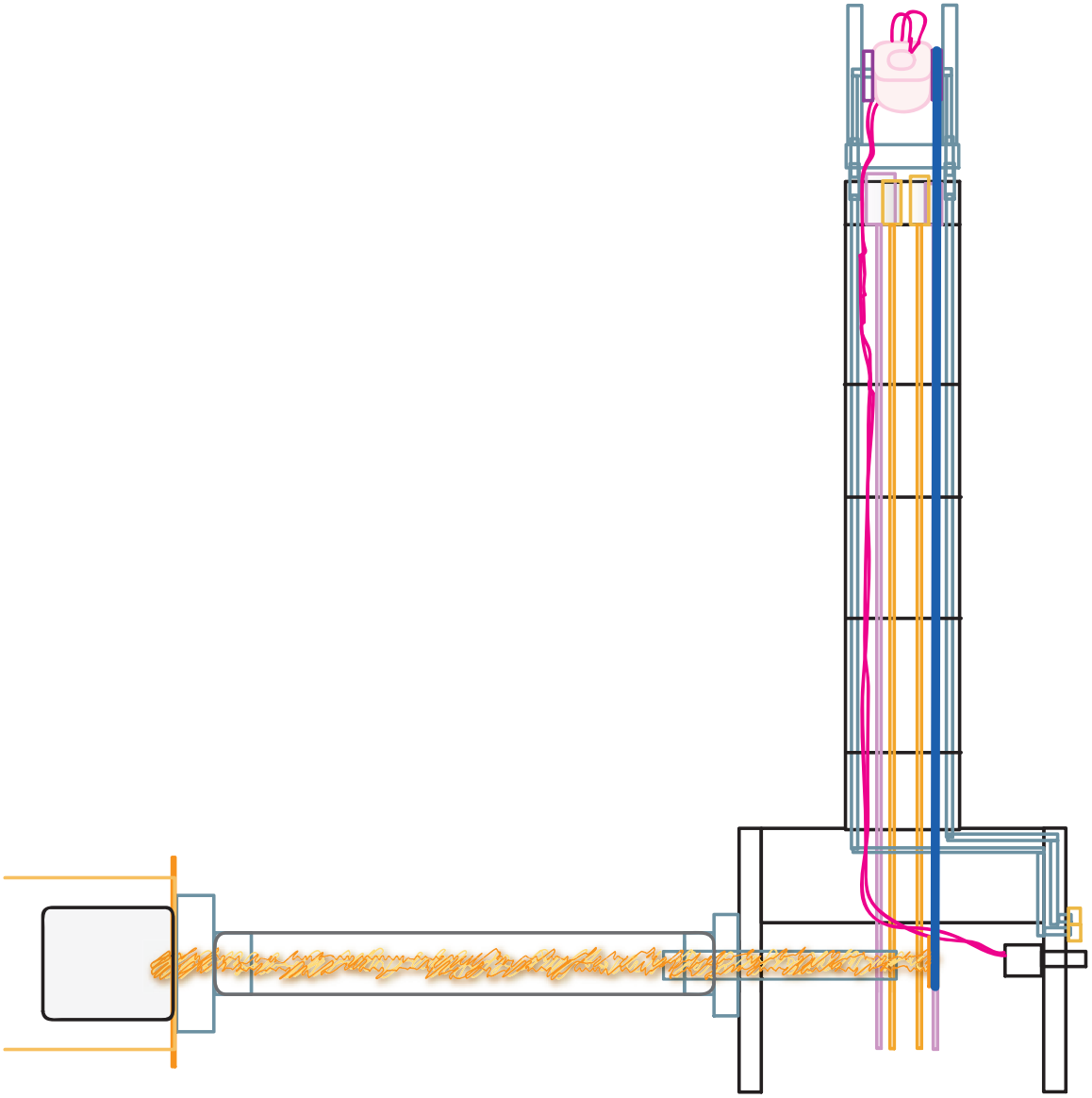

Figure 8.4: *A p-MAT probe. The stepping motor, controlled by an auxiliary computer, can switch between angles in tens of milliseconds. The pulley system is connected to the motor through a long rod. At the end of the rod is a disk which screws onto the rod. A similar disk is connected to the sample's stator. The two disks are connected with a strong polymer string. The disks and the string compose the pulley system. The stator is made out of kel-F to minimize proton signal. The leads for the coil are connected to disks which are held to the sides of the stator. These disks then sit on top of an equal radius copper semicircle disk lead, which is connected to the rest of the circuit. These make a tactile connection. This is used instead of wire leads directly since the switching of the stator would cause the lead to continually bend and straighten and break them eventually.*

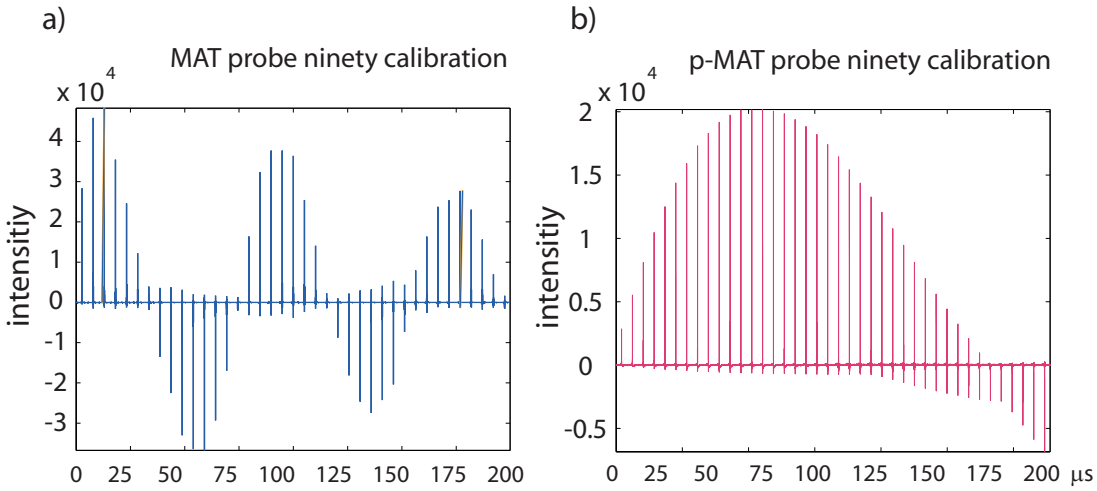

Figure 8.5: *The 90° time is found by varying the length of a single pulse and acquiring the FID. The data is stacked making a nutation curve. The 90° time is the first highest peak in the experiment. See section 4.1.1 for more details. At multiples of that time the magnetization is flipped eventually to 90° again, that is 450° and 810° a) A 90° calibration from the MAT probe. The efficiency of the probe was found to be 60% by comparing the third peak to the first peak. b) The 90° calibration from the p-MAT probe. The 90° time is at 65 µs at 640 watts of power. Using that much power past 200 µs could damage the amp so the third 90° peak was not observed.*

found to be 60 percent. At this point the MAT pulse sequence in 4.9 a) was tried with the probe.

After the initial tests of the probe the switching mechanism was put in. This constituted a stepping motor held away from the magnet, a pulley system, a new stator that could be moved, and a new coil.(See Figure 8.4)

8.3.2 Coils

The coil is the most important part of the probe. It both excites and detects the spins. For a dynamic angle probe the coil needs special consideration. If a saddle, bird cage, or solenoid is used the coil would move with the sample and the effective B_1 would change. This would lead to the 90° time at each angle not being equal. This is detrimental to a VACSY type experiment but does not eliminate the p-MAS experiment from working.

Possible coil types for p-MAT probe

The MAT sequence works best when the 90° time is small because of the rotor synchronization. As such the 90° time in Figure 8.5 is unacceptably long at 65 μs, the best time achieved to date. Several different coils shown in Figure 8.6 were tried which all gave longer 90° times. A split solenoid has been used because as the stator turns the coil remains equivocally in the same spot. This means that the 90° time is equal for all orientations. One coil being considered is a solenoid and having two separately calibrated 90° times for each angle used.

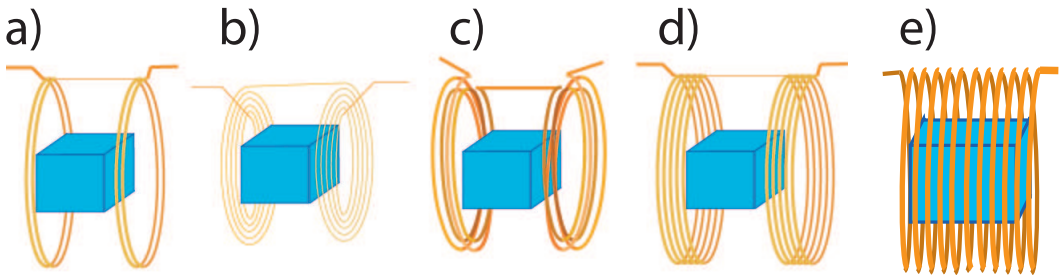

Figure 8.6: *Some of the possible coils tried in the p-MAT probe. All 90° times are for 640 watts of power. The coils tried so far have all been split solenoids with loops either stacked vertically or horizontally next to each other. a) The first coil tried. This coil is a split solenoid with two loops horizontally stacked next to each other. This coil originally gave a 90° time of 85 µs. After the other coils were tried this one was placed into the probe again as it had given the best 90° time. At that point this coil gave a 90° time of 65 µ, this change is attributed to using a different second inductor, L_H. b) This coil had two horizontally stacked loops, for ease of construction, and 8 more loops stacked vertically. This had 5 times the number of loops of the previous coil but gave a 90° time of 110 µs. c) This coil stacks two horizontal and two vertical. It also gave a 90° above 100 µs d) Using thin wire, to fit into the 2mm space on each side time above 100 µs d) Using thin wire, to fit into the 2mm space on each side of the sample, five loops were stacked horizontally. This coil gave a 90° above 100 µs d) Using thin wire, to fit into the 2mm space on each side time of 120 µs e) Since the split solenoid is not giving the desired 90° time a traditional solenoid maybe used instead. Using this coil, the 90° time will need to be calibrated for both angles used.*

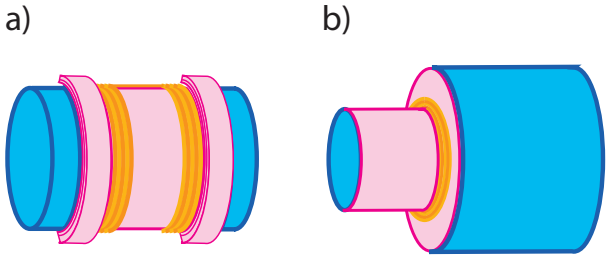

Figure 8.7: *A rod covered in tape with a gap made with tape was used to make horizontally wound coils. b) A two radius rod was used to make vertically wrapped coils.*

How to make coils

Coil wrapping can be a difficult task at first. A few tricks can help. The first thing to consider is something the coil can permanently rest on or in. For a normal stator this can be some groves on the inside which the coil is wound into. A surface coil can be etched onto a piece of plastic using chemicals. The coils for the p-MAT probes were made to hold their structure by themselves. To do this the coils were wrapped tightly and held together with super glue. The glue gave little background noise and was completely masked by the sample's signal. The space for each side of the split solenoid was not bigger than 2mm. This severely limited the number of turns that could be used.

For horizontally turned coils a straight rod could be used to wrap the coils. The rod was first lined with a single piece of tape so that the coil would not be glued to the rod and therefore permanent. Along this rod some more tape was wrapped at two locations with a gap sized to the space in the stator. The tape made a barrier to push the loops against and make them fit together as tightly as possible.

For vertically wound coils a special turning rod was made. This rod had two diameters. The coils were wound on the smaller diameter and braced against the wall of the larger diameter. The surface of the rod, was first lined with tape so that the coil could be removed.

Coil calculations

The longer 90° times for the coils were surprising since a coil with more loops should give a larger magnetic field, B_1, thus making a smaller 90° time. Calculations were used to try and explain what was happening using the already solved Bio-Savart equations for a loop of current [65]:

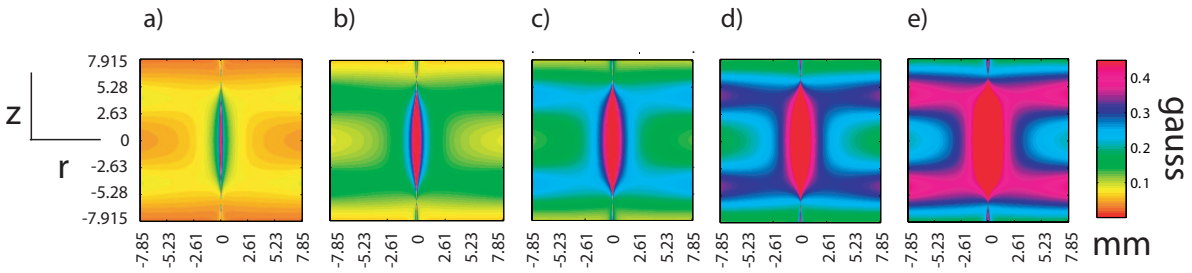

Figure 8.8: *Calculated field maps for a horizontal coild set up. The coil'd radius and spaceing is approxamatly 15.5mm. The z axis is the center of the coils. From a) to e) on additional coil is added to each side. The fields progressively become stronger as more coils are added.*

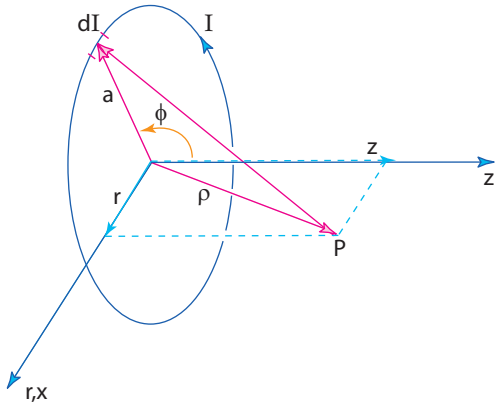

Figure 8.9: *Figure defining variables for Bio-Savart current loop equations, 8.3 and 8.4.*

$$H_z(z,r) = \frac{1}{2\pi}\left[(a+r)^2+z^2\right]^{-1/2}\left[K+\frac{a^2-r^2-z^2}{(a-r)^2+z^2}E\right] \tag{8.3}$$

$$H_r(z,r) = \frac{1}{2\pi}\frac{z}{r}\left[(a+r)^2+z^2\right]^{-1/2}\left[-K+\frac{a^2+r^2+z^2}{(a-r)^2+z^2}E\right] \tag{8.4}$$

The distance always from the coil is ρ which can be described by two variables, r and z since the coil is radially symmetric. The diameter of the coil is $2a$ and the current is I. K and E are the complete elliptic integrals of the first and second kind:

$$K(k) = \int_0^{\frac{\pi}{2}} \left(1-k^2\sin^2\gamma\right)^{-1/2} d\gamma \tag{8.5}$$

and

$$E(k) = \int_0^{\frac{\pi}{2}} \left(1-k^2\sin^2\gamma\right)^{1/2} d\gamma \tag{8.6}$$

Figure 8.8 shows a trend of increasing B_1 as we expected so there had to be other reasons for the observed 90° times. One possibility is that the resistance in the wire creates a RLC (resistance, inductor, and capacitor) circuit and the effective field is being reduced with each turn added instead of increased. However, this explanation does not seem to fit entirely. A more likely cause is that the two channels are not isolated in a way to optimize the high frequency. This is changed using the two inductors, L_S (sample inductance) and L_H (HF tuning inductance), in the system. The ratio of their inductance is what is important. For high field efficiency the ratio $\frac{L_S}{L_H}$ needs to be low, while for low frequency it needs to be high. [13] As the number of loops increases the inductance would increase and the ratio $\frac{L_S}{L_H}$ increased, thus giving worse 90° times. To address this problem, the number of loops could be reduced to one

on each side, and the inductance from L_H increased.

8.4 Proposed experimental methods

For the first p-MAT experiment the pulse sequence in 8.1 c) will be tried using oil, water, and beads, with hundreds of μm diameter, for a sample. This sample mimics that of a biological sample as the cell is mostly composed of water and oil (from the lipid bilayer). Also the beads provide a magnetic susceptibly which is present in biological samples.

8.5 Conclusions

The p-MAT experiment is well on its way to being accomplished. The results from which will be very useful in rotating field NMR experiments.

Chapter 9

Other Experiments

9.1 Magnetic Particle Steering

One interesting possible use of MRI instrumentation is influencing a system and then monitoring the changes using the same MRI intrument. Specifically the idea is to use MRI gradients to steer small magnetic particles. As most MRI instruments have three gradients this would mean that the magnetic particle could be steered in any direction of interest. This could have applications in a variety of ways. For example delivering medicines to a specific location or bringing one chemical to another for a reaction. [66] This could also be used to seperate magnetic materials from non-magnet materials. [67]

Particle movement directly caused by the MRI gradients has not been observed before because MRI pulse sequences generally do not steer particles even when strong gradients are used. This is because of the oscillatory nature of the gradients, which rapidly switch from positive to negative, prevents the movement to some extent. Another reason is that the majority of samples are not magnetic, as magnetic substances have magnetic susceptibilities and they distort the image.

9.1.1 Magnetic force

The force acting on a particle in a homogeneous magnetic field is a sum of magnetic, thermal, viscous drag and gravitational forces:

$$F = \overrightarrow{\nabla}(m \cdot \mathbf{B}) + \frac{3kT}{r} w(t) - 6\pi\eta r v + m_p g\hat{z} \tag{9.1}$$

Where $\mathbf{m} = \frac{4}{3}\pi r^3 \mathbf{M}$ is the magnetic moment, r the particle's radius, B is the applied magnetic field, T the system's temperature, w the Brownian motion, η the viscosity, v the velocity, m_p the particle's mass, and g the gravitational constant.

If the applied magnetic field is the static field, B_0, and a first order gradient the component form is:

$$B_i = B_0 \partial_{i,3} + r_j \frac{\partial B_i}{\partial x_j} \tag{9.2}$$

Assuming that the particles magnetic moment is always, or on average, pointing along the main magnetic field in z, such that $\mathbf{m} = m\hat{z}$, then the magnetic force expression only involves B_z gradients:

$$\frac{dH_x}{d\mathbf{r}} = m \begin{pmatrix} \frac{\partial B_z}{\partial x} \\ \frac{\partial B_z}{\partial y} \\ \frac{\partial B_z}{\partial z} \end{pmatrix} + \frac{3kT}{r} w(t) - 6\pi\eta r v + m_p g\hat{z} \tag{9.3}$$

Thus a conventional MRI gradient could be used to steer a particle in any desired direction.

9.1.2 Movement

Drag force

The most apparent force to overcome for steering magnetic particles is the viscous drag force. A particle 1μm in diameter at a velocity of 10 μm/sec in a viscosity of η=10^{-3} experiences a drag force approximately of:

$$0.2 \times 10^{-12} J/m, \tag{9.4}$$

Thermal force

The thermal force is much smaller than the drag force and thus can be ignored:

$$\frac{300K \cdot 10^{-23} J/K}{10\mu m} \approx 3 \times 10^{-16} J/m. \tag{9.5}$$

Magnetic force

The magnetic moment for a super paramagnetic particle 1μm is of the order 10^{-12} Am^2. The magnetic force for it is:

$$F_m = m\Delta B_z \tag{9.6}$$

To overcome the drag force, $0.2 \times 10^{-12} J/m$, the magnetic field gradient, ΔB_z, needs to be on the order of 0.1 T/m= 100 Gauss/cm.

9.1.3 Larger particles

Increasing the magnetic moment increases the magnetic force, thus the drag force becomes more readily overcome. Increasing the magnetic moment, $\mathbf{m} = \frac{4}{3}\pi r^3 \mathbf{M}$, can be accomplished by increasing the particle size as it is proportional to the particle's volume, by r^3. Size enlargement is effective because the drag force on a particle only increases linearly, by r. So increasing the radius by 10 scales the magnetic force by

$$F_{mag} \longrightarrow 1000 F_{mag} \tag{9.7}$$

while only scaling the drag by

$$F_{drag} \longrightarrow 10 F_{drag}. \tag{9.8}$$

9.1.4 Acceleration

Acceleration from Newtonian physics is $a = dv/dt$ with $v = dx/dt$ and x being position. The change in position due to acceleration is:

$$x(t) = x_0 + \frac{1}{2} a t^2. \tag{9.9}$$

The time to displace a magnetic particle starting from rest to go from $x_0 = 0$ to $x_{final} = x$, under the magnetic force is:

$$t = \sqrt{2x/a} = \sqrt{2x m_p / F_{mag}} \tag{9.10}$$

The range of force which typical gradients from MRI can make, 10 to 100 gauss/cm=.01 to .1 T/m, are between

$$F_{mag} = 10^{-12} Am^2 \times 0.1T/m = 10^{-13} N \tag{9.11}$$

and

$$F_{mag} = 10^{-12} Am^2 \times 0.01T/m = 10^{-14} N. \tag{9.12}$$

For a travel distance of $x = 1$ mm, for the higher gradient is

$$t = \sqrt{\frac{2mx}{F_{mag}}} = \sqrt{frac2 \cdot (4.6 \times 10^{-12} kg)\,(0.001m) 10^{-13} kg.m/s^2} = 0.3s \tag{9.13}$$

and the lower

$$t = \sqrt{\frac{2mx}{F_{mag}}} = \sqrt{frac2 \cdot (4.6 \times 10^{-12} kg)\,(0.001mm) 10^{-14} kg.m/s^2} = 0.96s \tag{9.14}$$

9.1.5 Procedure

Two different nanoparticles were studied, Co and FeO_3. Images were taken on a 400MHz INOVA system in a 10mm imaging probe. Images were taken of the protons in water around the nanoparticles. [68] These nanoparticles have a magnetic susceptibly and caused the water's T_2 to be short, causing in turn an extremely low signal in that region. Since the water is being

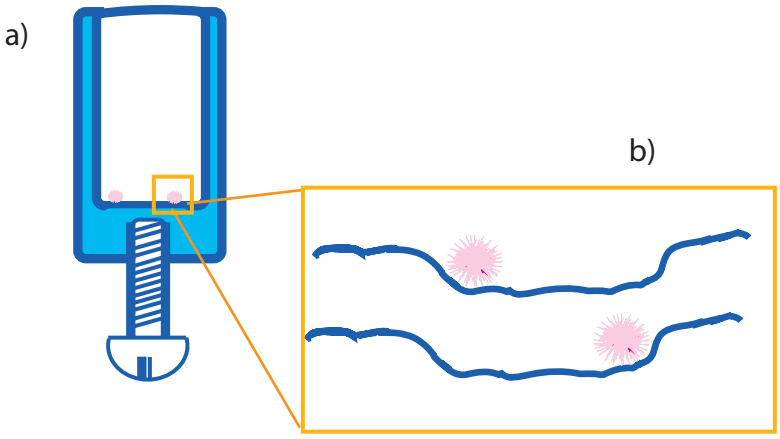

Figure 9.1: *a) The container(made from delrin) to place nanoparticles in the sweet spot for imaging. The nanoparticles were placed in a water solution where they could move freely. Gravitational forces were an obvious factor as the particles would move to the bottom of the container. b) Though machined as smoothly as possible, the bottom of the container possible had very small grooves which the nanoparticles would follow, evident from circular motion, and eventually get stuck in. In order to minimize this effect a smooth piece of plastic can be placed at the bottom and also could be coated with oil before putting the nanoparticles in.*

imaged and not the particle itself, the size of the particles can not be determined directly from the image.

To help keep the particle in the sweet spot of the magnet a special container was made whose height could be adjusted using a screw at the bottom of a regular NMR tube as shown in figure 9.1. The cobalt particles, $<1\mu m$ to 10 μm, could be seen with the naked eye to ensure that only a few particle were in the sample. The FeO_3 particles, $10\mu m$, needed to be checked under a microscope to check their abundance in a sample. If too many particles were in the sample, the image washes out and individual particles are not seen. After loading a sample the particles were allowed to settle to the bottom of the container.

MRI gradients have limits as to how long they can be turned on with a certain amount of power. One draw back from this is that a constant gradient could not be applied. Instead the gradients were repeatedly turned on and off as shown in figure 9.2. The gradients would be on for a few milliseconds and then off for a few milliseconds. This would be repeated anywhere between 500 and 3000 times. Different combinations of gradients were used in attempts to get

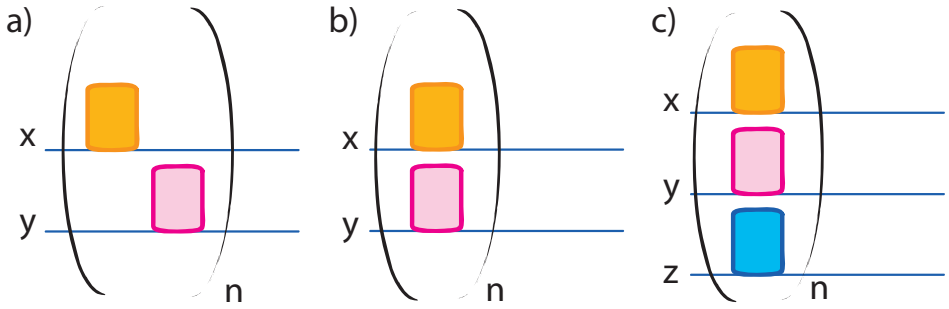

Figure 9.2: *The gradient could only be used for a certain amount of time at a certain power with out sustaining damage. To prevent damage the gradient was not constantly on. Several schemes were used in attempt to move the magnetic particles. The gradients would be rapidly shut on and off a large number of times, n. a) An x gradient would be applied followed by a y with a short down time. This pulse sequence minimized the time in which there was no gradient on. b) A x and y gradient were applied at the same time. This gave the largest gradient strength in steering a magnetic particle. c) An additional z gradient was applied to try and counter act any friction experienced from the container.*

the most movement.

9.1.6 Data

Figure 9.3 shows before and after images from pulsing on Co particles 2000 times. The particles moved slightly. After a second or third push from the gradients though the particles would stop moving. This could be due to the particles getting stuck in a groove in the container. (See figure 9.1.)

Some calculations were made for the Co particles before starting. The bulk magnetic moment for cobalt is 1.7 Bohr magneton, where a Bohr magneton is $\mu_B = 9.274 \times 10^{-24} J/T$. The magnetic moment for a nanoparticle is calculated with $m = 1.7 \times 4\pi \times \rho N_A \mu_B r^3/(3M)$. The magnetic force, thermal force, viscous drag force, and gravitational force according to particle size are graphed in figure 9.4. From this initial calculation, the drag force was assumed to be the dominating factor in keeping the nanoparticles from moving.

Obtaining minute movements from the gradients where attributed to two things. First, the

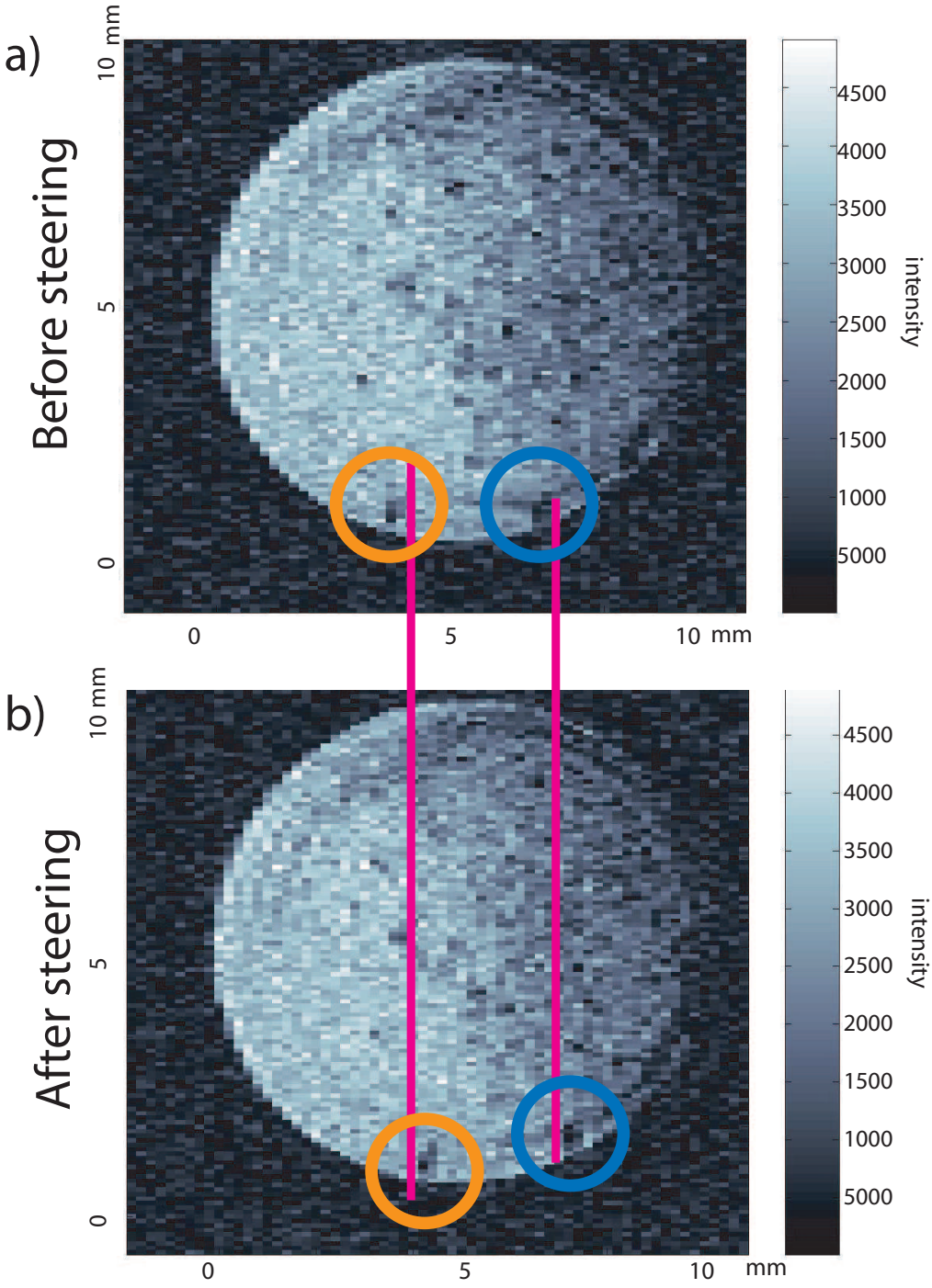

Figure 9.3: *Magnetic nanoparticles, Co, shown here, can be detected by water signal since they kill the surrounding signal. a) The nanoparticles before pulsing gradients on them. b) After 2000 repetition of the scheme shown in figure 9.2 b) the particles have moved to a small extent. This can be seen clearly from the two circled particles. In the before image both lie left of their hot pink line and after both are right of it.*

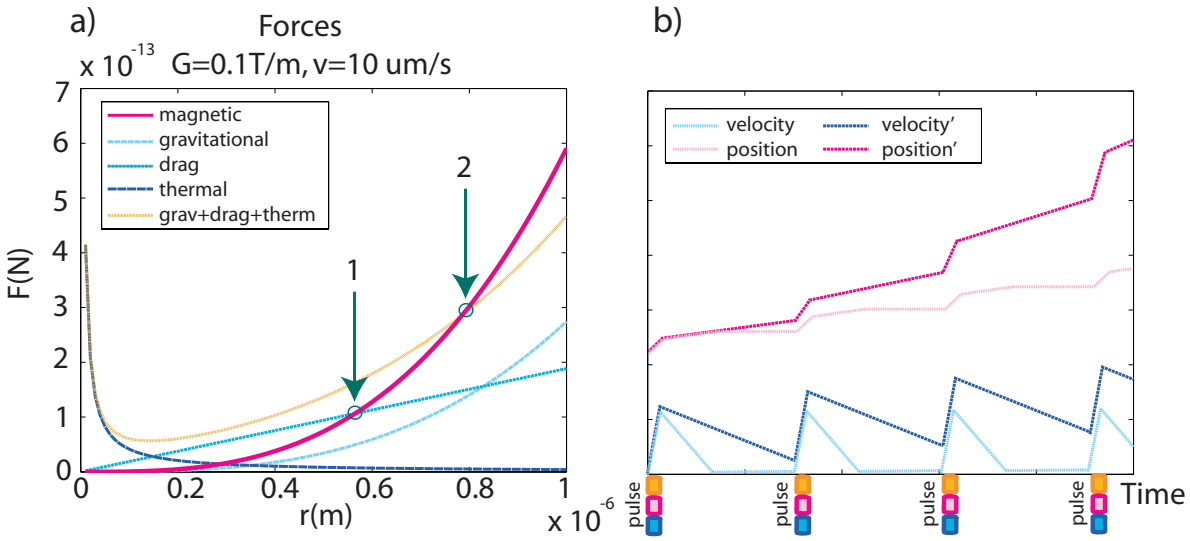

Figure 9.4: *a)The forces experienced on a magnetic nanoparticle, Co, of a certain size from a gradient of 0.1T/m. The velocity is assumed to be 10$\mu m/s$ for calculations in which velocity matters. The larger the particle, the stronger magnetic moment it will have and the more it can be influenced by the applied gradient. The drag force causes most of the resistance to the movement of a particle. If forces other than drag are disregarded, then the particle over 500nm for Co should be movable. However, when all the forces are added the particle size needs to be at least 800nm to be efficiently effected. b) Since the gradient cannot be turned on permanently at high fields the gradient pulses were rapidly turned on and off. In blue, possible particle velocity profiles are shown. In light blue, the particle gains some velocity, but, then between pulses it stops from the drag force. During this time the particle moves slightly sometimes shown in pink. A second possibility, shown in dark blue, is that before the particle stops completely, the next gradient pulse comes. In this case the maximum gradient speeds achieved continually increase and the particle moves further and further with each pulse, shown in hot pink.*

other forces than anticipated, specifically gravitational, had some influence on the system. As figure 9.4 a) shows a larger particle with a larger magnetic moment is needed to over come the resistance factor than was first thought. The particles situated themselves on the bottom of the container because of the gravitational force, this created friction between them and the container. The kinetic coefficient of friction for delrin is 0.25, however the static coefficient is not known. [69] It is possible that the particle could not overcome static friction. A second obstacle could be the surface of the container. Figure 9.1b) shows how the small nanoparticles could be caught in a groove of the container. Once it reached a barrier in the container, it stops moving. Attempts to suspend the particles in the water were made by having a very dilute solution of algerose; however, this increased the drag force too much to have movement.

There is a possibility that the movement observed was not caused by the gradient coil's magnetic field but by mechanical vibrations. There was no test done to determine if this was the cause of movement. The particle movement would still have been hindered from the surface of the container.

9.1.7 Steering Conclusions

The gradients used in MRI can be used to push magnetic particles slightly. The major hindrance to this is the strength of the gradients and the limitations on use of the gradient at high power. These difficulties are caused by the opposing forces make the gradient strength range to small for effective movement.

9.2 High pressure rotor design

9.2.1 Motivation

The study of chemical reactions in high pressure systems is both interesting and versatile. NMR when used as a tool in chemical dynamics and structure could give new insights into high pressure systems. Some samples whether liquid or solid react better under high pressure Anisotropies are not restricted to just solid samples, but any oriented system. One such system involves the catalytic addition of hydrogen in PASADENA. [70, 71] This system is studied under higher than atmospheric pressures, though it is just a few atmospheres of pressure, and has both solids and liquids in it. Systems have been made in which this system could be studied, but they are quite elabrate and potentially very costly. [72] The high cost and technical difficulty involved have acted as a hinderance to developing a system that would allow studies of the above mentioned system. Here a possible economical and quick solution to doing higher than atmospheric pressure solid state NMR methodology is presented.

9.3 Regular rotors

A rotor is used for spinning samples. There are three parts to a rotor, the shaft, the tip, and the plugs. (See Figure 9.3) The rotor is spun with two sources of air, the bearing, which pushes it up, and the drive, which turns it around. It is essential that the rotor be made with great precision. If the rotor is off balance than it will crash into the stator's wall.

The shaft is the main body of the rotor which encases the sample. This piece needs to carefully fit into the opening in the stator. If there is too much room it will sit on to the bottom of the stator which keeps it from spinning. If it is too tight the air will not be able to move around it. Flowing air catches flutes on the tip causing the rotor to spin. The flutes are

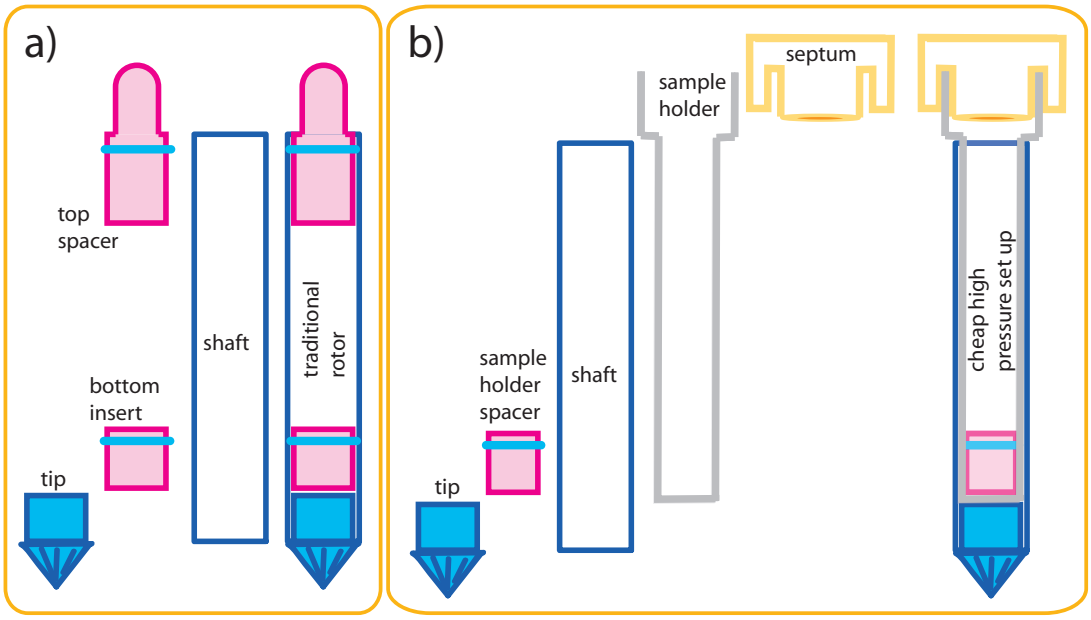

Figure 9.5: *a) Parts of a regular rotor. b) Parts of the higher that atmospheric pressure rotor.*

carefully angled to produce maximum speed. Spacers are used to correctly confine the volume of the sample to the homogeneous region of the coil. If the sample protrudes out of the coil it is unevenly excited as in figure 4.2 c).

Both solids and liquids can be packed as samples into a rotor, the techinnique varies for each but they both start out the same. First a spacer must be placed in the bottom of the shaft, its size will be determined by the probe that is being used. Then a tip must be placed into the shaft. If the tip is to loose then the shaft could slip and cause uneven spinning which would crash the rotor. Once the tip is in place then the sample must be prepared to be placed in the rotor.

The solid first needs to be ground into a fine powder with a mortal and pestle allowing the greatest amount of the sample to be packed in, while in powder form the sample can then be compressed into the holder. A funneled holder may help when packing a solid sample into smaller rotors. Once the sample is in the shaft the top insert is then placed . It is important to the stability of the rotor that the tip and the top insert are fully inserted. For liquid containing

samples special o-ring inserts are used to prevent the liquid from leaking out.

9.3.1 The design

Some experiments would require a rotor which can withstand higher pressures. Making one is not simple, however, some groups have done this. [72] There are two ways in which pressure escapes from a the standard rotor, both from the tip and the top insert. To prevent leaks from the tip the tip and shaft could be made into one piece, except that the tip is removable for several reasons; it is easier to remove the sample if the body can be opened from both sides. The body of the probe is made from a very hard ceramic material which would be hard to machine. A ceramic tip would chip easily and be rendered useless. Plastics are a possible solution to this but, if the shaft were made out of plastic then two things may happen. First, materials made out of plastics are difficult to machine resulting in possible inconsistencies and a taper, which would mean mean that the fit in the stator would not be equally tight all the way around. The other problem is that plastics are not as smooth as ceramics, so if the rotor hits the sides, it would have more friction and crash more easily.

An alternative to a single piece shaft is a tight fitting insert that could have a closed bottom. There would be less signal, as there is less volume, but the walls could be machined thinly. A larger rotor like a 7.5mm could be used as in Figure 9.3. In order to run high pressure experiments a special cap would need to be designed to hold in the pressure at the top. However, for only a couple of atmospheres a septum could be used to retain pressure. To accommodate this piece the rotor insert would be longer than the shaft so that the septum could fit on top of the whole apparatus which can be seen in Figure 9.3.

9.3.2 High pressure rotor conclusion

Possibilities of a more economical way to gain higher than atmospheric pressures in a rotor are under way. The system described above is still to be made and tested for its effectiveness but may be useful in taking spectra for the high pressure catalyst used in the PASADENA project. [73]

Bibliography

[1] C. Meriles, D.S. Sakellariou, H. Heise, A. Moule, and A. Pines. Approach to high-resolution ex-situ nmr spectroscopy. *Science*, 293:82–85, 2001.

[2] M.H. Levitt. *Spin Dynamics*. Wiley, Chichester, 2002.

[3] J. Cavanagh, W.J. Fairbrother, A.G. Palmer III, and N.J. Skelton. *Protein NMR Spectroscopy Principles and Practice*. Academic Press, San Diego, 1996.

[4] R.A. Serway. *Physics For Scientists and Engineers with Modern Physics*. Saunders College Publishing, Philadelphia, third edition, 1990.

[5] P.F. Bernath. *Spectra of Atoms and Molecules*. Oxford University press, New York, 1995.

[6] J.J. Sakurai. *Modern quantum mechanics*. Addison-Wesley, New York, revised edition, 1994.

[7] I.N. Levine. *Quantum Chemistry*. Prentice Hall, Upper Saddle River, New Jersey 07485, fifth edition, 2000.

[8] P. Atkins. *Physical Chemistry*. Oxford University press, New York, sixth edition, 1998.

[9] S.S. Zumdahl. *Chemical Principles*. Houghton Mifflin Company, Boston, fifth edition, 2005.

[10] E.M. Purcell. *Electricity and Magnetism Berkeley physics couse volume 2*. McGraw-Hill, Boston, 1985.

[11] E.O. Stejskal and J.D. Memory. *High Resolution NMR in the Solid Statel: Fundametals of CP/MAS*. Oxford University Press, New York, 1994.

[12] U. Haeberlen. *High Resolution NMR in Solids, Adv. Mag. Reson. Supplement1*. Academic, New York, 1976.

[13] F.D. Doty. Probe design and construction. *The Encyclopedia of Nuclear Magnetic Resonance*, 6:3753–3761, 1996.

[14] S. Han, J. Granwehr, S. Garcia, E.E. McDonnell, and A. Pines. Auxiliary probe design adaptable to existing probes for remote detection nmr, mri, and time-of-flight tracing. *Journal of Magnetic Resonance*, 182:260–272, 2006.

[15] S. Xu, M.H. Donaldson, S.M. Rochester, V.V.Yashchuk, D. Budker, and A. Pines. Application of atomic magnetometry in magnetic particle detection. *Applied Phys. Lett.*, 89:224105–224107, 2006.

[16] J.C. Watkins and E. Fukushima. High-pass bird-cage coil for nuclear magnetic resonance. *Review of Scientific Instruments*, 59:926–929, 1988.

[17] M.A. Macnaughtan, A.P. Smith, P.B. Goldsbrough, R.E. Santini, and D. Raftery. Nmr difference spectroscopy with a dual saddle-coil difference probe. *Anal Bioanal Chem*, 378:1520–1527, 2004.

[18] M. Gochin and A. Pines. High resolution nmr with a surface coil. *Journal of American Chemical Society*, 107:7193–7194, 1985.

[19] E. Harel, H. Hilty, E.E. McDonnell, and A. Pines. Time-of-fight flow imagind of two-component flow inside a microfluidic chip. *Physical Review Letters*, 98:017601, 2007.

[20] C. Hilty, T.J. Lowery, D.E. Wemmer, and A. Pines. Spectrally resolved magnetic resonance imaging of a xenon biosensor. *Chemical Physical Letters*, 45:70–73, 2006.

[21] V. Demas, C. Meriles, D.S. Sakellariou, S. Han, J. Reimer, A. Moule, and A. Pines. Towards ex-situ chemical shift mri in a one-sided nmr probe. *Magnetic resonance Engineering*, 29:137–144, 2006.

[22] L.-S. Bouchard. Summer lecture notes 2. Pines lab private Lectures, 2005.

[23] J.H. Hu, D.W. Alderman, C. Ye, R.J. Pugmire, and D.M. Grant. An isotropic chemical shift-chemical shift anisotropy magic-angle slow-spinning 2d nmr experiment. *Journal of Magnetic Resonance*, 105:82–87, 1993.

[24] J.H. Hu and R.A. Wind. Sensitivity-enhanced phase-corrected ultra-slow magic angle turning using multiple-echo data acquisition. *Journal of Magnetic Resonance*, 163:149–162, 2003.

[25] Y. Yarim-Agaev, P.N. Tutunjian, and J.S. Waugh. Sample spinning at the magic angle with rotation-synchronized rf pulses. *Journal of Magnetic Resonance*, 47:51–60, 1982.

[26] J.Z. Hu, A.M. Orendt, D.W. Alderman, R.J. Pugmire, C. Ye, and D.M. Grant. Measurement of c^13 chemical shift tensor principal values with magic-angle turing experiment. *Solid State Nuclear Magnetic Resonance*, 3:181–197, 1994.

[27] J.Z. Hu, W. Wang, F. Liu, M.S. Solum, D.W. Alderman, R.J. Pugmire, and D.M. Grant. Magic-angle-turning experiments for measuring chemical-shift-tensor principle values in powdered solids. *Journal of Magnetic Resonance*, 113:210–222, 1995.

[28] L. Frydman, G.C. Chingas, Y.K. Lee, P.J., Grandinetti, M.A. Eastman, G.A. Barrall, and A. Pines. Variable-angle correlation spectroscopy in solid-state nuclear magnetic resonance. *Journal of Chemical Physics*, 97:4800–4808, 2002.

[29] E. Wrenn Wooten, K.T. Mueller, and A. Pines. New angles in nuclear magnetic resonance sample spinning. *American Chemical Society*, 25:209–215, 1992.

[30] R.W. Martin, R.C. Jachmann, D. Sakellariou, U.G. Nielsen, and A. Pines. High-resolution nuclear magnetic resonance spectroscopy of biological tissues using projected magic angle spinning. *Magnetic Resonance in Medicine*, 54:253–257, 2005.

[31] C.A. Meriles, D. Sakellariou, and A. Pines. Resolved magic-angle spinning of anisotropic samples in inhomogeneous fields. *Chemical Physical Letters*, 358:391–395, 2002.

[32] D. Sakellariou, C. Meriles, R.W. Martin, and A. Pines. Nmr in rotating magnetic fields: magic angle field spinning. *Magnetic Resonance Imaging*, 23:295–299, 2052.

[33] R.C. Jachmann, D.R. Trease, L.-S. Bouchard andD. Sakellariou, R.W. Martin, R.D. Schluter, T.F. Budinger, and A. Pines. Multipole shimming of permanent magnets using harmonic corrector rings. *Review of Scientific Instruments*, 78:035115, 2007.

[34] G. Moresi and R. Magin. Miniature permanent magnet for table-top nmr. *Concepts in Magnetic Resonance part B*, 19:35, 2003.

[35] H. Raich and P. Blumler. Design and construction of dipolar halbach array with a homogeneous field from identical bar magnets nmr mandhalas. *Concepts in Magnetic Resonance part B*, 23:16, 2004.

[36] K. Halbach. *Nuclear Instruments and Methods in Physics Research Section A*, 169:1, 1980.

[37] C.A. Meriles, D. Sakellariou, A. Moule, M. Goldman, T.F. Budinger, and A. Pines. High-resolution nmr of static samples by rotation of the magnetic field. *Journal of Magnetic Resonance*, 169:13–18, 2004.

[38] D. Sakellariou, C.A. Meriles, R.W. Martin, and A. Pines. High-resolution nmr of anisotropic samples with spinning away from the magic angle. *Chemical Physics Letters*, 377:333–339, 2003.

[39] R. Schlueter, D. Humphries, and J. Tanabe. Pure permanent magnet harmonics corrector ring. *Nucl. Instr. Meth. Phys. Res. A*, 395:153, 1997.

[40] R. Schlueter and S. Marks. *IEEE Trans. Magn.*, 32:2710, 1996.

[41] M.E. Bollard, S. Garrod, E. Holmes, J.C. Lindon, E. Humpfer, M. Spraul, and J.K. Nicholson. High resolution ^{1}h and ^{1}h-^{13}c magic angle spinning spectroscopy of rat liver. *Magnetic Resonance in Medicine*, 44:201–207, 2000.

[42] R.D. Ross. The biochemistry of living tissues: examination by mrs. *Nuclear Magnetic Resonance in Biomedicine*, 5:303–324, 1992.

[43] R.D. Ross. B. sitter and U. sonnewald and M. spraul and H.E. fjosne and I.S. gribbestad. *Nuclear Magnetic Resonance in Biomedicine*, 15:327–337, 2002.

[44] J.L. Taylor, C.L. Wu, D. Cory, R.G. Gonzales, A. Bielecki, and L.L. Cheng. High resolution magic angle spinning proton nmr analysis of human prostate tissue with slow spinning rates. *Nuclear Magnetic Resonance in Biomedicine*, 50:627–632, 2003.

[45] O.M. Rooney, J. Troke, J.K. Nicholson, and J.L. Griffin. High resolution and diffusion and relaxation-edited magic angle spinning ^{1}h nmr spectroscopy of intact liver tissue. *Magnetic Resonance in Medicine*, 50:925–930, 2003.

[46] R.A. Wind, J.Z. Hu, and D.M. Rommereim. High-resolution 1h nmr spectroscopy in a live mouse subjected to 1.5 hz magic angle spinning. *Magnetic Resonance in Medicine*, 50:1113–1119, 2003.

[47] W.T. Dixon. Spinning-sideband-free and apinning-sideband-only nmr spectra in a spinning sample. *Journal of Chemical Physics*, 77:1800–1809, 1982.

[48] O.N. Antzutkin, S.C. Shekar, and M.H. Levitt. Two-dimensional sideband separation in magic-angle spinning nmr. *Journal of Magnetic Resonance*, 115:7–19, 1995.

[49] C.L. Wu, J.L. Taylor, W. He, A.G. Zepeda, E.F. Halpern, A. Bielecki, R.G. Gonzales, and L.L. Cheng. Proton high-resolution magic angle spinning nmr analysis of fresh and previously frozen tissue of human prostate. *Magnetic Resonance in Medicine*, 50:1307–1311, 2003.

[50] A. Bax, N.M. Szeverenyi, and G.E. Maciel. Correlation of isotropic shifts and chemical shift anisotropies by two-dimensional fourier-transform magic-angle hopping nmr spectroscopy. *Journal of Magnetic Resonance*, 52:147–152, 1983.

[51] Z. Gan. High-resolution chemical shift and chemical shift anisotropy correlation in solids using slow magic angle spinning. *Journal of the American Chemical Society*, 114:8307–8309, 1992.

[52] J.Z. Hu, W. Wang, and R.J. Pugmire. *Encyclopedia of Nuclear Magnetic Resonance*. Wiley and Sons, New York, 1996.

[53] J.Z. Hu and R.A. Wind. The evaluation of different mas techniques at low spinning rates in aqueous samples and in the presence of magnetic susceptibility gradients. *Journal of Magnetic Resonance*, 159:92–100, 2002.

[54] R.A. Wind, J.A. Hu, and D.N. Rommereim. High-resolution 1h nmr spectroscopy in organs and tissues using slow magic angle spinning. *Magnetic Resonance in Medicine*, 46:213–218, 2001.

[55] S.P. Brown and S. Wimperis. Inhomogeneous broadening of two-dimensional nmr lineshapes. *Chemical Physics Letters*, 237:509–515, 1995.

[56] D. Sakellariou, S.P. Brown, A. Lesage, S. Hediger, M. Bardet, C.A. Meriles, A. Pines, and L. Emsley. Highresolution nmr correlation spectra of disordered solids. *Journal of the American Chemical*, 125:4376–4380, 2003.

[57] L. Schroder and P. Bachert. Evidence for a dipolar-coupled am system in carnosine in human calf muscle from in vivo 1h nmr spectroscopy. *Journal of Magnetic Resonance*, 164:256–269, 2003.

[58] C. Boesch and R. Kreis. Dipolar coupling and ordering effects observed in magnetic resonance spectra of skeletal muscle. *Nuclear Magnetic Resonance in Biomedicine*, 14:140–148, 2001.

[59] R.W. Martin, E.K. Paulson, and K.W. Zilm. Design of a triple resonance magic angle sample spinning probe for high field solid state nuclear magnetic resonance. *Review of Scientific Instruments*, 76:3045–3061, 2003.

[60] R.H. Havlin, G.H.J. Park, T. Mazur, and A. Pines. Using switched angle spinning to simplify nmr spectra of strongly oriented samples. *Journal of the American Chemical Society*, 125:7998–8006, 2003.

[61] S.R. Williams, D.G. Gadian, E. Proctor, D.B. Sprague, D.F. Talbot, I.R. Young, and F.F. Brown. Proton nmr studies of muscle metabolites in vivo. *Journal of Magnetic Resonance*, 63:406–412, 1985.

[62] J.Z. Hu. High-resolution 1h nmr spectroscopy in rat liver using magic angle turning at a 1 hz spinning rate. *Magnetic Resonance in Medicine*, 47:829–836, 2002.

[63] J.H. Hu and R.A. Wind. The evaluation of different mas techniques at low spinning rates in aqueous samples and in the presence of magnetic susceptibility gradients. *Journal of Magnetic Resonance*, 159:92–100, 2002.

[64] K. Schmidt-Rohr, D. Nanz, L. Emsley, and A. Pines. Nmr measurement of resolved heteronuclear dipole couplings in liquid crystals and lipids. *Journal of Physical Chemistry*, 98:6668–6670, 1994.

[65] H.E. Knoepfel. *Magnetic Fields: A comprehensive Theoretical treatise for Practical Use*. John Wiley and Sons, Inc, New York, 2000.

[66] R. Evans, C.R. Timmel, P.J. Hore, and M.M. Britton. Magnetic resonance imaging of the manipulation of a chemical wave using an inhomogeneous magnetic field. *American Chemical Society*, 128:7309–7314, 2006.

[67] C.T. Yavuz, J.T. Mayo, W.W. Yu, A. Prakash andJ.C. Falkner, S. Yean, L. Cong, H.J. Shipley, A. Kan, M. Tomson, D. Natelson, and V.L. Colvin. Low-field magnetic separation of monodisperse fe_3o_4 nanocrystals. *Science*, 314:964–967, 2005.

[68] E.M. Shapiro, S. Skrtic, and A.P. Koretsky. Sizing it up:cellular mri using micron-sized iron oxide particles. *Magnetic Resonacne in Medicine*, 53:329–338, 2005.

[69] Ensinger-Hyde. *Delrin*. Ensinger-Hyde, Pennsylvania, 2004.

[70] T. Posset and J. Blumel. New mechanistic insights regarding pd/cu catalyst for the sonogashira reaction: Hrmas nmr studies of silica-immobilized systems. *Magnetic Resonance in Medicine*, 54:253–257, 2005.

[71] C.R. Bowers. Sensitivity enhancement utilizing parahydrogen. *Encyclopedia of Nuclear Magnetic Resonance*, 9:750–770, 2002.

[72] A. Rezzouk, Y. Errammach abd F. Rachdi, V. Agafonov, and V.A. Davydov. High-resolution ^{13}c nmr studies of the tetragonal two-dimensional polymerized c_60 phase. *Physica E*, 8:1–4, 2000.

[73] S. Burt and S. Anwar. private communication, 2005.